Universidad
Carlos III de Madrid

TESIS DOCTORAL

Rapid manufacturing methods for geometrically complex nuclear fusion devices: The UST_2 stellarator

Autor:

Vicente Manuel Queral Mas

Director:

Dr. Víctor Tribaldos Macía

DEPARTAMENTO DE FÍSICA

Leganés, abril 2015

Universidad Carlos III de Madrid
www.uc3m.es

TESIS DOCTORAL

Rapid manufacturing methods for geometrically complex nuclear fusion devices: The UST_2 stellarator

Autor: *Vicente Manuel Queral Mas*

Director: **Víctor Tribaldos Macía**

Firma del Tribunal Calificador:

(Nombre y apellidos) (Firma)

Presidente:

Vocal:

Secretario:

Calificación:

Leganés, de de

A mis padres.
A mi abuelo Pascual.

Universidad
Carlos III de Madrid

Rapid manufacturing methods for geometrically complex nuclear fusion devices: The UST_2 stellarator

Thesis for the degree of Doctor
presented by

Vicente Manuel Queral Mas

Adviser

Dr. Víctor Tribaldos Macía

DEPARTMENT OF PHYSICS

Leganés, April 2015

Abstract

Energy sources have been decisive in the development of human history. However, today abundant and inexpensive energy sources are declining. Fusion energy might contribute to overcome this problem. For instance, stellarators, which are magnetically confined fusion devices whose magnetic field is mainly generated by external coils, are promising among the numerous fusion approaches. The advancement of the stellarator research line is hindered to some extent by their high geometrical complexity that results in long production cycles and high costs.

This thesis investigates whether a manufacturing method, based partially on additive manufacturing, and fully integrated with the physics and engineering design, may speed up and lower the construction costs of certain stellarators. If such a method were feasible, a faster production cycle for experimental stellarators might also advance fusion plasma science.

A research methodology that is essentially exploratory and applied is followed. Initially, concepts for new construction methods, based on literature searches and author creativity, are formulated. Next, these concepts are experimentally validated or rejected. Moreover, the design and construction of a small stellarator with major radius of 0.125 m (the UST_2) is attempted to integrate and validate the concepts. Generation of knowledge about the feasibility of the methods and know-how are pursued.

Literature concerning fabrication methods used in W7-X, HSX, NCSX and other devices is reviewed, particularly the coil winding and positioning methods, coil frame and vacuum vessel fabrication, as well as the assembly of such components. In addition, the QPS, NCSX-like and three quasi-isodynamic stellarator magnetic configurations are assessed using the CASTELL code. CASTELL is a code developed by the author to calculate, among others, guiding centre orbits and to interact with the NESCOIL code to generate coil configurations.

After completing the literature review, fabrication methods have been studied, combined and some are tested. Subsequently, three main engineering concepts are formulated: i) additive manufacturing combined with casting, consisting of an additively manufactured light truss structure enclosed within a thin external surface, where the internal volume is filled with a material that solidifies or cures after filling, ii) coil frame, fabricated following the previous concept, that includes grooves in the external surface in which conductors are wound, and iii) a single conductor pancake compressed and embedded in each groove.

Several results are reported. A construction method for stellarators based on additive manufacturing and resin casting has been conceived, developed and tested. However, the measured dimensional errors are $\pm 0.3\%$, which are excessive. Nonetheless, using high-quality 3D printers and enhanced procedures may improve accuracy. The light truss structure concept has been designed, 3D printed in polyamide and satisfactorily validated. Thus, the rapid manufacture of strong, geometrically complex structures at relatively low cost has been proven. The method combines a small quantity of expensive, but weak, 3D-printing material with bulk inexpensive, but strong, cast resin, which can be fibre reinforced. It is considered that this concept could be extended to a 3D printed metallic shell and internal metal casting.

A Last Closed Flux Surface that includes a straight non-torsion plasma section has been calculated for UST_2. For that, a three-period quasi-isodynamic magnetic configuration was modified so as to allow possible enhanced engineering and maintenance features such as large planar tilting coils and detachable sectors. However, confinement is deteriorated.

A convoluted sector of the vacuum vessel for the UST_2 has been devised, designed and fabricated as a copper liner that is externally reinforced by cast epoxy resin. Winding the cables in the grooves was straightforward and accurate. Coil frame positioning, envisaged as coil frames sliding on a flat smooth surface until contact on a mandatory circular central ring, was demonstrated by UST_2 half-period assembly. Finally, electron beam field line mapping experiments were undertaken in one half-period and confirmed the correctness of the explored methods.

An affirmative answer results for the posed question. At least one faster construction method, with reduced costs, has been identified for a small stellarator. It can be considered a modest, but relevant, contribution to the broader fusion device construction problems and to fusion energy.

Summarised contents

Contents

Chapter 1

Introduction

1.1 Outline of introduction

Fusion energy may contribute to lessen the present energy and environmental problems. The stellarator, a type of geometrically complex fusion device, is one approach for fusion energy. Geometrical complexity implies somewhat long production cycles and high cost of the devices.

Stellarators are commonly manufactured by casting, forging, machining and welding. Study and application of recent manufacturing methods for the construction of stellarators has been uncommon. Accordingly, this thesis investigates whether a manufacturing method, based partially on additive manufacturing, may speed up and lower the construction cost of certain stellarators.

An exploration of traditional and new manufacturing concepts is carried out in order to create improved fabrication techniques for coil frames and other components for stellarators. Concepts are formulated and subsequently they are experimentally validated or rejected. The work is developed with low funds in a personal laboratory.

1.2 The energy problem. Fusion energy

The world energy consumption has grown from the origin of humanity. The world energy consumption includes the energy spent by the world population in the form of food, used in agriculture, industry, services, transport, and domestic uses. Fig. 1.1 shows an estimation of the evolution of the world energy consumption during the last 2000 years. The graph indicates a notable increase in energy utilization from

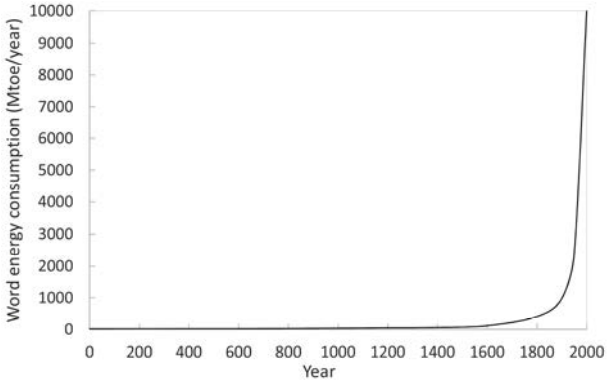

Fig. 1.1. Estimation of historical total world energy consumption. Source: compilation from Refs. [1-4].

1700, accelerated after 1900. Different interrelated factors and feedback yielded the extraordinary increase of world energy consumption in such period. Population was able to grow [1] from around 170 million in 1 AD to around 7000 million in 2014. Energy use together with other factors motivated the chance of population growth. Coal and later petrol improved food transport, enhanced agricultural techniques (e.g. synthetic fertilizers, powerful mechanization, greenhouses), liberated population from field work and thus, allowed flourishing other important activities like science, innovation and trade. In parallel to the population growth, the average world per capita energy consumption also increased notably, from roughly 0.1-0.2 toe/capita-year (t/c-y) in 1 AD [2,5] to 1.88 t/c-y [3] in 2011. Currently, in some regions the energy use is still much lower than in the developed countries. In 2011 [3], the consumption in toe/capita-year in Africa was 0.67, in India 0.6 and in China 2. As comparison, in Japan was 3.6 t/c-y and in USA 7 t/c-y. There is a correlation between the Human Development Index and per capita energy consumption, [6]. Few doubts remain that many deemed advances are impossible without some level of energy consumption at affordable cost.

In 2012 fossil fuels still accounted for 82% of the primary energy supply [3]. Hydroelectric, nuclear fission and energy from wastes complete the energy map. In 2011 still only 3.4% of the world final consumption came from wind, solar and geothermal energy [3]. Petrol wells of lowest extraction cost are declining [7]. If CO_2 is not stored, coal produces significant climate change and pollution. In any case, fossil fuels will deplete. Renewable energies may solve part of the problem but they hardly will allow the past growth ages created by abundant fossil fuels.

Currently, fission energy is one of the non-fossil significant energy sources. There are some lines of research trying to lessen its drawbacks, like breeder reactors, small modular reactors, thorium-based reactors and enhanced passive safety. In contrast, fusion would enjoy of natural passive safety (major accidents are practically impossible due to the natural self-extinction of the plasma reactions under anomalies). The moderate decay heat of in-vessel materials reduces the risk of explosions and melting of closure elements [8]. The inventory of mobilizable activated materials is low if tritium and erosion activated powders are appropriately removed. Deuterium and lithium fuels are much abundant [9,10] and inexpensive than uranium or thorium. Moreover, fusion power plants have the prospective of more favourable scaling, that is, plants of several GW_e power would result in notably cheaper electricity [11] without the fission safety concerns [12]. And essential, no actinides and no long life activated wastes are generated if materials are chosen appropriately [8].

Nevertheless, it could be argued that fusion plants are complex and require large, accurate and high technology components. High plant availability of a complex system can only be assured by appropriate design for fast maintenance [13,14], strict reliability requirements and expensive heavy remote maintenance systems [15,16]. Also, Tritium is a permeable gas, more difficult to handle than Uranium. Low-level wastes from divertors, blankets, shield, vacuum vessel and support structure will likely be larger than in fission plants [17]. Neutron damage and erosion of first wall, blanket and divertors will force the replacement of such components several times during the life of the plant, accounting for an important part of the cost of electricity, [18]-p.43. Summarising, it may be claimed that high construction

costs [19], notable cost of replaced elements and long maintenance downtimes will hinder competitive fusion for many decades.

In spite of that, the appealing of nuclear fusion, in contrast to the other sources, is the ambition of generating huge amounts of clean and cheap energy, at least as inexpensive as fossil fuels. And to try to contribute to avoid the frightening singularity (see e.g. [20]-p.184) in the history of humanity which started around 1800, which, without fusion energy or perhaps fission [21] will likely finish sometime during the XXI century.

In principle, there are various possible fusion reactions [18]-p.22 acceptable for fusion energy. However, the nuclear reaction of Deuterium (D) with Tritium (T) is the easiest to achieve [22,23]. This reaction has [18,22] the higher reaction rate for the same conditions, much lower bremsstrahlung losses, ignition possible at higher concentrations of impurities, fuel availability if lithium breeding is used, and requires lower magnetic fields for confinement. The reaction products are mostly ^{4}He and an energetic neutron:

$$D + T \rightarrow {}^4He\ (3.5\ MeV) + n\ (14.1\ MeV) \qquad (1.1)$$

Though this reaction is the easiest to achieve, it generates an energetic neutron and requires Tritium. Both aspects have many detrimental effects in a power plant. Neutrons generate a considerable amount of radioactive wastes [24], damage the first wall and blankets [25] and require thick shielding to allow superconducting coils [26]. Tritium is a radioactive hydrogen isotope almost naturally non-existent on earth and it permeates easily through walls [10]-p.22. The generation of tritium requires a breeder system based on neutron/lithium nuclear reactions [10]-p.7. The space occupied by the breeder system [27], the safety requirements due to the use lithium and compounds [28,29], the complex maintenance of the breeders [16], the usually required ^{6}Li enriched lithium [27,30], the tritium balance and recovery issues [31], imply a considerable increase of complexity and costs of the power plant. In spite of the extra difficulties, the reaction (1.1) is still the mainstream reaction considered for fusion energy production.

1.2.1 Fusion energy approaches

There are several approaches to produce nuclear fusion energy on earth. The inertial confinement fusion (ICF) and the magnetic confinement fusion (MCF) are the two prevailing research lines. There are some intermediate approaches, for example, magnetized target fusion (MTF) [32]. MTF pursues much higher plasma density and smaller plasma volume than conventional magnetic confinement fusion. The diversity of fusion energy approaches is graphically shown in Fig. 1.2, [33]. In magnetic fusion, the tokamak concept is the most developed one, followed by the stellarator concept. The other magnetic confinement concepts have been developed to a less extent. Other approaches are the muon catalysed fusion [34] and the dubious cold fusion [35]. In muon catalysed fusion, the fusion reaction is catalysed through the formation of a muon mesomolecule.

Laser driven inertial confinement fusion currently presents some difficulties, like the low efficiency and high cost of lasers, the accuracy and cost of the numerous pellets required, the symmetry of the heating beams and accurate location of the pellet with respect the

beams. However, it enjoys some potential advantages like the comparatively small, simple and accessible vacuum chamber, small blankets and the lack of superconducting coils and cryogenics. High plasma densities of the order of 10^{31} m^{-3} and temperatures of the order of few keV are sought by compressing a small pellet of diameter <~0.5 mm by laser beams or ion beams drivers. Other advantages, drawbacks and details about the inertial confinement fusion approach can be found in Refs. [36,37].

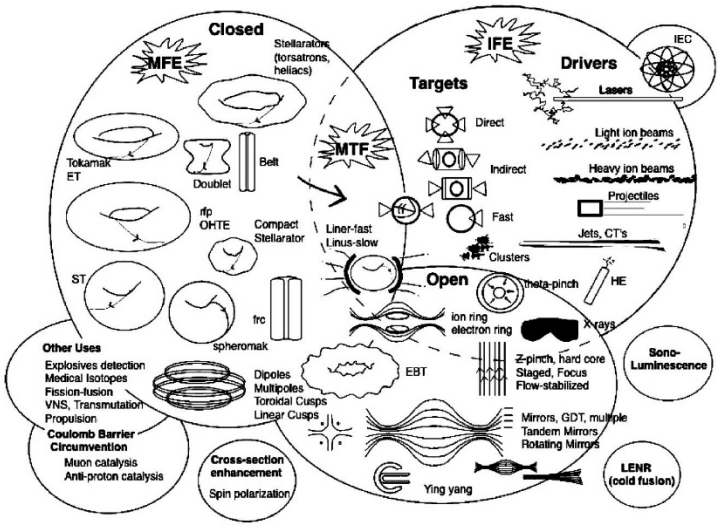

Fig. 1.2. Different fusion approaches. Reproduced with kind permission of Springer Science+Business Media from [33]. © 2005 Springer Science+Business Media, Inc.

The mainstream magnetic confinement fusion concepts also undergo some specific issues like too high plasma turbulent transport, large devices difficult to maintain in a radioactive environment, difficulties in power extraction, expensive superconducting coils, and large, heavy and complex blankets difficult to maintain and prone to failures. Advantages with respect to inertial confinement might be the potential for steady-state operation and the apparent more favourable scaling of power with size. Magnetic confinement fusion aims at obtaining plasma density of the order of 10^{20} m^{-3} and temperatures of the order of few keV by keeping the ions and electrons on magnetic field lines. Details about magnetic confinement fusion can be found in the Refs. [38-40]. There are many magnetic confinement fusion approaches [33] that might achieve competitive fusion reactors, for example based on: common tokamak [19], spherical tokamak [41,42], stellarator [43], relatively compact stellarator [44], hybrids fusion-fission [45], Field Reversed Configuration [46], Reversed Field Pinch [47], dipole [48] and spheromak [49,50].

A brief comparison of the advantages and drawbacks of tokamaks and stellarators, the current dominant concepts, is carried out next. The study of drawbacks is crucial since the improvement of a single drawback surely would contribute to fusion energy.

The essential difference between stellarators and tokamaks is the way the torsion of the magnetic field lines is produced, Fig. 1.3. A (pure) tokamak generates the poloidal component of the magnetic field by a current in the plasma. A (pure) stellarator generates the poloidal component of the magnetic field only by current in coils. There are intermediate

cases, named hybrids, e.g. the Compact Toroidal Hybrid (CTH) [51], able to work in middle points from a pure stellarator to a pure tokamak. In real stellarators, a fraction, even if small, of the rotational transform is always generated by a plasma current.

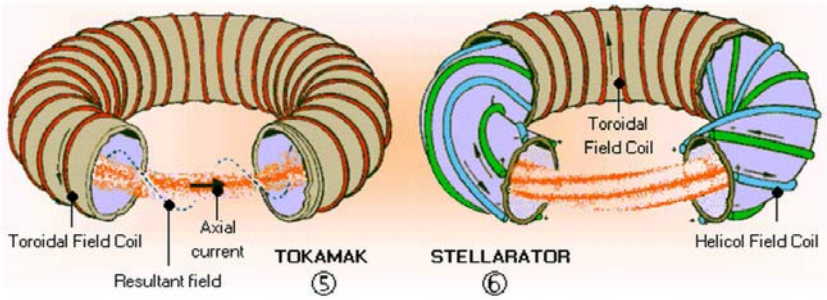

Fig. 1.3. Magnetic field lines, coils and currents in a tokamak and a stellarator. Figure reproduced from [52].

1.2.2 Problems in stellarator research

Stellarators have potential **advantages** over tokamaks [18,53]. Stellarators are steady state devices by nature. This quality provides important advantages: irrelevant fatigue of the structures and coils, higher current in the same superconducting coil and no need of energy storage for start-up. Current drive is not necessary in stellarators. Current drive requires complex devices working steady state 365 days per year. Thus, there is low recirculated power in the stellarator power plant and consequently, higher plant engineering efficiency Q_{eng} may be achieved. Simple start-up, no vertical instabilities, simple control and inexistence of major disruptions are other main advantages. Simple control implies lower complexity and absence of energy storage for fast control. Major disruptions and fatigue of materials has an important impact on cost due to the higher structural requirements. From the physics side, it is not clear yet whether the turbulent transport in stellarators might be lower than in tokamaks [54-56] under certain circumstances. Finally, the diversity of stellarator magnetic configurations might give extra freedom for divertor design, maintenance and other enhancements.

Nonetheless, stellarators exhibit also some **weaknesses**. Both in stellarators and tokamaks, particles moving on the magnetic field lines may be trapped in magnetic mirrors depending on the pitch angle of the particle and the mirror ratio [40]-p.160. However, in stellarators there are particles, named helically trapped particles since they are trapped in the helical periods/ripples of the magnetic field, which turn poloidally less than half a poloidal turn between bounces. The drift ([40]-p.402, [57]) of such particles is not compensated and they are quickly lost. Stellarators need to be optimised in order to confine the helically trapped particles as well as possible. A satisfactory optimization is whatsoever straightforward. Moreover, so far, the result of an excellent optimization gives very convoluted plasma shapes, i.e. see Fig. 3.6. The required convoluted plasma shape implies the need of highly precise twisted components for the whole fusion device. The vacuum vessel, the divertors and the support structures follow such contorted plasma shape. Also, the coils for the best confinement stellarators are currently defined as twisted coils of

complex geometry. The geometrical complexity of the components at high accuracy, up to now, has implied hardly affordable costs and long development and construction periods. In comparison to tokamaks, the geometrical complexity of the components involved in stellarators might seem to counterweight the advantages. However, the attractiveness of stellarators for possible competitive fusion reactors would increase if some new concepts, or certain technology advancements, or some integration enhancements were produced.

Other drawbacks of stellarators, less related with the current work, are: neoclassical transport is higher in stellarators than in tokamaks for typical low collisionality reactor conditions [58]. Aspect ratio is larger than in spherical or slim [59] tokamaks whatever design of stellarator is chosen. Large aspect ratio tend to increase plant cost [60,61]. Present $<\beta>_{lim}$ of stellarators is much lower than in spherical tokamaks [41]. Lower $<\beta>_{lim}$ implies higher cost of coils for the same fusion power. The future hypothetical use of advanced fuels is impossible at low $<\beta>_{lim}$ [22]. A summary of advantages of stellarators is given in Ref. [53]. Advantages and drawbacks of stellarator reactors can be deduced from Ref. [41]. Ref. [62] compares plasmas in stellarators and tokamaks.
In summary and simplifying, all the problems in stellarator research might be grouped in two top problems:

1. **The magnetic configuration problem.** Laborious search and calculation of magnetic configurations with satisfactory properties (e.g. simultaneously: high plasma stability, proper divertor features, low turbulent and neoclassical transport, configuration given feasible and reasonable coils, etc.).
2. **The construction problem**. High geometrical complexity of accurate components that implies high cost and long production cycles.

The next section is devoted to outline previous common solutions given to the second problem. Possibly, the optimization of magnetic configurations has progressed much more than the advancement of construction methods. In relation to that, Dr. Farrok Najmabadi commented "*Pace of 'Technology' research has been considerably slower than progress in plasma physics. Advanced technologies have a dramatic impact on attractiveness of fusion*" [63]. In view of the fact that there is a gap in the knowledge of the second problem, and since the second problem is of my interest and suited to my formation, hence, the construction problem is confronted in this thesis.

1.3 Previous solutions to the construction problem of stellarators

Some previous solutions to the construction problem of stellarators are described next. Details about such solutions are given in Chapter 2, 3 and 6. Literature about previous solutions for the magnetic configuration problem is also reviewed in Section 3.1.

'Construction' of a stellarator is a broad term involving many elements. However, only the construction of the core of a stellarator is considered next, essentially coils, coil frames and supports, and the assembling methods for such components.

1.3.1 Coil frames in different devices

CTH is a hybrid torsatron-tokamak, [52,64]. The CTH helical coil is wound in the grooves generated by ten aluminium frames, which form a torus, Fig. 1.4. The frames are fabricated by aluminium casting and mechanising. Metrology and spacer shims are used for the adjustment of the 10 frames and finally the frames are bolted. After frame assembling, manual winding of the conductors in the helical coil frame is carried out. Finally, in-situ vacuum epoxy impregnation is produced, Fig. 1.5.

The fabrication method is accurate and mechanising is not excessively complex. The concept implies the division of the torus frame in several toroidal sectors. The created flat surfaces can be more easily mechanised and assembled. However, in CTH a helical coil is generated, not modular coils. Modular coils are discrete twisted coils located similarly as toroidal field coils in tokamaks, [18]-p.859. Modular coils can create generalised magnetic configurations [18] and thus, potentially may achieve superior plasma performance.

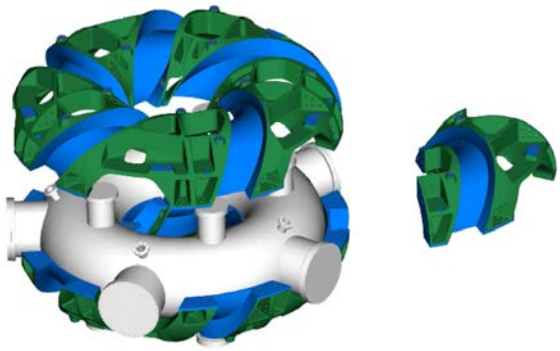

Fig. 1.4. CAD figure of ten bolted frames forming the torus, and one single frame. Figure reproduced with permission from [65].

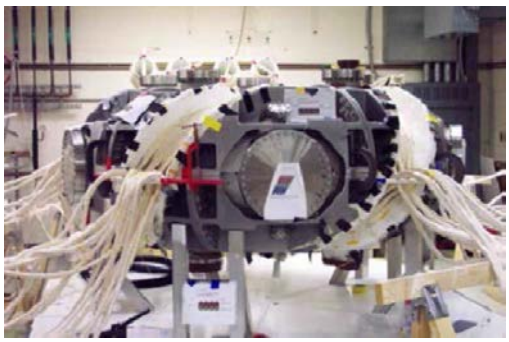

Fig. 1.5. Winding of the conductor in the grooves of the aluminium helical frame. Reproduced with permission from [52].

A solution to some extent similar to the CTH one was utilised for the construction of the TJ-IU torsatron [66]. In this case, a toroidal vacuum vessel was initially manufactured from two forged halves. Each half is shaped as a torus cut through the equatorial plane. Externally to the vacuum vessel toroidal surface, forged plates compose the walls of helical grooves intended for the coil winding [66].

Another solution somewhat similar to CTH but for modular coils was developed for the NCSX stellarator. Information about this approach is found in [67] and Section 3.2.3.1.

1.3.2 Independent coils attached to a structure

In the W7-X case, the approach for the positioning of the coils is based on a stainless steel ring of pentagonal shape, named coil support structure (Fig. 1.6), located at the centre of

the torus. The modular coils are individually bolted [68] to the coil support structure by the inboard of the coil in order to support the magnetic Lorentz forces. The coils are joined among them by intercoil pads and supports [69]. Section 3.2.4.1 gives further information.

A concept somewhat similar is utilised for the construction and assembly of HSX stellarator [71]. In this case a support structure, defined as various box-beam structures, holds each support ring from three adjustable points, Fig. 3.14. A support ring is a planar shape which holds each coil.

The solution to the assembly problem implies the manufacture of independent coils that are finally assembled. This approach has the advantages and drawbacks discussed in Section 3.2.2. and compared in Section 6.2.3.

Fig. 1.6. Coil support structure (green). Reproduced with permission from [70].

1.3.3 Additive manufacturing

Few applications of additive manufacturing for fusion devices have been studied and developed so far. In one of such studies, the potential use of additive manufacturing to produce stellarator components was already proposed in 2008. It was studied as a possible advanced construction method for the coils of the ARIES-CS stellarator reactor [72]. Steel was planned as 3D printing material. Three segments of 1000 ton each would be 3D printed. A specifically developed 3D printer for the task was intended, Fig. 1.7. The fabrication method is promising. Nevertheless, it still has to be developed for large size and proper cost.

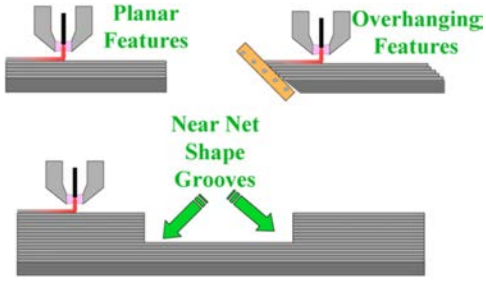

Fig. 1.7. Fabrication concept by additive manufacturing for the ARIES-CS coil structure. © 2008 by the American Nuclear Society, La Grange Park, Illinois. Reproduced with permission from [72].

More recently, a real application of additive manufacturing in fusion produced a demonstration prototype for permeation experiments under vacuum [73]. The component is applied to blankets and not to the structure of a stellarator. However, it is a brilliant example of the possibilities of metal additive manufacturing for fusion.

As an example of indirect method, 3D printed plastic patterns were used to cast aluminium pieces for the construction of the SCR-1 stellarator [74]. The walls of the grooves for the modular coils were cast by sand casting using the 3D printed patterns. Indeed, metal casting based on 3D printed patterns is commonly applied in many industrial sectors.

1.3.4 Simplified coils

Since the fabrication of coils, coil structures and other components for worthy plasma performance in stellarators is complex and expensive, a complementary approach is the

attempt to simplify the convolution of the coils and the general assembly. Some few attempts have been performed to simplify the coils trying to keep suitable neoclassical confinement and plasma stability. The approach followed in Heliotron J [75] seems satisfactory, though the coil system is not exceptionally simple. Very simple coils are used in CNT stellarator [76], in the Proto-CIRCUS hybrid [77] (Fig. 1.8), which employs tilted coils, and in certain theoretical compact stellarators [78]. However, the plasma performance for such three devices is unclear and perhaps poor for a reactor. In any case, the research of simple coils for stellarators, keeping the physics properties, is worthy and complementary to any effort in manufacturing complex stellarator structures.

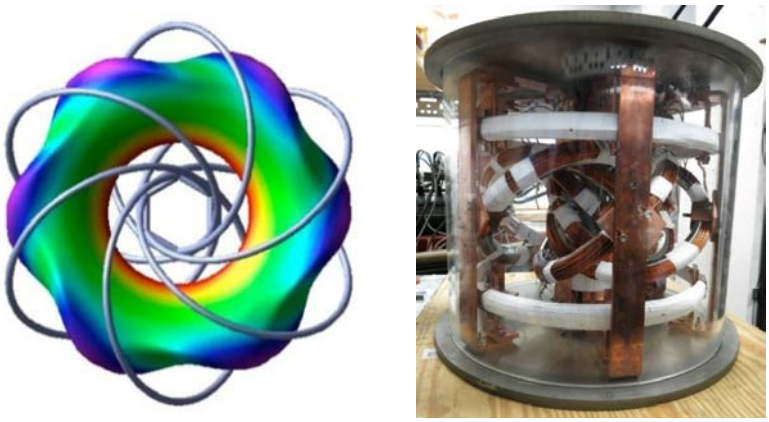

Fig. 1.8. Proto-CIRCUS tokamak-stellarator hybrid [77]. Concept showing the 6 tilted coils (left). Real device after construction (right). Reproduced with permission from Ref. [79] and picture courtesy of Proto-CIRCUS team.

1.3.5 Other solutions

Other previous solutions to the construction problem are described in Section 3.2. In this section, previous winding methods, coil positioning methods, techniques for the fabrication of convoluted vacuum vessels and component assembly are reviewed. Comparison of the different methods is performed in Chapter 6.

A particular set of concepts was developed by the author during 2005 and 2006 for the construction of a small stellarator (see Chapter 2 and Ref. [80]). Simplified modular coils located on a toroidally and poloidally circular winding surface were conceived. The combination of a single monolithic frame with grooves and compression of two conductor turns per layer in the groove resulted in simple positioning of the coils and fast winding. A special milling machine working on toroidal coordinates was capable to mechanise the simplified coil grooves in the monolithic frame.

1.4 Justification of the research

Among the mentioned solutions, additive manufacturing is the less explored technique for stellarator construction. It happens to some extent because additive manufacturing is a

recent technology. Additive manufacturing is increasingly becoming cost-effective for relatively small, geometrically complex parts, when few identical items or single customized items are required. However, currently two important drawbacks of additive manufacturing, in particular for toroidal magnetic confinement fusion, are the required large size of components and the high 3D-printing cost for large pieces. Only the fabrication of small stellarators (R ~ 1 m) would be feasible with the present commercial printers.

The maximum printing size of commercial Selective Laser Sintering (SLS) plastic printers is e.g. 750 x 550 x 550 mm for the 3D Systems 'sPro 230' model. A large and notably precise 3D-printer is the D-Shape model [81] of 6 m x 6 m printing area, using a mixture of sand and binder. Several metres length prototypical titanium 3D printers are being developed in China, e.g. see [82].

A rough estimation of the cost of commercially manufactured 3D printed pieces is currently ~2 €/cm^3 for SLS in polyamide and ~50 €/cm^3 for Direct Metal Laser Sintering (DMLS) in titanium. The cost of a piece also depends on other factors like the hollowness, the size and the quality of the piece.

The lack of competitiveness of additive manufacturing for many applications and the still relatively small commercial printers hinder the current widespread application of additive manufacturing for fusion. In spite of that, it is expected a great increase in performance and reduction of cost in the next years, much faster than the common terms in fusion research.

On the other hand, the more traditional manufacturing methods like casting, forging, mechanising and welding are already greatly developed and allow few new exploration and integration[1] possibilities. Integration in fusion devices tend to be poor due to the complexity and diversity of matters involved.

The information from the previous sections suggests that additive manufacturing, likely complemented or combined with traditional manufacturing, is appropriate to fill a gap in the knowledge of rapid manufacturing methods for geometrically complex fusion devices.

Consequently, this thesis investigates whether a manufacturing method based partially on additive manufacturing, properly integrated with the physics and engineering design, may speed up and lower the construction cost of certain stellarators.

In other words, the objective of the present work is the research and development of new enhanced manufacturing methods based on additive manufacturing for the fabrication of the accurate and complex geometries of stellarators and other fusion devices, and the integration of additive manufacturing with the physics and engineering design.

[1] Integration, in this particular case, means proper combination of the physics and engineering designs, and adequate combination of engineering design and the planned manufacturing methods.

As evidenced in this chapter, lessening the construction problems is crucial for stellarator research. Moreover, stellarators are valuable as a potential alternative to tokamaks. Furthermore, a diversity of fusion approaches is vital, especially if tokamaks experience difficulties for competitive fusion energy.

A fast cycle production of experimental stellarators might result in faster advance of fusion plasma science. Several different conceived optimised magnetic configurations could be experimentally tested in a reasonable term. Additionally, the diversity of stellarator magnetic configurations might give extra freedom for the future development of innovative divertor designs, maintenance and other enhancements.

A valuable contribution to the knowledge of construction methods and generation of construction know-how are foreseen from the present work.

1.5 Research methodology and scope

1.5.1 Methodology

The research methodology followed in the work is based on a research essentially exploratory. Initially the concepts and hypothesis about the possible construction methods are formulated. Subsequently the concepts or hypothesis are experimentally validated or rejected.

The developed research is applied research. Applied results to the creation of real objects, in particular stellarators, are aimed. Therefore, the knowledge generated is essentially the creation of new methods and the generation of technical know-how.

Though the research is essentially exploratory and applied, the simulation and calculation based on mathematical models is pursued in some parts of the work.

A three phase process is followed: first construction methods are sought, second magnetic configurations are studied, and third both research activities are combined in the fabrication of a stellarator based on the construction methods and the selected magnetic configuration. The first and second phases are developed mostly in parallel.

Prior to the first phase, a review of the literature about the previous construction methods for stellarators is performed in order to understand the status of the technique and get inspiration for new manufacturing concepts. Also, a review of some existing magnetic configurations is performed so as to take advance of the previous remarkable plasma science effort.

1.5.2 Scope of the work

The aspects included in the scope of this thesis and out of the scope are listed next.

In the scope:

- Possible geometrical structures for components are studied and developed.

- Geometrical integration of the different elements is studied and pursued.
- Study and implementation of magnetic configurations, properly integrated with the engineering design, is intended.
- Devise, test and implementation of innovative fabrication methods.
- Preliminary validation of the work performed.

Out of scope:

- The accurate dimensioning of the mechanical structures so as to withstand forces for a specified magnetic field is not tackled.
- Forces and stresses on the structures are not studied. An estimation of forces and stresses is presented in Ref. [83].
- Plasma experiments are not pursued in this work.
- The size of the device and magnetic field required for significant plasma experiments are not studied.
- The application of the developed construction methods to large devices or reactors is not confronted.
- Since the work is notably integrative, the details of some aspects are not studied.

1.6 Funds and means for the work

Funds for the work came from the author and from a crowdfunding campaign, accounting for a total of approximately 6000 €.

Several IT resources were provided by CIEMAT. For example, CATIA (a CAD software), NESCOIL [84] and DESCUR [85] codes (codes for stellarator calculations) and other less important codes were utilised for the work. Also, computers to run the codes.

The exploration and experimental validation of the concepts, from initial simple tests to the final validation of methods and components, have been performed in the personal laboratory owned by the author. In this laboratory many elements are ready available for quick tests of incipient concepts. Therefore, numerous branches of possibilities are early trimmed and some few are expanded, thus, decreasing exploration time.

In particular this personal 120 m^2 laboratory is equipped with:

- Many types of materials like plastics, rubbers, metals, wood, in different formats such as wire, rods, ingots, sheets or profiles. Numerous types of glues, plasters, resins and fibres.
- Basic mechanical workshop composed of hand and fixed drills, saws and grinders, manual tools, etc. Small torches, small kiln, sand and foundry elements. Different soldering alloys, and solder fluxes. Solvents, lubricants and waxes.
- Multitude of electronic components and varied basic electric material.
- Measurement and inspection instruments like multimeters, caliper gauges, hardness gauge, infrared thermometer, digital scales, microscopes, volume measurement, and digital cameras.
- Computers for calculation, control and data acquisition, high vacuum system, power supplies and air compressor.

- Auxiliary elements: bolts, nuts, fasteners, o-rings, ropes, pipes, containers and other similar components.

This personal laboratory has been developed and maintained by the author during about 30 years.

The fabrication, assembling and test of all the concepts and components investigated in this thesis, except for the elements indicated as commercial ones, have been carried out by the author in this laboratory.

1.7 Thesis outline

Chapter 2 summarises the work performed during 2005 and 2006 for a miniature stellarator. The conceptual and detailed design, the manufacturing by a special milling machine and the e-beam field mapping experiments are outlined. Several investigated concepts are key for the subsequent research.

Chapter 3 reviews the literature about some magnetic configurations developed by researchers and still not implemented in a real stellarator. Besides, it reviews winding and coil positioning methods, component fabrication and assembling methods for stellarators. It represents the background knowledge to attempt the advancement of the construction methods in the subsequent chapters.

Chapter 4 stablishes the conceptual design of a small stellarator, named UST_2, in order to validate the developed manufacturing methods. The objectives and the physics and engineering conceptual design are defined.

Chapter 5 complements the previous chapter. It describes the features of a code, named CASTELL, developed to perform certain calculations for stellarators, like generation of coils and calculation of particle trajectories. The process to calculate the plasma Last Closed Flux Surface for UST_2 is described.

Chapter 6 presents the research performed in order to find improved alternatives for the manufacture and assemble of different components of a stellarator, focussed for the previously conceptualised UST_2. A modified additive manufacturing method is conceived, experimentally tested, improved, and finally experimentally validated again. Also, concepts explored for coil positioning and coil winding are described. The results for each concept are shown. Particular alternatives are selected as the best mutually integrated concepts. The selected concepts are utilised for the next validation phases, described in the next two chapters.

Chapter 7 describes the process followed to manufacture the coil frame, vacuum vessel and winding coils, and the assembly of the elements. Lessons learned, know-how generated and results are presented. At this stage one halfperiod of a small stellarator has been built. The next phase is the experimental validation of the work.

Chapter 8 reports the e-beam field line mapping experiments carried out to compare the calculated electron trajectories in a halfperiod model of the stellarator with the experimental e-beam trajectories in the real halfperiod of UST_2. The results are summarised.

Chapter 9 summarises the results of the work.

Chapter 10 presents the conclusions and the possible future work.

Chapter 2
UST_1 stellarator

The work carried out on UST_1 stellarator was developed from 2005 to 2007. UST_1 is relevant for the current work since the present research of new construction methods cannot be well understood without a vision of the effort performed on UST_1 stellarator. Several concepts developed for UST_1 have inspired new ideas and methods. Also, the kernel of the code used in this thesis was developed during the UST_1 endeavour. Different manufacturing and assembling methods were devised and implemented for UST_1.

The physics conceptual design is described first. The engineering design derives from the physics design and is reported later. The construction by a special milling machine is presented. Finally, the e-beam field line mapping experiments carried out are described. A summary of the work is exposed in this chapter.

2.1 Motivation and objectives

The motivation and objectives of the work carried out on UST_1 were:

- The development of innovative construction methods for stellarators. Methods to reduce construction cost and to simplify assembly were primarily sought.
- Training of the author and of other students.
- Validation of the developed methods by construction of a small stellarator.
- Generation of demonstration effect, that is, encouraging plasma research groups in universities and small laboratories to build small experimental stellarators, valuable for the assessment of new confinement concepts, tests of diagnostics and training.
- Carry out R&D as a base for a future improved stellarator.

The development has to be understood in the framework of low funds and human resources. Thus, the relevance of the work is based on the conceived methods and the high degree of simplicity achieved, not on the size of the device or the plasma performance.

2.2 Physics design of UST_1

Integration of the physics design, engineering design and available funds were pursued from the very beginning in an iterative design process. For example, the aspect ratio and size of the stellarator was adapted to commercial off-the-shelf pipe for the vacuum vessel, and mean on-axis magnetic field was chosen for the low cost 2.45 GHz magnetrons.

2.2.1 UST_1 essential physics features

The first insight for the UST_1 physics design came mainly from CTH torsatron [86], W7-X coils [87] and the modular coils depicted in Ref. [40]-p.398. In the end, UST_1 resulted somewhat geometrically similar to a CTH torsatron using modular coils and having the plasma shape similar to LHD torsatron.

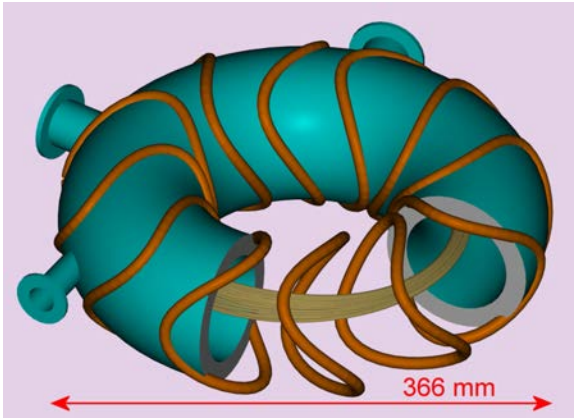

Fig. 2.1. Sketch of the UST_1 conceptual design.

Fig. 2.1 shows a sketch of the conceptual design of UST_1. Table 1 summarises the UST_1 properties. The rotational transform is selected in the gap below 1/3 to avoid low order rational surfaces. Only the rather low order 2/7 rational surface appears, see Fig. 2.2.

Fig. 2.2 shows a Poincaré plot of the vacuum magnetic configuration at two toroidal angles. Magnetic islands are observed. The black solid line represents the vacuum vessel. Fig. 2.3 represents the iota profile. The flattening of the iota profile at $r = 21.4$ mm is triggered by the island 2/7. Calculations are performed by the CASTELL code (see Chapter 5 for further information about the code).

Element	Specification
Number of periods	2
Plasma volume (litres)	1.1
R, plasma major radius (mm)	125.3
a, ave. plasma minor radius (mm)	21
B_0 Magnetic field on axis (T)	0.089/0.045
ι_0 , rotational transform at axis	0.32
ι_a , rotational transform at edge	0.28

Table 1. Essential properties of UST_1 stellarator.

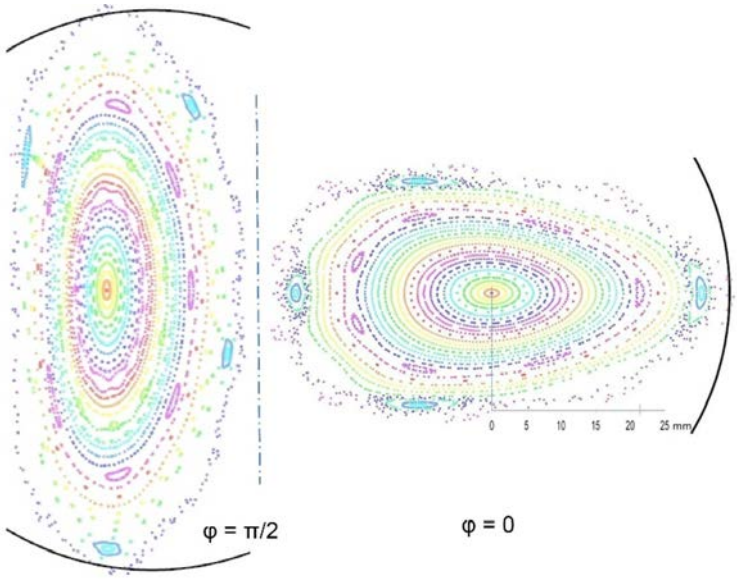

Fig. 2.2. Poincaré plots of vacuum magnetic configuration.

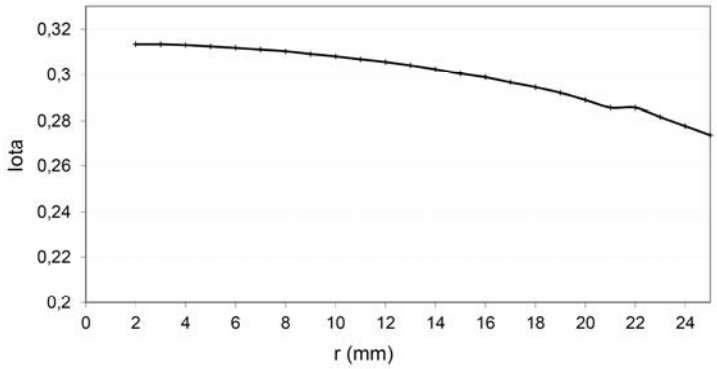

Fig. 2.3. Iota profile in UST_1. 'r' is the minor radius on the x+ coordinate axis for each initialised particle.

2.2.2 Optimization of magnetic field and coils

A partial optimization of UST_1 was carried out by means of CASTELL code.
Different properties were considered during the optimization process:
- The minimum distance between contiguous coils was required larger than two coil diameters to avoid overlapping of coils.
- The rotational transform was selected slightly lower than 1/3.
- The standard deviation of the |B| minima values on one magnetic surface was minimized.
- The approximate plasma volume was maximized. The plasma volume was estimated from the approximate area enclosed in the more external continuous closed curve found on the poloidal cut φ=0, e.g. see green dotted curve in Fig. 2.2 to better understand the concept.
- Magnetic well depth > 0 on most of the magnetic surfaces was required.

A process using the CASTELL code (version of 2006) was followed to select the Shaping parameters shown in Table 2. The winding surface was initially fixed. A four dimensional space of parameters was scanned in three optimization loops. A wide interval of parameters was set in the first loop. Testing 10000 different coil structures lasted 24 hours of calculations in a PC. Many coil structures were rejected when the calculated rough rotational transform was found outside the target interval. Accepted coil structures were followed by calculations of: refined iota at magnetic axis and plasma edge, approximate plasma volume, standard deviation of the |B| minima values on a magnetic surface, minimum distance between coils, and magnetic well. At the end of each loop, a spreadsheet was created and the results were ordered according to iota. The coil structures giving rotational transform in the proper gap were studied based mainly on the plasma volume and |B| minima standard deviation. New narrower intervals for the four parameters were set heuristically from the obtained best coil structures and another optimization loop was run. The optimization was modest since the degree of freedom of the coil shapes is constrained on a toroidally and polloidally circular torus.

The expression relating the toroidal and poloidal coordinates of a point of the filamentary coil is:

$$\varphi = \varphi_c - R_0/R \; p \; \lambda \; \sin(2\theta) \qquad \pi/2\, i < \theta < \pi/2\,(i+1)\; ;\; p = p_i\; ;\; i = 0, \ldots, 3$$

Being:

(R, φ, θ) : Toroidal coordinates of each point of the filamentary modular coil. The points are located on a torus of minor radius a = 57.1 mm.

R_0 : Major radius of the toroidal winding surface.

φ_c : Reference toroidal angle position of each coil. $\varphi_c = 2\pi k/12$, $k = 0, 1, 2$

p_i : Shaping parameters of the coil, e.g. see the shaping parameters shown in Table 2. The shaping parameters of the coil are four parameters defining the amplitude of the sinusoidal deformation of the coil at four quadrants of the poloidal coordinate.

λ : Magnitude of shaping of the coils. $\lambda = 0.15$ for UST_1. Higher λ produce higher rotational transform.

UST_1 is formed by 12 modular coils, three coils in each halfperiod. The successive modular coils in each halfperiod turn poloidally by changing the origin of θ coordinate. The coils for the other three halfperiods are produced by stellarator symmetry.

2.3 Engineering design and construction of UST_1

2.3.1 Conceptual engineering design

A thick monolithic toroidal plaster surface is conceived around the toroidal vacuum vessel. The coils would be defined as grooves mechanised in the thick winding surface so as to avoid the use of winding moulds [88]. The grooves would be mechanised with a special

toroidal milling machine in order to avoid positioning of the coils and achieve higher precision in the magnetic field.

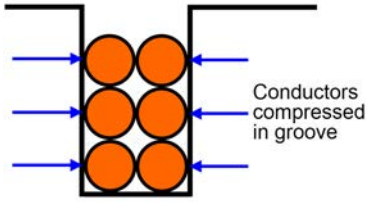

Fig. 2.4. Concept of two conductors per layer compressed on the walls of the winding groove.

Two turns per layer and three layers are planned in the groove. Therefore, the conductor would be compressed (Fig. 2.4) on the walls of the groove to avoid the use numerous fasteners [89]. The conductor is manufactured from a 6 mm^2 bunch of Cu filaments sleeved in a heat-shrink tube 0.3 mm wall thickness. The effective copper section in the groove is 50%. The value is relatively low due to the circular shape of the conductor. Pressure due to Lorentz force on the groove is low, lower than 10 N/cm^2. So, extra conductor fixations or epoxy impregnation is not considered.

2.3.2 UST_1 main engineering specifications

Table 2 summarises the coil specifications.

Element	Specification
Type of coils	Modular coils
Number of coils	12 (3 shapes)
Turns per coil	6
Shaping parameters of the coils	p_0=1.45 , p_1=1.3 , p_2=1.55 , p_3=0.65
Winding pack size (mm)	7 width x 10.5 depth
Structure of the winding pack	1 double pancake per coil
Winding surface shape	Circular, poloidally and toroidally
Major / minor radius of winding surface (mm)	119.2 / 57.1

Table 2. Summary of coil specifications.

2.3.3 Vacuum vessel

The vacuum vessel is circular, poloidally and toroidally, with major radius 119.2 mm and minor radius 40 mm. It is formed by five commercial 72º copper elbows of 0.8 mm wall thickness externally reinforced with brass rings. Three large perpendicular ports and a small tangential port are available. The components are soldered by Sn-Ag solder and internally thoroughly cleaned. Fig. 2.5 shows the finished UST_1 vacuum vessel.

Fig. 2.5. UST_1 vacuum vessel.

2.3.4 Monolithic coil frame

The monolithic coil frame is a single solid continuous toroidal thick surface covering the vacuum vessel. The thick surface is made of plaster. Common plaster type 'Iberyeso E-35' was utilised. It has enough strength for compression (hardness Shore D = 50) and easy mechanization. Shore D is a type of material hardness measure based on the permanent indentation produced in the material by a normalized tip and exerted force. The monolithic plaster frame is moulded in two stages. First, the half part below the equatorial plane is moulded in an expanded polystyrene mould, Fig. 2.6. Later, the remaining half is moulded. After moulding, the torus is smoothed down by the same toroidal milling machine utilised to mechanise the grooves. The result is shown in Fig. 2.7.

Fig. 2.6. Expanded polystyrene mould and vacuum vessel covered by a separation layer.

Fig. 2.7. Finished smoothed and completely circular monolithic frame without grooves.

2.3.5 Coil production and positioning

The positioning of the coils would be unnecessary and the positioning accuracy would be high if the coils were generated as grooves in the monolithic frame. A special milling machine was thought in order to accurately mechanise the grooves. Thus, the coil adjustment and metrology worktime would also be avoided.

Twelve grooves 7 mm wide and 12 mm deep (Fig. 2.8) are mechanised in the plaster frame by the special milling machine working on toroidal coordinates, see Section 2.4. The groove width is identical to the diameter of the milling cutter so as to produce one groove with only one poloidal turn of the milling head.

The mechanization of each groove was fast and simple, lasting about 2 hours each groove.

Fig. 2.8. Monolithic frame and grooves for the coils.

2.3.6 Coil winding

As described in Section 2.3.1, the two turns per layer and 3 layers of conductor are introduced in the groove (Fig. 2.9) and compressed on the groove walls. Thus, the turns do not unwind during the winding process and numerous fasteners are not needed. The black conductor shown in Fig. 2.9 is an auxiliary conductor used to temporarily fix the first turn of the pair of turns per layer. The second turn is introduced in the groove and compressed on the walls of the groove while the auxiliary conductor is removed, Fig. 2.9-right. As conceived, the turns did not unwind while winding the conductor. The final 12 modular coils composed of 6 turns per coil are shown in Fig. 2.10.

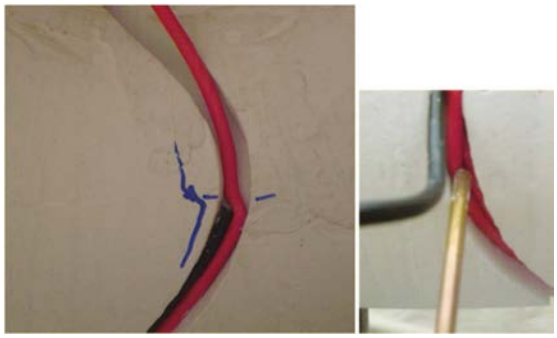

Fig. 2.9. Process of winding the first turn of one modular coil (left). Compression of conductor on the groove walls (right).

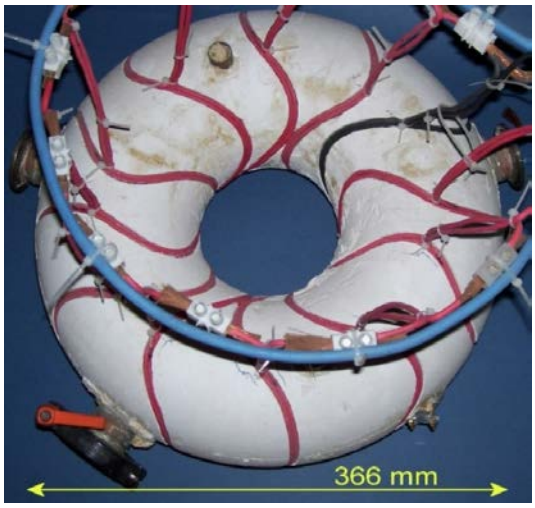

Fig. 2.10. Plan view of the 12 manufactured modular coils.

2.4 Toroidal milling machine

The concept and implementation of the toroidal milling machine are summarised next. Further information can be found in Ref. [80].

The milling head of this special milling machine moves in toroidal and poloidal coordinates. The toroidal milling machine (Fig. 2.11 and Fig. 2.12) is composed of a turning horizontal base, a vertical circular guide, a circular sector, and the milling head. The turning horizontal base supports the stellarator and is able for 360º rotation with respect the vertical symmetry axis of the torus. The base supports four slender columns located at the vertices of a square. The four legs of the stellarator lay on those columns. One of the three columns can be removed by sliding (when it collides with the milling head) without disengaging the other columns. This feature is worthy since the toroidal winding surface is never fully disconnected from the supports during the mechanization of the whole series of coil grooves, therefore simplifying the process and increasing accuracy.

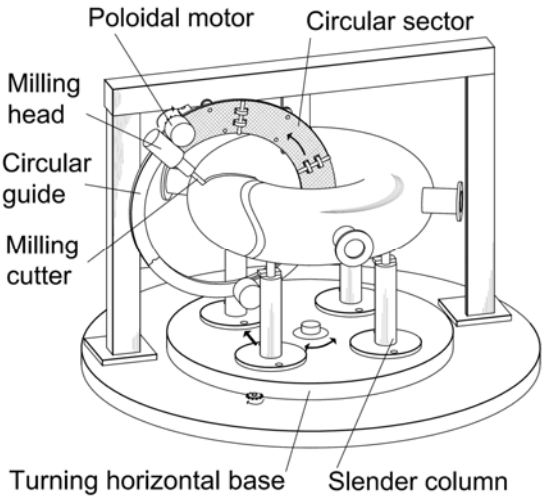

Fig. 2.11. Schematic view of the toroidal milling machine.

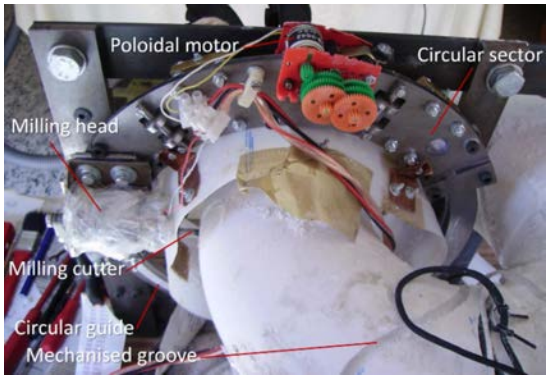

Fig. 2.12. Picture of a detail of the toroidal milling machine.

The circular guide is a metallic flat ring split in two identical halves to allow the introduction of the torus in the circular guide. A flat circular sector of about 120º equipped with wheels adjusts and moves poloidally without play on the circular guide similarly to a train on the rails. The poloidal motor, fixed on the circular sector, engages with the lateral of the circular guide and drives the poloidal movement. The slender columns allow a full 360º poloidal turn of the circular sector around the winding surface.

A milling head, which points towards the toroidal axis of the winding surface, is attached to one end of the circular sector and moves together with the circular sector. The milling head is small in order to pass through the central torus hole. The diameter of the milling cutter is the same as the groove width in order to produce the groove with only one poloidal turn of the milling head. It simplifies the milling process.

The main **advantages** of this special milling machine are:

- Positioning and adjustment of the coils is unnecessary because all the grooves are mechanised on a single toroidal surface. Only the mechanization of grooves is performed.
- Fabrication errors of the grooves are similar to the ones in CNC (computer numerical control) milling machines, very small.
- Construction time decreases and the mechanization process is simplified.

However, this milling machine might be unsatisfactory for non-circular winding surfaces, like e.g. the ones in W7-X and NCSX, since the inboard part of the coils are very convoluted in a small space. Also, the developed milling machine would be inadequate for very compact stellarators like QPS.

2.5 The UST_1 facility

The different systems of the UST_1 facility are outlined next. In spite of the simplicity, the facility is able to evacuate, feed, control, and diagnose the stellarator. Fig. 2.13 shows a picture of part of the facility.

Vacuum system.

The UST_1 vacuum system is composed essentially by a roughing mechanical oil pump Pfeiffer DUO 004A (4 m^3/h), a diffusion pump Leybold (~150 L/s). Vacuum gauges: 'Edwards' active inverted magnetron gauge (1Pa - 10^{-6} Pa), 'Lesker' thermocouple gauge 100 Pa - 0.1Pa, and Bourdon manometer. One 'AMETEK Dycor Quadlink' quadrupole mass spectrometer (RGA) and the necessary fittings and valves. Vacuum level typically reached 5 x 10^{-3} Pa.

Power supplies.

Seven lead batteries 12 V, 45A-h, are installed in series supplying 400 A to the stellarator. The power generated by the batteries is 35 kW. 19 kW are supplied to the coils and 16 kW are lost in the internal resistance of batteries, connections, main switch and leads. There is no current regulator in the system, the current drops ~12% during the pulse due to copper temperature increase and fatigue of the batteries.

Heating system.

Only ECRH heating at 2.45 GHz is installed. The heating system is based on a magnetron from a commercial microwave oven. The waves are transmitted by a coaxial cable and emitted into the vacuum vessel by a ¼ λ stub antenna. The small size of the stellarator hinders the wave injection by a waveguide.

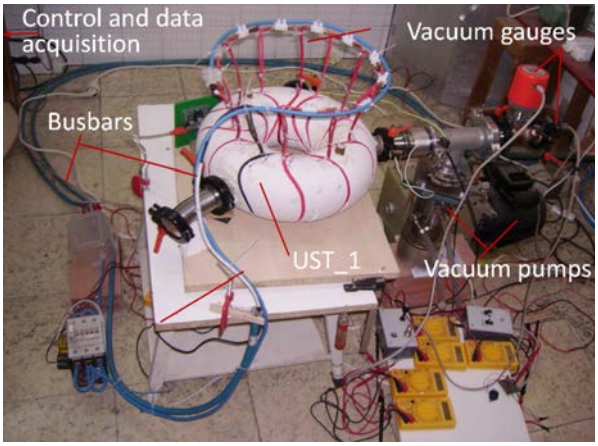

Fig. 2.13. UST_1 and vacuum system.

Control system.

Two PCs are installed, one for the high speed digital camera and one for the slow control of the pulse. A C-language code interacts with two A/D cards that control all the systems and receive analogic data from diagnostic. The vacuum system is controlled manually.

Diagnostics.

The available diagnostics are: digital camera of 400Mb/s Firewire transmission, 30 fps, 640 x 480 pixels, non-compressed image, e-beam field mapping system, Langmuir probe, and residual gas analyser.

Not all the diagnostics can be installed simultaneously due to the scarcity of ports.

2.6 E-beam field mapping experiments

E-beam field line mapping experiments were performed to validate the accuracy of the resulting magnetic configuration.

The conventional fluorescent movable rod method [90] was utilised. A sketch of the e-beam field mapping experimental setup is shown in Fig. 2.14. A very simple mechanism is utilised for the fluorescent rod movement. The rod is a copper wire 1.5 mm diameter and 120 mm long (Fig. 2.15) covered with P-24-GE fluorescent doped ZnO powder. The powder is deposited on the wire by a methanol-powder solution. The rod lays equilibrated on a thin tip. An external magnetic short impulse is given on a tiny ferromagnetic piece fixed on one end of the rod and the rod starts oscillating. A camera 400Mb/s 30 fps installed at the port P4 films the oscillating rod. The achieved simplicity of the mechanism is one notable result.

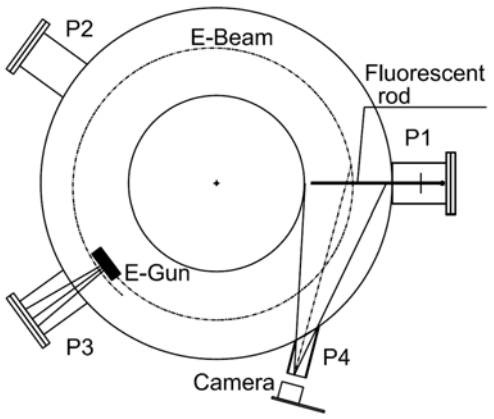

Fig. 2.14. Field line mapping experimental setup.

Fig. 2.16 shows the e-gun built and used for the experiments shown next. It is built from a cut 10 W, 12 V commercial halogen light bulb introduced in an internally blackened metallic cover. One larger e-gun 'E-Gun-2' was also built.

Fig. 2.15. Oscillating fluorescent rod.

Several difficulties appeared during the e-beam experimental sessions, among them:

- The e-beam collided with the rear part of the e-gun after the third turn of the beam since the rotational transform is approximately 1/3. Accurate strategic positioning of the tiny E-Gun-3 was required to solve the issue.
- The E-Gun-3 was fragile and gave lower beam current and higher background light than the larger E-Gun-2.
- The low sensitivity of the camera hardly recorded the fluorescent points. Relatively high electron energy (~100 eV) was set for higher brightness but large electron drifts appeared due to the small size of UST_ 1 (small curvature radius).

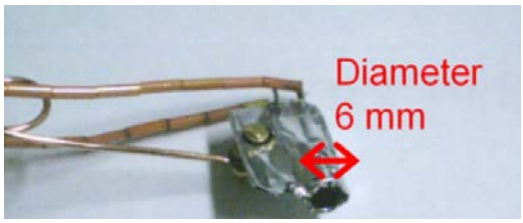

Fig. 2.16. Small 'E-Gun-3' of 6 mm diameter.

Fig. 2.17 shows the overlapping of 12 frames obtained from the pulse #202 (24-08-2006) with the calculated beam-rod intersections. The experimental conditions during the pulse #202 were: $B_0 = 34$ mT, acceleration voltage 95 V, vacuum level 3 x 10^{-3} Pa.

A notable degree of accuracy was achieved in the design and construction of the stellarator since the experimental magnetic surfaces notably agree with the calculated surfaces. Nevertheless, measurement errors of the system are ~±1 mm. Therefore, slight magnetic errors, significant for plasma confinement, may still exist. Thus, the validation of the quality of the construction is only partial.

After e-beam mapping, an ECRH system 2.45 GHz, based on a commercial magnetron oven, was installed and plasma pulses were produced. Impurities desorbed from the surface of the vacuum vessel during the plasma pulse hindered the production of satisfactory plasmas.

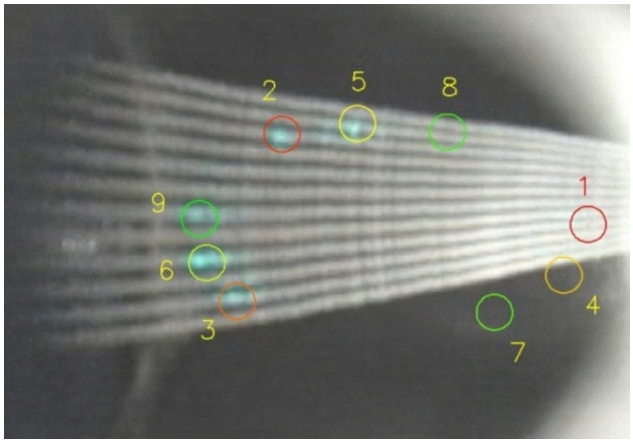

Fig. 2.17. Comparison of experimental fluorescent points (cyan points) and calculated points (circles).

2.7 Cost and worktime breakdown

The total cost of the materials used in the facility was about 3000 € (€ year 2006). Most of the elements were second hand components. The vacuum system was the most expensive system, accounting for 50% of the budget.

Worktime is divided between R&D time and construction/installation time. The two types of worktime are somewhat mixed. Table 3 shows the time breakdown of the different activities performed.

Activity	Dedicated time (hours)
1. Develop CASTELL code, optimise coils.	440
2. Vacuum: Training, orders, assembly, leak test.	378
3. Toroidal milling machine: Conception, design, tests and construction.	264
4. General training, calculations, devise.	196
5. Search components, orders.	158
6. E-guns: Training, construction, installation.	105
7. Vacuum vessel: Devise, design, solder parts.	102
8. Coil monolithic frame: Design, test, production.	46
9. Conductor manufacture. Modular coil design and test. Integration.	54
10. Mechanize the grooves in the plaster frame.	35
11. Other activities.	828
TOTAL	**2606**

Table 3. Worktime breakdown of the different activities.

2.8 Experiences learned

The experiences learned, focused on the construction of a future stellarator, are listed next.

- Winding one turn per layer compressed in the groove may be faster than winding two turns per layer.
- The manufacture of the special sleeved conductor took a long time. Thin wall commercial copper conductors are available for a few ranges of diameters.
- Excessive desorption during pulses hindered the generation of proper plasmas.
- The toroidal milling machine is unsuited for very convoluted winding surfaces. Additive manufacturing methods might be superior to the subtractive construction method presented here.
- The toroidal milling machine is expensive unless several similar stellarators are fabricated.

2.9 Summary

The objectives of UST_1 work were essentially to develop innovative construction methods for stellarators and training of the author. After some research, UST_1 was defined as a two field period compact modular stellarator of aspect ratio 6, plasma major radius R = 125 mm and 12 resistive modular coils. Rotational transform is slightly lower than 1/3 to avoid major low order rational surfaces. A partial optimization of some key stellarator parameters was carried out by means of the CASTELL code, which is a code developed from scratch.

The main concocted engineering concepts were: **i)** the use of grooves mechanised in a thick winding surface so as to avoid the use of winding moulds [88] and **ii)** the use of two conductors per layer compressed on the walls of each groove. A special toroidal milling machine was devised, patented, designed and built to accurately mechanise the grooves in the thick winding surface.

After construction, e-beam field line mapping experiments were performed to validate the design of the stellarator and the used construction methods. Correct magnetic surfaces as calculated were experimentally obtained by the e-beam field line mapping experiments. The cost of the materials, equipment and instruments for the whole UST_1 facility was around 3000 €. UST_1 stellarator was dismantled in 2014. Further information is provided in the web site Ref. [91].

2.10 Main results

► The combination of a single monolithic frame with grooves and compression of two conductor turns per layer in the groove resulted in simple positioning of the coils and fast winding.

- A construction method for stellarator coils based on a toroidal milling machine has been developed.
- A special milling machine working on toroidal coordinates has been developed, utilised and validated.
- A particularly simple and economical e-beam field mapping system has been devised and utilised.
- UST_1 has contributed to train plasma and fusion engineering students.
- Inspiration and encouragement has been generated in other researchers. For example, the SCR-1 stellarator has been built in Costa Rica [74,92] based on the UST_1 design. The definition of the SCR-1 coils is the same as the UST_1 ones scaled two fold.

Fig. 2.18 'Stellarator of Costa Rica' SCR-1. Picture courtesy of ITCR (Instituto Tecnológico de Costa Rica).

2.11 Conclusions

The research of physics and engineering concepts, the physics and engineering design, and the construction and operation of a low-cost stellarator have been carried out. The knowledge and know-how generated might be valuable for universities or certain laboratories. In spite of that, two weaknesses of the work could be mentioned. First, the obtained magnetic configuration is poorer than other magnetic configurations obtained by physicists during the last twenty years, see e.g. [93]. Second, the toroidal milling machine is unsuited for very convoluted winding surfaces and for compact stellarators. Moreover, the toroidal milling machine is expensive unless several similar stellarators are fabricated. Thus, the question of how to produce at moderate cost a device presenting any required magnetic configuration raises.

Therefore, the next chapter is devoted to the search of literature about both matters. Regarding the second weakness, previous construction methods are studied as a background to try to devise a better construction method than the one used for UST_1.

Chapter 3

Study of current magnetic configurations and construction methods

There are several types of magnetic configurations of stellarators. All types are not studied in this chapter. For example, torsatrons/heliotrons may be advantageous for possible innovative divertor implementation (see also Section 4.1.3 point F6). However, neoclassical confinement of heliotrons until now, e.g. LHD [58], is lower than in recently developed modular stellarators [58]. Heliotron J [75] is an advanced heliotron aimed at improved neoclassical confinement, though it comprises toroidal field coils which hinder spacious helical divertors [94]. Modular stellarators [18]-p.859 can produce generalized magnetic configurations and thus, they are the only type of stellarators considered next.

The assessment of stellarator magnetic configurations is worthy for the subsequent selection or enhancement of a particular configuration.

The first section of this chapter evaluates magnetic configurations for stellarators already developed by physicists but not implemented yet in a real device. The second section outlines prior techniques utilised for the fabrication and assembly of real stellarators.

3.1 Assessment of different stellarator magnetic configurations

Only the magnetic configurations developed by physicists and received from the authors are reviewed and studied. The definition of the coils was obtained for Aries-CS, HSR-3 and HSR-4 stellarators. The LCFS of the stellarators NCSX-TU (NCSX-like with potentially improved turbulent transport) and QIPCC (quasi-isodynamic with poloidal closed contours) of 2, 3 and 6 periods were received. For QPS stellarator both the coil definition and the LCFS were obtained.

HSR-3 and HSR-4 are Helias-type reactor designs [43]. These concepts were discarded for the planned UST_2 stellarator since more modern similar concepts, like QIPCCs, were available.

ARIES-CS is a quasi-axisymmetric reactor design [60,95] based on the NCSX concept [96]. The ARIES-CS optimization was carried out for a reactor. Self-consistent bootstrap current is required to obtain the calculated optimised magnetic configuration. This option was discarded for UST_2 due to the difference between the bootstrap current in a reactor and the negligible bootstrap current in UST_2 stellarator. The utilization of the ARIES-CS configuration would have likely resulted in lower confinement for the small UST_2.

The remaining configurations are QPS [97], QIPCCs [93, 98] and NCSX-TU [99].

3.1.1 Comparison table

Table 4 compares key properties of QPS, QIPCCs and NCSX-TU configurations.

Device	<β> for best plasma perfor-mance	Estimation[1] of neoclassical confinement	Possible improved turbulent transport	<β> limit. Rotational transform	Aspect ratio. Others
QIPCC2 [100]	Stiff behaviour independent of <β> value. Negligible bootstrap	Acceptable confinement	Yes [62]	$<\beta>_{lim}$ ~ 2.7%. ι ~ 0.53 - 0.54	A= 3.6. A~axis = 6, [100]. Large excursion of helical axis → engineering issues. Plasma cross section has tips, Fig. 3.2. It hinders feasible real coils.
QIPCC3 [93]	Id. QIPCC2	Excellent confinement (CASTELL and MOCA codes)	Yes [62]	$<\beta>_{lim}$ ~ 3.9%. ι ~ 0.67 - 0.71	A=6.8. Slightly large aspect ratio but acceptable. Triangular shape provides central space.
QIPCC6 [98]	Id. QIPCC2	Excellent confinement	Yes [62]	$<\beta>_{lim}$ ~ 8.5%. ι ~ 1	A=12. Large aspect ratio. COE increases at large aspect ratio, [60,61].
QPS [101]	<β>~2%	Relatively poor confinement for <β>=0	Yes [102]	$<\beta>_{lim}$ ~ 2% ι ~ 0.16 - 0.26	A=2.7. Compact, but difficulties in inboard blankets if a reactor. COE may increase [61] at low A.
NCSX-TU [99]	<β>~4%. High bootstrap	Acceptable confinement for <β>=0	Yes [99]	$<\beta>_{lim}$ ~ 4%	A=4.4

Table 4. Comparison of key properties for the assessed devices.

Certain further details about the devices listed in Table 4 are given next. No extra details are provided for the QIPCC6 configuration.

[1] From CASTELL code, for <β>=0. See Chapter 5 for more details about neoclassical estimations with CASTELL code. MOCA [103], a validated code for neoclassical transport calculations [58], confirmed the neoclassical confinement estimaton from CASTELL for the QIPCC3 configuration at <β>=0.

3.1.2 Additional details for QIPCC2 configuration

The quasi-isodynamic with poloidal closed contours configuration of two periods (QIPCC2) [100] exhibits a large vertical excursion of the magnetic axis, Fig. 3.1. The large vertical excursion implies a more complex engineering design.

The aspect ratio calculated as R/a is $A_{R/a}$ = 3.6. Due to the large vertical excursion of the magnetic axis, the aspect ratio calculated considering the length of the magnetic axis results $A_{\sim axis}$ = 6 [100]. $A_{\sim axis}$ aspect ratio may be considered as the engineering aspect ratio. $A_{\sim axis}$ is similar to the aspect ratio of the QIPCC3 configuration.

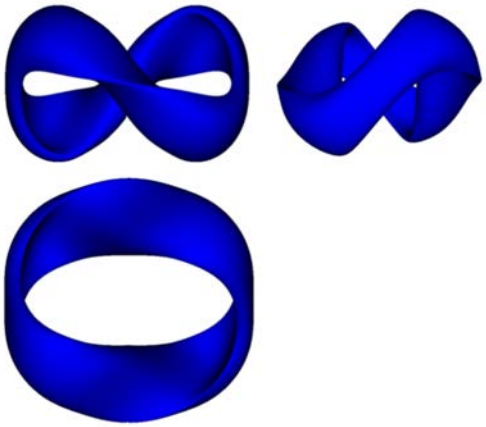

Fig. 3.1. Plan, elevation and profile view of QIPCC2 LCFS.

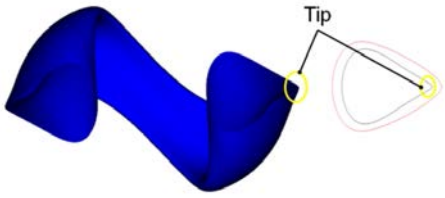

Fig. 3.2. Poloidal section of the plasma surface. An outboard tip is observed.

The graphical representation of the LCFSs in this memory is obtained from a text file in '.RAW' format generated by CASTELL code and represented by VisIt visualization tool.

The LCFS, at the low field section of the plasma, presents a tip at the outboard of the poloidal cross section, Fig. 3.2. Thus, the winding surface has to be located very near the LCFS to properly reproduce the LCFS by NESCOIL code [84]. Fig. 3.3 shows the effect of the number of coils and the distance of the winding surface from the LCFS. The winding surface is approximately equidistant from the LCFS. The set of coils generated on a winding surface at 0.3 m distance from the LCFS (minor plasma radius a ~ 1 m for the original QIPCC2) did not reproduce correctly the original LCFS, Fig. 3.3-left. A set of 400 coils on a winding surface at 0.1 m distance from the LCFS generated magnetic surfaces which fairly reproduced the original LCFS, Fig. 3.3-right.

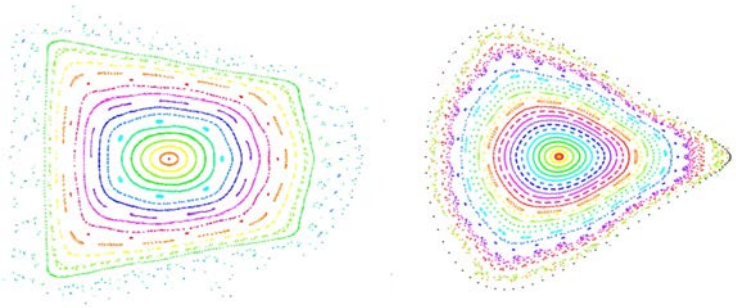

Fig. 3.3. Poincaré plot at φ=0 obtained from 40 coils on a winding surface located at 0.3m from the LCFS (left) and from 400 coils at 0.1m from the LCFS (right). The external black points in the right figure indicates the LCFS.

All the Poincaré plots in this memory are

obtained by guiding centre orbit integration performed by CASTELL code. CASTELL code generates a text file containing a series of sets of 3D points. The file is loaded and coloured by a Visual Basic automation interface for AutoCAD code.

A more rounded LCFS' might be obtained by taking an internal magnetic surface, like the dark blue surface in Fig. 3.3-right. The Fourier coefficients [84] of the LCFS' are generated by DESCUR code [85] from a magnetic field line obtained from CASTELL code, corresponding to a non-rational magnetic surface. DESCUR code calculates the Fourier coefficients of a magnetic surface from 3D points located on poloidal cuts of the magnetic surface and, if needed, points of the magnetic axis. The LFCS' is shown in blue in Fig. 3.4-left and the original LCFS in red.

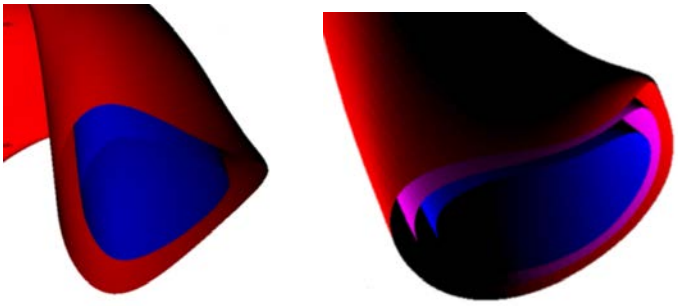

Fig. 3.4. Internal LFCS' in blue (left) and an intermediate magnetic surface in magenta (right).

Linear combinations of the Fourier coefficients of LCFS and LCFS' give intermediate magnetic surfaces, e.g. magenta surface in Fig. 3.4-right. The Poincaré plot obtained from the respective coils reproduces accurately the rounded LCFS', Fig. 3.5. LCFS' exhibits higher aspect ratio than the original LCFS.

Fig. 3.5. Poincaré plot at φ=0 for LCFS' resulting from 180 coils. LCFS' is the solid cyan line.

Other drawbacks of QIPCC2 configuration are:

- Low Beta limit. It is irrelevant for UST_2 but not for larger devices.
- The LCFS' is less compact than the original LCFS.
- Both LCFS and LCFS' also presents a large vertical excursion of the magnetic axis.

3.1.3 Extra details for QIPCC3 configuration

The three-period configuration, QIPCC3 [93,104], has aspect ratio A ~ 6.8, $<\beta>_{lim}$=3.9%, and good neoclassical confinement. The vertical excursion of the magnetic axis is moderate. The LCFS is shown in Fig. 3.6 and the poloidal cross section of the LCFS at φ=0 and φ=π/3 in Fig. 3.7. The poloidal cross section has no tips and it is fairly rounded. A first set of coils located at large distance from the plasma was easily obtained from NESCOIL, Fig. 3.8. Correct reproduction of the magnetic surfaces by 180 coils was obtained by CASTELL code, Fig. 3.9. The QIPCC3 LCFS is shown as a red solid line in Fig. 3.9.

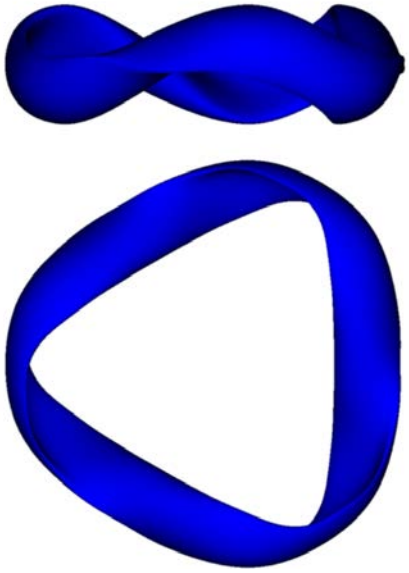

Fig. 3.6. Plan and elevation view of the QIPCC3 LCFS.

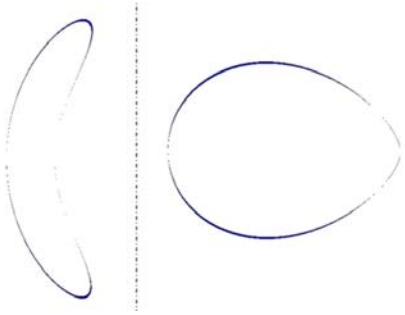

Fig. 3.7. Poloidal cross sections of the QIPCC3 LCFS.

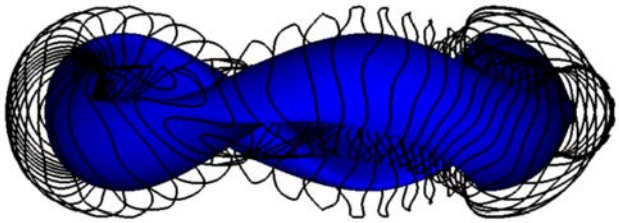

Fig. 3.8. A first set of non-optimised coils for QIPCC3.

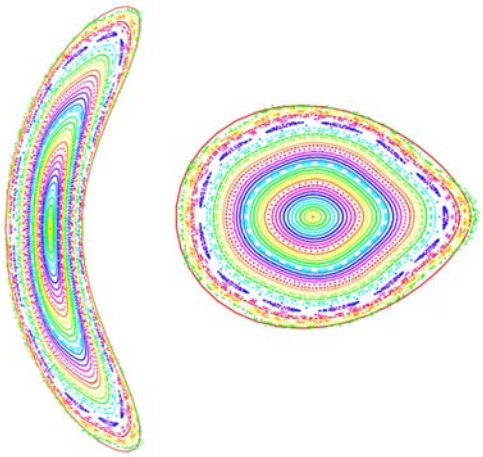

Fig. 3.9. Poincaré plot at $\varphi=\pi/3$ and $\varphi=0$ of the QIPCC3 vacuum magnetic configuration.

3.1.4 NCSX potentially turbulence improved, NCSX-TU

An improved NCSX-like stellarator exhibiting potential reduced turbulent transport is described in [99]. A reduction of turbulent transport of about a factor two with respect to NCSX has been calculated. A satisfactory experimental test of such configurations would greatly impact in fusion research since, for example, obtaining twice the equivalent confinement of H-Mode in tokamaks would be invaluable [105].

Dr. H. E. Mynick suggested the possibility of a device able to produce both configurations, the NCSX and the NCSX-TU. The idea of a device able to model both stellarators would better prove the magnitude of turbulence optimization achieved. A swept of infinite

intermediate configurations could be performed. Some preliminary tests and calculations were produced to assess the possibility of such hybrid configuration for UST_2.

The next process was followed:

Initially, an auxiliary LCFS' is obtained as a linear combination ($\lambda = 0.5$) of the NCSX LCFS (Fig. 3.10) and the NCSX-TU LCFS. A winding surface defined as 3D-points is generated by CASTELL code as an equidistant surface from the LCFS'. The Fourier coefficients of the winding surface are obtained by DESCUR code. The winding surface is illustrated in Fig. 3.10. A set of soils C1 is obtained by NESCOIL for NCSX-TU on the winding surface. C1 coils are introduced as a background magnetic field in NESCOIL and coils C2 are obtained for the NCSX LCFS. Two sets of coils C1 and C2 are created. C1 generates NCSX-TU, and C1+C2 generates NCSX. The coils C1 and C2 are wound on the same winding surface only as a matter of theoretical test. A second equidistant winding surface should be used in reality. The resulting coils are shown in Fig. 3.11. The magnetic surfaces obtained from the coils were unsatisfactory. Different number of coils and distance to a specific winding surface for NCSX-TU were tried. The combination of the plasma tip in NCSX-TU (Fig. 3.10, bean shape in magenta) and the effect of the plasma current needed in NCSX-TU (not included in the CASTELL code model) seems the origin of the poor replication of the NCSX-TU LCFS.

The alluring experiment combining NCSX and NCSX-TU is not selected for UST_2 due to the issues found. It might be attempted for a future larger more powerful device.

Fig. 3.10. NCSX LCFS in red and NCSX-TU LCFS in magenta. A tentative winding surface is shown in blue.

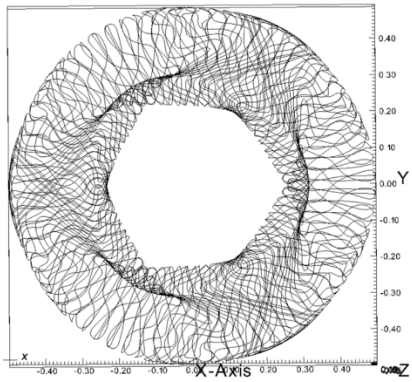

Fig. 3.11. Overlapped coils C1 and C2, only to assess the feasibility of the concept.

3.1.5 Details for QPS configuration

The vacuum LCFS of QPS is represented in Fig. 3.12-red. The result of a VMEC [106] free boundary calculation for $<\beta>=2\%$ is displayed in Fig. 3.12-magenta. A similar calculation is shown in Ref. [101]. The magnetic surfaces calculated by CASTELL code from the definition of the received coils are shown in Fig. 3.13.

QPS is very compact, favourable in general. QPS may exhibit reduced turbulent transport due to the low poloidal viscosity and high radial variation of the radial ambipolar electric field [102]. However, the notable properties of QPS are achieved for $<\beta>\sim2\%$ and

UST_2 will reach $<\beta>\sim 0\%$. Moreover, QPS may be too compact to allocate inboard blankets in case of a reactor and, Cost of Electricity (COE) may increase [61] at low aspect ratio. Also, $<\beta>_{lim}=2\%$ is only a modest value.

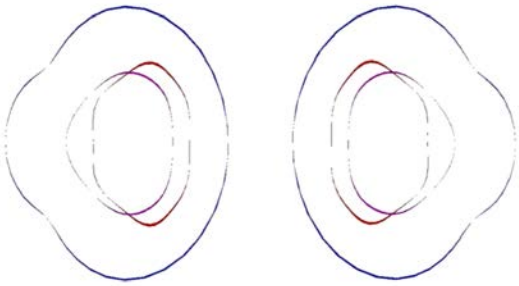

Fig. 3.12. LCFS for vacuum (red), LCFS for $<\beta>=2\%$ (magenta), and winding surface (blue).

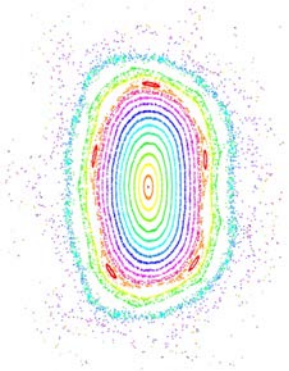

Fig. 3.13. Poincaré plot at $\varphi=0$ for vacuum magnetic surfaces. Magnetic islands due to the low order rational 1/5 = 0.2 appear.

3.2 Review of methods for stellarator fabrication

In the next, the term *stellarator* includes only the core of the device: the coil frame, the coils and the vacuum vessel. The heating systems, power supplies, diagnostics and controls are included, as usual, in the term *stellarator facility*. A modular stellarator ([18]-p.859) composed only by a set of independent twisted toroidal field coils is understood when the term stellarator alone is used in the next. The minimum components for a short plasma pulse stellarator are considered. They are essentially, coils, coil frames and vacuum vessel. Divertors and limiters are not studied for UST_2 in spite of their importance. Only resistive coils are taken into account.

In a simplified vision, construction of a stellarator may be considered composed of three processes: fabrication of mechanical components, fabrication of coils and assembly.

3.2.1 Winding methods

Winding packs for modular coils are produced by (see also [80]):

i) **Use of winding moulds and epoxy impregnation**. e.g. in HSX, [71]. A winding mould is utilised to shape and wind the cable turns. Final epoxy impregnation is performed to keep the shape of the winding pack.

ii) **Use of winding moulds and casing**. e.g. in W7-X. The process is, [88,107]: Conductors are wound on a winding mould, multitude of fasteners are used to fix the conductors until impregnation, subsequent vacuum impregnation, introduction of the winding pack in the casing half shells, and final welding of the halves.

iii) **Winding in/on several winding forms or coil frames**. For example, **a)** In CTH [51,64]: Manual winding of the conductors in the helical coil frame grooves and final in-situ epoxy impregnation of the winding, **b)** in NCSX [67,108]: The conductors are wound on the T shape of each modular coil winding form. Numerous fasteners are required. From 1000 to 7000 labour hours were needed to wind each coil. 1000 hours were achieved after a process of learning by doing.

iv) **Compressive winding in grooves**. e.g. in UST_1, [80]. It can be considered a variant of winding the conductor in grooves located in coil frames, alternative iii). The particularity is that only one or two conductor turns per layer are wound. Therefore, the conductor is compressed on the lateral of the walls of the groove. For that, the dimension tolerances of the groove and the conductor have to be compatible. Thus, numerous fasteners are not needed to avoid unwinding of the conductor during the winding process. Therefore, the winding process is faster and accuracy of the winding pack is increased.

3.2.2 Coil positioning methods

The positioning and assembly of the modular coils are carried out by several methods [80]. Among them, methods requiring the fabrication and adjustment of independent coils, methods requiring the adjustment of several frames which contain winding grooves, and methods considering a single monolithic frame:

a) **Independent coils**. In HSX stellarator the positioning procedure [71] consists of: three adjusters per coil are used to align the independent modular coils, a coordinate measurement machine is used for metrology, and finally the four periods are connected. In W7-X the coils are bolted [68] to a central coil support structure (Fig. 1.6) and supported among them by inter-coil supports of two types, welded connections between coils and gliding Al-bronze pads. First, the coils are fabricated and later they slid on the vacuum vessel for installation at the required position.

   The variant employed in NCSX [67,108] may be considered as an independent coils alternative. 18 winding forms are built for 18 coils. Each coil is wound in one winding form. The winding forms slid on the vacuum vessel and they are finally joined among them. It results a solid and accurate toroidal structure.

b) **Several frames containing winding grooves**. In CTH stellarator the procedure is [51]: Aluminium casting and mechanising of 10 frames, the 10 frames compose a toroidal helical coil frame (Fig. 1.4), the frames are located on and around the vacuum vessel, metrology and spacer shims adjust the 10 frames, final bolting of the frames. The winding packs are wound after the frames are installed on the vacuum vessel.

c) **Single monolithic frame with grooves**. A single monolithic toroidal thick surface equipped with grooves is fabricated. The piece may be fabricated by a milling robot having many degrees of freedom, a rapid prototyping method, or a special toroidal milling machine. The UST_1 modular coils were generated by this method [80].

3.2.3 Fabrication of mechanical components

The coil casings, coil frames and vacuum vessels are usually fabricated by casting, cutting, forging, welding and mechanising, e.g. see [68,86,109]. Such methods are a combination of additive and subtractive fabrication methods. The use of additive manufacturing for stellarators has been proposed in Ref. [72] but likely it has been attempted for the first time in the present work [83]. Combination of additive manufacturing (3D printing) and conventional fabrication methods can be envisaged.

Maximum fabrication and positioning errors around 0.1% are suggested in Refs. [71,110,111] and of the order of 0.01% in Ref. [112]. Magnetic field errors $\Delta B/B$ should be lower than 10^{-4} [68,113]. The positioning errors have to be understood as maximum deviations among the different periods of the stellarator in relation to the major radius of the device. Important degradation of confinement comes from breaking the stellarator symmetry [112]. The dimensional errors are less significant if all the periods are identical among them and correctly positioned, though somewhat different from design.

3.2.3.1 Coil casing and coil frame fabrication

W7-X, CTH and NCSX cases are summarised next.

W7-X: The next information comes from Ref. [88]. The coil casings for the superconducting coils for W7-X are made by casting stainless steel half shells. The winding pack is impregnated in epoxy resin and embedded in the half shells. The two half shells are welded. Final machining of the high precision surfaces and holes for fixation is produced according to measuring marks on the winding pack. Later, welding copper cooling strips on the external surface of the casing and final acceptance tests.

CTH: The helical coil frame of CTH is composed by ten identical coil frames [86]. Each coil frame is made of A356 aluminium casting alloy [114]. After casting, the piece is machined to the desired accuracy at specified locations. Each coil frame weights about 150 kg. The interior of the helical trough is machined to a tolerance of -0.00 +0.76 mm.

NCSX: Data comes from Ref. [67]. A cast-and-machine process is used for the manufacture of the coil winding forms. Sand casting with wood patterns is utilised. One mould is created for each winding form. Accurate dimensional control and casting modelling is performed. After casting, the next operations are carried out: cut off risers, laser metrology, clean-up of cast surfaces, magnetic permeability checks, X-ray inspection, heat treatment, and flaw repair. Each winding form weights about 3600 kg. Machining was performed by large and accurate multi-axis milling machines. It is one of the most difficult processes. Intended dimensional tolerance of the piece after machining was ± 0.25 mm.

3.2.3.2 Vacuum vessel fabrication

A short review of vacuum vessel fabrication procedures used in NCSX, HSX and W7-X stellarators is performed next. The information is valuable for the research of new methods for the production of the UST_2 vacuum vessel.

NCSX: The next information is obtained from Ref. [109]. The vacuum vessel shell is formed by 10 mm thickness Inconel-625 plate. Three identical 120º vessel segments form

the vacuum vessel. Each 120º segment comprises two welded 60º segments. Each 60º segment is fabricated by welding ten press-formed panels together over a 60º welding fixture. Each press-formed panel is built by: first press forming, trimming borders to size, annealing, and second press forming. The shape tolerance of each press-formed panel is quickly checked by a set of 10 panel gauges, one for each panel. The 60º welding fixture is used to precisely position the panels prior to welding. This fixture is ingeniously designed as several pieces in order to allow extraction of the fixture from the interior of the 60º segment after welding. A laser coordinate measuring machine is used to check the position of the press-formed panels prior to welding. After formation of the 60º segments, they are joined and welded on a 120º fixture. The 120º fixture allows position adjustment of the 60º segments, allows access for welding and other features. After the 120º vessel segment is fabricated, holes for ports are milled by a five axis milling machine. The ports are welded, the 120º segment is leak tested and the ports are finally cut in order to allow installation of the modular coils on the vacuum vessel.

HSX: The next data is obtained from Ref. [71]. The vacuum vessel shell is formed by 6.35 mm thickness stainless steel sheet. Eight identical segments compose the vacuum vessel. Each segment is fabricated by four explosive-formed pre-forms. Each explosive-formed pre-form is built by the process: U shape sheet is introduced in a split strong mould for explosive forming, several explosive charges are detonated in the U shape sheets, and finally the generated pre-forms are trimmed to size. The four pre-forms are welded together to create one rough segment of the vacuum vessel. After annealing, the segment is introduced in the mould for a final explosive forming and a final annealing is produced. The mould for explosive forming has a set of grid lines to coin reference lines on the external part of the vacuum vessel during explosion. The grid lines are used for metrology purposes and to locate the ports. The ports are laser cut on the shell.

W7-X: Data comes from Ref. [115]. The vacuum vessel is made of 17 mm thickness austenitic stainless steel plate. Five almost identical 72º vessel modules compose a vacuum vessel of about 12 m of external diameter. Each module comprises two half-modules. Each half-module is produced by welded poloidal rings of 1.8º toroidal width. The poloidal rings are composed of four welded plates, which are hot-formed at 1100ºC. Port openings are water-jet cut. The half-modules and the five modules are finally manually welded on site. Leak testing and laser tracking system are used to assure quality.

3.2.4 Assembly of components

Assembly and positioning of coils, coil frames and vacuum vessels have been carried out in different ways in diverse devices.

3.2.4.1 W7-X assembly

The named coil support structure [116] is utilised to attach and locate the modular coils. The coil support structure (Fig. 1.6) is a stainless steel ring of pentagonal shape located at the centre of the torus. The piece is 10 m diameter and weights 80 ton. It is fabricated as 10 cast modules. Each module is accurately mechanised by large multi-axis milling machines.

The modular coils are individually bolted [68] to the structure by the inboard part of the coil to support the centering forces. Centering forces appear due to the higher magnetic field at the inboard than at the outboard of the coils. Off-plane forces are supported by inter-coil supports. There are two types of inter-coil supports: **i)** welded half boxes between coils at the outboard part of the coil and **ii)** gliding Al-bronze pads between neighbouring coils for the narrow supports [68].

3.2.4.2 HSX assembly

A support structure defined as various box-beam structures [71] holds each support ring from three points, Fig. 3.14. A support ring is a planar shape holding a modular coil and an auxiliary coil. Three adjusters per ring, which are attached to the box-beam structure, allow fine-tuning of the position and alignment of the coils. An accurate coordinate measurement machine is used to measure witness points located on the rings and coils. The adjusters are tuned to achieve the correct position. Finally four field periods are connected and all the components are referenced to a single global machine coordinate system.

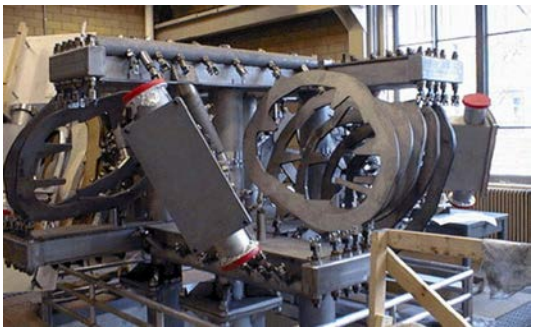

Fig. 3.14. Box-beam structure holding some support rings. Coils are not installed yet in this picture. Reproduced from [117].

3.3 Conclusions

Different magnetic configurations, developed by leading physicists, have been studied and compared. Nevertheless, the selection of an appropriate configuration for a small device, which will be built with low funds, still has to be undertaken. The next chapter deals with such selection, among other matters.

Fabrication methods for windings, coil casings and frames for some stellarators have been compiled and analysed. The positioning of the coils and the assembly methods have been reviewed. An enormous complexity and high accuracy in the construction and assembly is observed. It implies high construction costs and long periods of design and construction. This study may give insight about what not to do if simpler assembling, maintenance and construction methods are aimed. Also, the review may trigger visions for simpler alternative assembly and fabrication methods for UST_2. Based on that, the next chapter will establish some engineering concepts for the UST_2 design.

However, only pure technical factors like the previous ones are insufficient for any research. Objectives, some of them somewhat strategic, are needed to push a work towards a direction. The next chapter also defines such objectives.

Chapter 4

Conceptual design of UST_2

The starting point for the conceptual design of UST_2 are general objectives, physics objectives and engineering objectives. In this chapter, the term *conceptual design* includes both physics and engineering conceptual designs.

An iterative approach of gradual increasing definition of all the elements is advantageous. Fig. 4.1 shows graphically the concept of iterative approach. It implies that integration of the physics design and engineering design was sought from the very beginning.

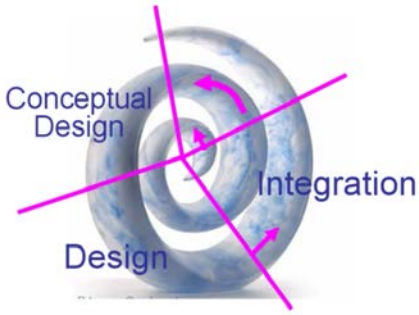

Fig. 4.1. Concept of iterative approach.

The process of generation of alternatives for the physics and engineering conceptual design and for the construction methods was carried out during the year 2013.

4.1 Motivation and objectives for the work on UST_2

The motivation for the R&D of rapid manufacturing methods for geometrically complex fusion devices is justified in Chapter 1. Summarising, the motivation is founded on the still scarce studies dealing with the construction problem of stellarators from the point of view of the recent rapid manufacturing methods and the advantages they imply.

4.1.1 Motivation for the construction of a stellarator

The R&D of rapid manufacturing methods for fusion devices does not necessarily require the construction of a real device to validate the results of the research. However, the attempt to build a small stellarator as a test of the new fabrication methods provides two extra gains:

- Such stellarator, though being small and built by new unrefined methods, may be valuable for universities or research centres for basic plasma experiments, diagnos-

tics development and student training. Small stellarators have been and are used for such functions, like for example the Tohoku University Heliac [118] and TJ-IU torsatron [119].

- A more compelling validation of the construction methods would be achieved if a real device is built and experimentally tested. Otherwise, the validation procedure would be too abstract and less complete.

It is worthy to keep in mind that in any real construction of an object, the relevance lies not only on the generated object but also in the process to generate the new object, that is, the **know-how** generated. And, as important is what was done for success as what should not be done to avoid failure.

4.1.2 General objectives

The **general objectives of the work performed on UST_2** are:

- **A.** Develop innovative construction methods to speed up the production cycle and lower the costs of certain stellarators. Chapter 1 established the critical importance of both aspects.
- **B.** Validate the construction methods by fabricating a stellarator of enough quality to be used by universities. Section 4.1.1 justifies the relevance of this general objective.
- **C.** Consider as much as reasonably possible a physics and engineering design also appropriate for a large stellarator, including features suitable for a reactor.

4.1.3 Objectives for the UST_2 physics design

Some objectives have been imposed in order to guide the process of R&D and try to find satisfactory stellarator properties. Some of the properties would only be noticed in a large stellarator or a reactor.

The objectives related to the physics design are:

- **F1**. Use as much as possible the current available magnetic configurations for stellarators. The design of a well optimised magnetic configuration lasts years of work from many physicists and it is unfeasible in the current framework (see also Section 4.2).
- **F2**. Slightly modify the selected available magnetic configuration if feasible and convenient. This objective may be convenient in order to generate useful research work since the new configuration might provide some advantages (see also Section 4.2).
- **F3**. Such magnetic configuration shall enjoy low neoclassical transport. It is a necessary condition but not sufficient for suitable energy and particle confinement.
- **F4**. Reasonably pursue a magnetic configuration with somewhat reduced turbulent transport. It is still hardly possible, but at least a research group in the world is trying to obtain turbulence improved magnetic configurations, see e.g. [99].

- **F5**. Seek a relatively compact stellarator, A ~ 5 - 7. Middle aspect ratio is in general favourable for engineering and cost [61]. Too low aspect ratio hampers the inboard blankets due to reduced space [44] and increases magnetic field at the inboard part of the coils. Cost of Electricity (COE) tend to increase at low aspect ratios [61].
- **F6**. Search magnetic configurations capable for a future potential implementation of innovative high power divertors. Divertors importantly limit the potential of fusion as a competitive energy source, both for stellarators and tokamaks, [120,121]. Space inside the torus is limited and very expensive. Steady state power extraction in common solid divertors has achieved 10 MW/m^2 in finger units and from 10 to 23 MW/m^2 in other designs [122], low values for competitive fusion energy. Divertor legs external to the torus [94] is an interesting approach for high power extraction in torsatrons without increasing the size of the power core. A small powerful power core is the key for competitive fusion, see e.g. [123]. Therefore, it would be valuable for UST_2 to consider a magnetic configuration having prospective capability for significant and simple power extraction.

4.1.4 Objectives for the UST_2 engineering design and construction

The mechanical components for stellarators are mostly fabricated (Section 3.2) by casting, cutting, forging, welding and mechanising. The fabrication of coils is performed on forms, in grooves, or on forms and in casings. Essentially the assembly is either based on adjustment of independent coils referenced to a structure, or based on the mutual contact and adjustment of frames containing grooves or profiles.

The number of design and construction alternatives resulting from the combination of methods is large. Some objectives have been imposed to the research to reduce the number of alternatives and guide the R&D. Some objectives are strategic and not purely technical.

Objectives for the fabrication of mechanical components:

- **M1.** Try to find and utilize new construction methods, different from casting, forging, welding and mechanising. New unknown paths are required to yield some probability to find better ideas than the older ones.
- **M2.** If feasible and convenient, combine the new construction methods with such traditional methods.

Objectives for the fabrication of coils:

- **C1.** Use the results from the UST_1 work to select a coil winding method. Efficiency and certainty is sough in this case. The coil winding method developed in UST_1 was successful.
- **C2.** Use the studies performed for UST_1 about positioning of coils. The long work carried out in UST_1 for the coil positioning should generate a positive impact on UST_2 design.

- **C3.** Integrate the coil positioning with the constraints coming from the new fabrication methods. Integration is critical. For example, many issues in ITER are caused by lack of integration.

Objectives for the assembly and operation:

- **A1.** Simplify and increase the accuracy of the assembly of the coil frames by integration with the new fabrication methods and with the physics design. The justification is the same as in 'C3'.
- **A2.** Try to obtain a modular device for easy assembly. Equal and detachable modules are in general favourable for construction, assembly and maintenance.
- **A3.** Seek a design for easier maintenance and faster in-vessel access. Long maintenance periods in a future power plant is a major concern in fusion since plant downtime greatly impact on COE.

4.2 Physics design of UST_2

The UST_2 physics design is generated from the next steps:

1) Review of the current magnetic configurations (Section 3.1).
2) Selection of the most appropriate configuration to fulfil the physics and engineering objectives stated in Section 4.1.3.
3) Enhancement, from the point of view of engineering, of the selected magnetic configuration by means of numerical methods.

Several alternatives are possible so as to obtain a conceptual physics design for UST_2:

a) **Choose an already designed magnetic configuration**. Many optimised magnetic configurations for modular stellarators have been developed during the last decade and none of them has been built. Thus, an interesting possibility is to choose one of such magnetic configurations, perform the detailed engineering design and build it by the explored construction methods.
b) **Slightly modify an already designed magnetic configuration.** This alternative may be satisfactory if the degree of modification is modest.
c) **Design a new optimised stellarator**. The design of a well optimised magnetic configuration lasts years of work from many physicists. This option was rejected.

Alternative a) complemented with alternative b) is chosen since alternative c) is unfeasible for the present work.

4.2.1 Selection of a magnetic configuration for UST_2

Section 3.1 reviews and studies different magnetic configurations.

QIPCC3 exhibits (Table 4) excellent confinement, stiff behaviour independent from <β>, high rotational transform and triangular shape. As weaknesses, the aspect ratio of QIPCC3 is considered slightly large and beta limit is modest.

QIPCC2 is discarded due to the increase of engineering complexity due to the large vertical excursion and since almost all properties are poorer than the ones in QIPCC3 configuration.

QPS is not considered for UST_2 since UST_2 works at <β> ~ 0 and QPS is designed for <β> ~ 2%. Then the performance would deteriorate. Also, $<\beta>_{lim}$ ~ 2% is modest and inboard engineering issues are envisaged.

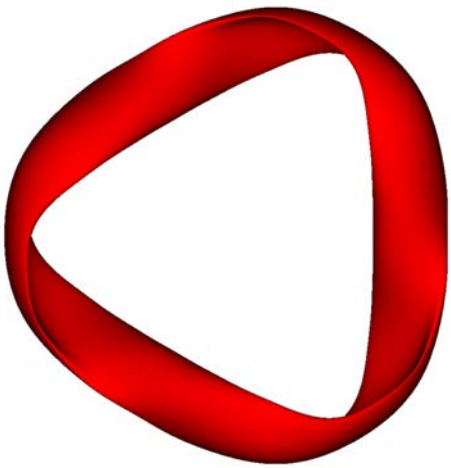

Fig. 4.2. Top view of the LCFS of QIPCC3 configuration.

NCSX-TU is discarded since the design should be adapted to the particular conditions of UST_2, that is, almost no bootstrap current and <β> ~ 0.

The best balance of properties in relation to the physics and engineering objectives established in Section 4.1 is identified in the QIPCC3 magnetic configuration.

QIPCC3 (Fig. 4.2) magnetic configuration is chosen as the reference magnetic configuration for UST_2.

4.2.2 Modification of the selected magnetic configuration

The selection of QIPCC3 as reference magnetic configuration for UST_2 was taken in May 2013. After that, a slight modification of the configuration was conceived.

Some possibilities were speculated considering the physics and construction objectives.

Conceived improvements:

a) It was hypothesised whether a magnetic configuration presenting aspects of the configurations appearing in Refs. [124 - 128] (Fig. 4.3) might be obtained. The implementation of the idea might be carried out by removal of the torsion of the QIPCC3 LCFS at the middle of the mirror section of the plasma. The plasma cross section at the middle of the mirror section may be extruded creating a short cylinder of non-circular section. The process to obtain a configuration keeping good neoclassical confinement, stability and proper rotational transform seemed not straightforward. Finally, the process was based on the generation of a geometrically modified LCFS exhibiting such straight section and the calculation of the performance of the resulting configuration. Iterations were produced to try to find a satisfactory configuration. This process is described in Chapter 5.

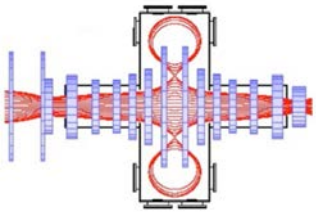

Anchor divertor as planned in GAMMA 10. Source of figure [126].

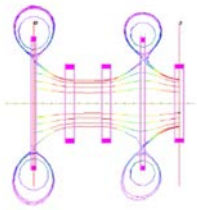

Toroidal divertor devised for EPSILON linked mirrors. Source [125].

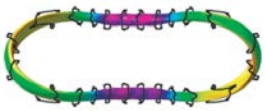

A new two period quasi-isodynamic configuration. Source [127].

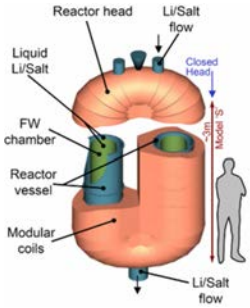

Model S (Small) of Allure Ignition Stellarator [128].

Fig. 4.3. Different concepts and plasma shapes for inspiration.

b) The straight plasma sections might be utilised in the future to install and study toroidal divertors similar to the ones devised in Refs. [123,124,126]. Toroidal divertors may extract particles outside the coils where large and powerful structures could be installed without increasing the cost of the coils due to increase of in-vessel volume. The toroidal divertors would try to achieve, for modular coils, the same advantage of the helical divertors in the LHD heliotron [94].

c) Simultaneously to the previous thoughts, it was speculated whether extra in-vessel space at the straight plasma section might be obtained as a result of having such straight plasma section. It was thought to create large planar coils at the straight plasma region without changing the modified magnetic configuration. These large planar non-circular coils are somewhat similar to the five larger modular coils defined in W7-AS [129]. These large coils are located outside the main smooth and continuous winding surface.

4.2.3 Physics properties of UST_2

Fig. 4.4 shows a plan view of the UST_2 LCFS obtained by CASTELL code from the Fourier coefficients. The physics properties calculated from the LCFS are summarised in Table 5. V_p , R, a and A are obtained by a VMEC fixed boundary calculation at negligible plasma pressure (vacuum calculation). ι_0 , ι_a and magnetic well are obtained from CASTELL and VMEC, also in vacuum. Table 5 summarises the physics properties of UST_2. Fig. 4.5 presents a Poincaré plot of the vacuum

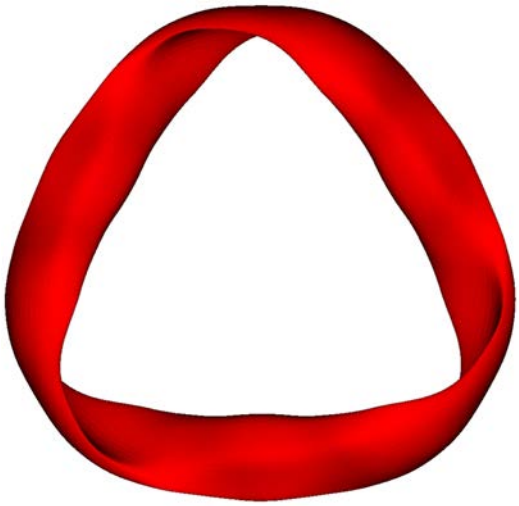

Fig. 4.4. Plan view of the vacuum LCFS of UST_2.

magnetic configuration at two toroidal angles. The small island on rational 8/11 =~0.727 is observed at r = 19 mm. Fig. 4.6 shows the iota profile. All the calculations are performed by the CASTELL code.

Element	Value
Number of periods	3
V_p, Plasma volume (litres)	9.5
R, ave. plasma major radius (mm)	292
a, ave. plasma minor radius (mm)	40.6
A, aspect ratio	7.2
$<B_0>$ (T)	0.089
ι_0 , rotational transform at axis	~ 0.74 (0.732 from VMEC)
ι_a , rotational transform at edge	0.70 (0.70 from VMEC)
Max. magnetic well	0.21 % (0.194 % from VMEC)

Table 5. Essential physics properties of UST_2 stellarator.

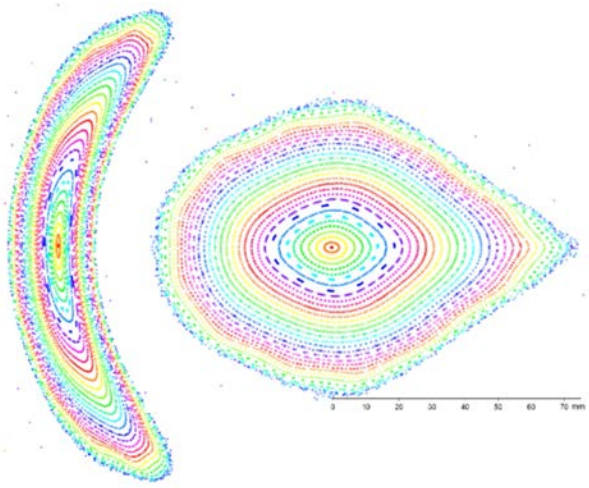

Fig. 4.5. Poincaré plots at φ=π/3 and φ=0 of UST_2 vacuum magnetic configuration.

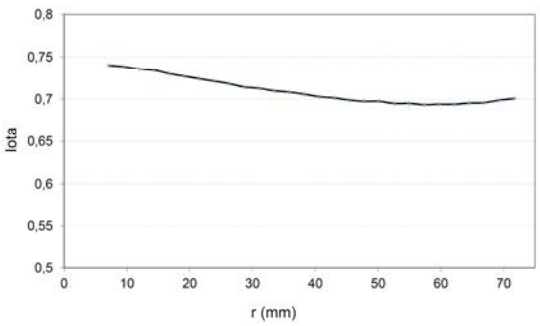

Fig. 4.6. Iota profile. 'r' is the minor radius on the x+ coordinate axis.

4.3 Conceptual engineering design of UST_2

Two main elements are conceived in order to fulfil some of the engineering objectives stabilised in Section 4.1.4. The concept of Large Tilting Coils for fast and safe maintenance and the concept of Detachable Periods are summarised next. The concept of Coil Frame for the modular coils is studied and developed in Chapter 6.

4.3.1 Concept of Large Tilting Coils

Large planar coils at the straight section may speed up and simplify the in-vessel access, among other functions. In-vessel access is important for experimental devices but it is critical in fusion reactors. Tokamaks and even more stellarator reactors, e.g. see [16], require complex and expensive remote handling systems [130] to perform the maintenance of the torus and the fusion facility. Any progress in the direction of simplifying the in-vessel access and remote maintenance is valuable. However, the accurate (re)positioning of the planar coils is a concern. Also, the design of the busbars for the planar tilting coils would be complex.

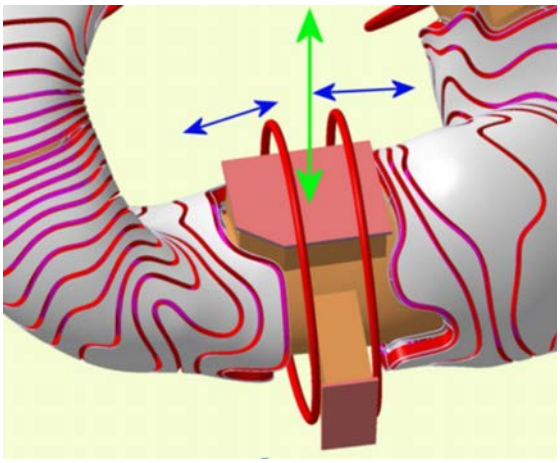

Fig. 4.7. Wide opening for fast in-vessel access.

Fig. 4.7 and Fig. 4.8 show the concept of Large Tilting Coils devised for enhanced in-vessel access. Two large planar non-circular coils (Fig. 4.8 element n. 1) are located perpendicular to the magnetic axis at the straight section of the plasma. The internal open space of the large coil is wider than the contiguous modular coils (Fig. 4.8 element n. 5) of the coil frame. The large coils are capable of two movements: **i)** tilting around an axis (Fig. 4.8 n. 2) perpendicular to the magnetic axis and located below the plasma column, **ii)** optionally, translation in the direction of the magnetic axis towards the coil frame. The design shall allow the movement of the large coils on the modular coils.

Some of the ports (Fig. 4.8 n. 7), located below the large coils, are wide ports since the magnetic configuration allows it. Such wide ports are freed after tilting the large coils, thus, allowing a fast, spacious and safe in-vessel access.

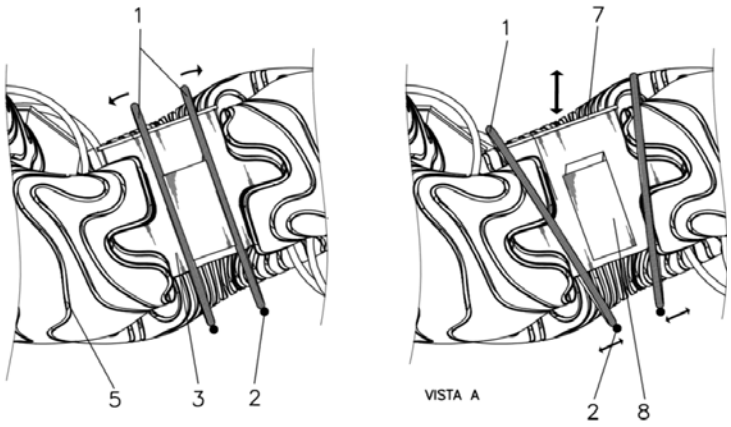

Fig. 4.8. Elements of the Large Tilting Coils concept.

4.3.2 Concept of Detachable Periods

The aim of the concept is to allow periods or halfperiods of the stellarator to be easily separated from the contiguous periods. The existence of the straight section and the large coils may facilitate the splitting of the periods and halfperiods of the stellarator. Additional-

ly, the access to the vacuum vessel flanges for splitting is enhanced. It is relevant in case the vacuum vessel is located inside the coil frames, as in UST_2. The separation of periods still can be speculated if the straight section is not present, as for example conceived for the ARIES-CS reactor stellarator [131].

Splitting the stellarator would increase modularity for easy assembly and maintenance. For a reactor, a full halfperiod could be removed from the torus and immediately, a refurbished or new one would be installed. The maintenance of the halfperiod (first wall, blankets, divertors, perhaps coils) would be carried out off-line, while the power plant would be already producing electricity.

However, the alternative of separation of periods may imply extra design difficulties in the case of a superconducting stellarator [131] due to the existence of the cryostat and the required thermal supports for the elements. Also, increased magnetic errors after the installation of a new halfperiod are a concern in this approach.

In spite of that, experimenting with detachable periods or halfperiods is valuable and supports the Objective A2 established in Section 4.1.4.

The process of detachment of one halfperiod is depicted in Fig. 4.9.

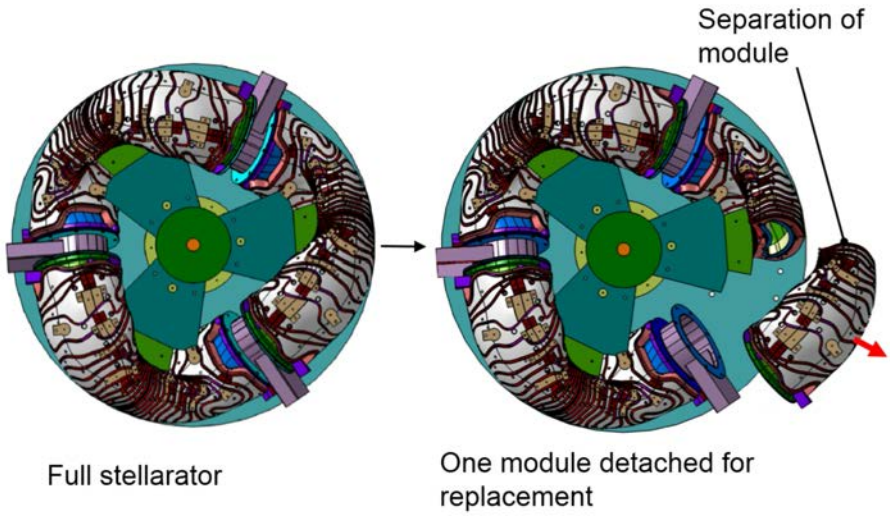

Fig. 4.9. Concept of detachable periods or halfperiods.

4.3.3 Other concepts and decisions taken

Decisions about other aspects of the conceptual engineering design are required. Key aspects not studied in the two previous sections are:

- Employment **of resistive copper coils or superconductive coils**. The study of HTS superconducting coils was started during UST_1 design. During 2005 only BSCOO HTS superconducting coils were commercially available. The cost of only the superconducting wire for UST_1 was about 6000 €. In 2012 YBCO HTS superconducting wire, having much better performance than BSCOO, is commercially available. Samples of YBCO from the company Superpower Inc. were received. The possibility of using HTS superconducting coils was assessed. At least, one attempt has been recently performed to use YBCO

HTS superconducting coils in the small Golem tokamak [132]. The alternative of superconducting coils was rejected due to the excessive cost (tens of thousands of euros) and extra complexity of the liquid nitrogen cryostat. **Resistive copper coils were chosen.**

- **Coils outside the vacuum vessel or inside the vacuum vessel**. Coils inside the vacuum vessel are implemented in CNT stellarator [133] and was planned for QPS stellarator [97]. Coils inside the vacuum vessel imply extra vacuum difficulties and increased complexity of the winding packs. If high vacuum is to be achieved, the coil frames (if not fully metallic) have to be covered by metal sheets or other vacuum compatible materials. Coils in UST_2 have complex shape and are numerous. For UST_2, the cost and complexity of designing and building an internal vacuum vessel appears lower than the cost and complexity of covering all the coils with strong metallic tight-welded sheets and to create a large external vacuum vessel equipped with ports. **Coils outside the vacuum vessel were selected.**

- **Coils connected in series or in series-parallel.** Table 6 compares both alternatives.

	Type of coil connection	Advantages	Drawbacks
C1	All the coils connected in series.	- Low precision power supplies are acceptable. - More appropriate for power supplies with higher internal resistance.	- Higher working voltage. - Higher safety measures needed.
C2	Several sets of coils connected in series. The sets can be connected in series or in parallel.	- A lower voltage power supply is sufficient if the sets are connected in parallel. - Obtains C1 alternative if the sets are connected in series. - More appropriate for power supplies with low internal resistance, e.g. batteries. - Allows some flexibility for the magnetic configuration if several power supplies are available.	- Slight increase of complexity at windings. - Low precision power supplies are only suitable if the current in the sets of coils connected in parallel is well balanced.

Table 6. Comparison of connection of coils in series and in series-parallel.

The coils will be grouped in sets since alternative C2 includes C1 and the increase of worktime to create different sets of coils connected in series is negligible. The coils are connected in series in each set. The number of sets will be decided during the detailed design of the stellarator.

- **Circular or square conductor**. Square (flexible) copper conductors exhibit larger effective copper section. Nevertheless, they are more difficult to wind in a twisted groove than circular flexible conductors. As experimented in UST_1, a circular conductor rotates on its longitudinal axis during winding in the twisted groove, easing the winding process. Moreover, off-the-shelve flexible square conductor is in principle unavailable. A **circular conductor is selected**.

- **Installation of divertor or not**. Neither toroidal external divertor [123,134] nor internal island divertor [135] have been considered. It remains for a future work.

4.3.4 Coil and vacuum vessel specifications

From the selected alternatives described in the previous sections, a conceptual engineering design is obtained. Fig. 4.10 illustrates all the elements involved. The coil frame concept is not discussed in this section since it is studied in detail in Chapter 6.

The large planar coils are located at the straight sections. Curved sectors joining straight cylindrical non-circular sections are obtained. The vacuum vessel is represented in orange. The possibility of large ports at the vacuum vessel for fast in-vessel access is also shown.

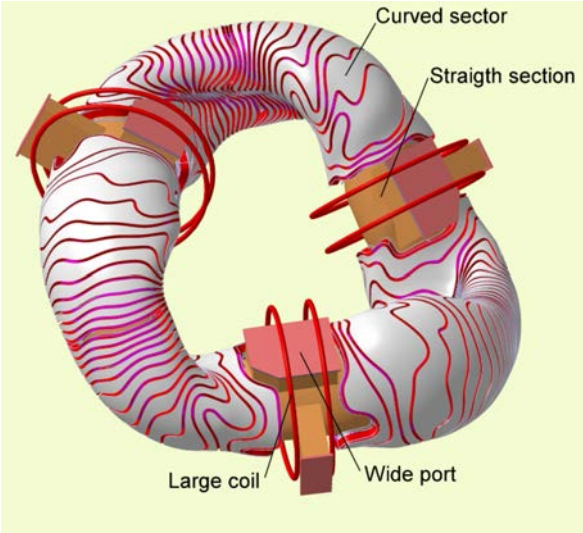

Fig. 4.10. Geometrical conceptual design of UST_2.

Coils are the key components in magnetic confinement fusion and they constrain other elements of the engineering design. Table 7 summarises the coil specifications.

Element	Specification
Type of coils	Modular coils
Number of coils	90
Number of non-planar coils	84 (14 x 6)
Number of planar non-circular coils	6
Turns per coil	3 in modular, 4 in planar coils
Winding pack size (mm)	4 width x 12 depth
Structure of the winding pack	1 pancake per coil
Conductor type	Thin insulation flexible copper wire TXL 10 AWG
Section of the conductor (mm^2)	5.26
Current in conductor (A)	630 (for B_0 0.1 T)
Coil current (A-turn)	1890 (for B_0 0.1 T)
Distance winding surface to LCFS (mm)	35
Minimum distance between coils (mm)	0.56 (among filamentary coil definition)

Table 7. Summary of coil specifications.

Table 8 specifies the general features of the vacuum vessel.

Element	Specification
Structure	Modular sectors joined by o-rings
Number of sectors	6 equal curved sectors and 3 central straight sections
Number of ports	3 large ports at the straight sections
Shape	Equidistant to the LCFS

Table 8. Summary of vacuum vessel specifications.

4.4 Integration of all the elements involved

The development of the physics and engineering conceptual design followed an integrated iterative process. Now, a final revision of the compatibility of all the aspects is worthy so as to achieve satisfactory integration and avoid later ruinous failures. Special attention is given to the interfaces among the elements.

The elements involved are:
- The magnetic configuration with straight sections.
- The maximum distance from the winding pack to the LCFS.
- The minimum curvature of the conductor.
- The necessity of proper crossovers to minimise magnetic errors.
- Positioning features to minimise magnetic errors.
- The large planar coils and the modular coils.
- The vacuum vessel internal to the coil frame.
- Means to allow the introduction of the vacuum vessel in the coil frame.
- The conductor, the winding packs and the grooves of the coil frame.
- Width, depth, curvature and dimension tolerance of the grooves.
- The legs and base of the coil frames.
- The attachment and adjustment of the stellarator to the vacuum system.

The magnetic configuration seems feasible with the use of the large planar coils. The fixation of the large planar coils appear feasible. The distance between the winding pack and the LCFS resulted small in this shaped and very optimised stellarator. The space for the vacuum vessel is limited and special attention will be needed. Wide tolerance has been stablished in order to cope with the vacuum vessel fabrication errors. A gap of 5 mm has been established between the exterior of the vacuum vessel and the interior of the coil frame. The joining of the different sectors of the vacuum vessel is a concern. However backup solutions, like building the vacuum vessel as a sole piece, are available in case of difficulties. The minimum curvature of the conductor does not look a concern since the

coils are formed by a thin single pancake. Therefore, the conductor can be correctly bent inside the groove without losing the centreline. The positioning features have not been defined yet but insight indicates that satisfactory alternatives should exist for accurate positioning. The introduction of the vacuum vessel in the coil frame appears feasible, at least by means of the alternative of splitting the coil frame in two halves. Other alternatives may be considered. From the UST_1 experience, the option of a single pancake in the groove seem reasonable and feasible. The legs and the base of the coil frames look realistic though the large vertical excursion of the magnetic axis of this magnetic configuration indicates some extra difficulties.

Consequently all the essential elements for UST_2 stellarator appear integrated and the interfaces among such elements, at the current level of research, seem well solved. Thus, the process of detailed design and construction can further advance.

4.5 Conclusions

An available magnetic configuration, the QIPCC3, has been selected as a starting point for the UST_2 design. A physics conceptual design properly integrated with the engineering design has been defined. An engineering concept that allows torus modularity and enhanced in-vessel access has been conceived. However, only the Fourier coefficients of QIPCC3 are available. Neither the Fourier coefficients of the LCFS for the modified magnetic configuration nor the definition of the stellarator coils exist. Computing work is needed to obtain the modified LCFS and a coil definition. The next chapter is devoted to the development and description of such work.

Chapter 5

Calculation of UST_2 configuration by CASTELL code

CASTELL (Calculator of stellarators) is a Java object oriented code developed from scratch to perform certain calculations and optimizations based mainly on guiding centre orbit integration. It has been developed from 2005 to 2014. Around 80 Java classes and 20000 lines of code are implemented. Graphical data output is based on the generation of text format files able to be represented by different codes. VisIt, MeshLab and Autocad codes can represent the output from CASTELL code.

The code is object oriented. Therefore, for example, the change from calculations in the UST_2 device to calculations in HSX device is as simple as changing the working object. All the properties of each particular fusion device are transferred to the successive objects and methods.

The code has been developed in parallel to the needs for the design of UST_1 and later UST_2 stellarator. Thus, there have been two main periods of development.

5.1 Functionalities of the code

The current functionalities are listed next in two groups, the functionalities implemented before and after the start of UST_2 work.

Main functionalities and methods of the code in year 2012 (before developments for UST_2):

- Calculation of the magnetic field at any 3D point by Biot-Savart integration based on a set of coils. Calculation of magnetic field at any point by interpolation from a 3D grid calculated by Biot-Savart.
- Initialization of electrons, protons and other particles in different spatial and energy distributions, e.g. particles on a magnetic surface, in a circular torus, on the magnetic axis, etc.

- Implementation of a collision operator based on the collision frequency. It is mainly used for estimations of neoclassical confinement.

Computation/calculation by guiding centre orbit integration of:

- Particle trajectories with drifts and without drifts.
- Iota profile, magnetic well profile, magnetic ripple profile, calculation of poloidal cross section of a plasma torus (related to plasma volume), deviation of the values of minimum of |B| on a magnetic field line, % of trapped particles, minimum distance among coils, simulation of hundreds of particles and calculation of the particle loss rate through the LCFS (related to neoclassical transport), calculation of the position of the magnetic axis, and representation of magnetic surfaces.
- Generation of parametric 3D coils as series of 3D points: Helical coils, circular TF and tilted coils, straight conductors, poloidal coils and certain simple modular coils.
- Optimization of coils by a loop of executions defined by an n-dimensional space of parameters. The parameters are used as inputs for the execution of the code in the loop. Parameters defining the shape of the modular coils, the current in different sets of coils (e.g. the poloidal and central interlocked coils in CNT stellarator), or the plasma density, were common parameters for this version of CASTELL.

Functionalities of the CASTELL code implemented during UST_2 development:

- Calculation of modular coils from the Fourier coefficients of the potential [84] obtained from NESCOIL code. These Fourier coefficients define a potential $\Phi(u,v)$ from which a surface current density related to the coils can be obtained [84].
- Interfacing of CASTELL and NESCOIL codes. CASTELL code sends the geometrical Fourier coefficients [84] of a LCFS to NESCOIL, NESCOIL performs the calculations and CASTELL receives the Fourier coefficients of the potential. Note that CASTELL was run under Windows and NESCOIL under LINUX.
- The code is capable of two consecutive NESCOIL executions. The second execution includes the effect of the magnetic field produced by coils calculated in a first execution. In the case of UST_2, a first NESCOIL run is the origin of the large planar coils and the second run generates the modular coils, see Section 5.3.
- Calculation and representation of $\mathbf{B} \cdot \mathbf{n}$ errors on a LCFS. The maximum and average value of the normal component of the magnetic field on a given LCFS are calculated. It is utilised mainly to assess the quality of the modular coils obtained by NESCOIL.
- Geometrical modification of poloidal cuts of a LCFS. The poloidal cuts can be translated, radially expanded, neared, etc. It is used to obtain the straight section of the UST_2 LCFS.
- Implementation of a Levenberg–Marquardt optimiser to obtain the geometrical Fourier coefficients of a series of points corresponding to a set of poloidal cuts of a LCFS. DESCUR code [85], an IPP Max-Planck code, performs the same function more accurately. However, DESCUR code was not integrated with the optimization CASTELL loops.
- Operations with surfaces represented as Fourier coefficients: scaling, changing signs for compatibility of codes, calculation of equidistant surfaces.

- The optimization structure based on an n-dimensional space of parameters is upgraded from the UST_1 CASTELL version. The new version can use the Fourier coefficients of a LCFS as parameters. Other new features are implemented to improve the magnetic configuration after the straight section is generated from the original QIPCC3 configuration.
- Generation of a 'vacuum vessel' or other material objects as a 3D grid. The 'vaccum vessel' is generated by orbit integration on non-rational surfaces and by a storage process. The material objects are used for neoclassical transport estimations and may be utilised for divertor studies.
- Calculation of plasma volume for any plasma geometry, not necessarily toroidal, e.g. a plasma knot.

5.2 Implemented objects

The code implements the objects (Java Classes) and packages of objects listed next.

5.2.1 Packages of objects

The next elements essentially are folders where a set of related objects are located.

FusDevices: Fusion Devices. Package containing objects 'fusion device', for example HSXDevice. Also a parent object fusion device, common to all the fusion devices, is available. All the stellarators cited in this memory and one tokamak are modelled as a fusion device object.

Experiments: Different experiments to obtain a result from the calculation/simulation. For example, the object PlasmaVolumeExperiment is a particular predefined run (a type and number of particles simulated, initialization position of particles, energy, parameters to save particular data, etc.) focussed on the calculation of the plasma volume of a magnetic configuration. Another experiment is MagAxisExp defined for the calculation of the magnetic axis. And some other experiments.

ParticlesClasses: Definition of different types of object 'particle'. A parent particle named 'Particula' is also available (see below). The present available 'particles' are Alpha, Antiproton, Electron, Muon and Proton.

SimulationClasses: It contains different types of simulations (with no drifts, with magnetic drifts, with electric field plus magnetic field drifts) and the different operations that are available or required for each type of simulation. For example the simulation with drifts (BDriftsSimulation object) detects collisions of particles with the 'vacuum vessel', produces (virtual) collisions depending on the collisionality, saves number of bounces, the time and death of each particle, stores information about the trajectories and cumulative trajectories, etc. However, the simulation without drifts (PoincareSimulation object) only saves information of particle trajectories.

5.2.2 Main objects implemented

Coil: (Coil.java): The object defines and generates coils in the 3D space as a series of vertices of a 3D polyline. The coil can be obtained from a file from its filamentary definition or be generated as a HelicalCoil, PoloidalCoil, StraightLine, TFCoil, etc.

CoilSystem: Generates a series of objects Coil according to the definition in the FusDevice object or takes the filamentary definition of a set of coils from a file.

Main Methods implemented:

- Methods to fill the CoilSystem from several common file formats of filamentary coil definition (NESCOIL format, TJ-II like format, etc.).
- Methods to generate a series of coils of similar structure, for example, a series of circular tilted coils located similarly to the TF coils in tokamaks.
- Methods to generate stellarator symmetry of sets of coils.
- Methods to generate equidistant coils to previously defined coils (useful to assess the effect of the different layers of turns in a coil, and other functions).
- Methods to set the currents of sets of coils.
- Method to calculate the minimum distance among coils and the length of conductor of the coils.
- Methods to save the CoilSystem in a file in several common formats (NESCOIL format, 3D points format, etc.).

MagneticGrid: Calculates, creates, exports and imports an object Grid. The Grid is a 3D array which store 3D vectors defining the magnetic field at the grid vertices. Used to speed up the calculations. The Grid is calculated from the definition of coils by means of the Biot-Savart law. Methods are implemented to calculate the magnetic field at a point by interpolation and to calculate the gradient of the magnetic field.

MaterialGrid: A 3D array containing a short type value (to save memory) per vertex that indicates the material or structure existent in the 3D space. For example the 'vacuum vessel' is denoted as cells filled with the value 50. The position of a divertor could be indicated with other value. The respective methods are able to fill the grid from a file or by setting cells, save the grid for representation and storage, and some other functions.

Particula (Particle): The object stores the information relative to each particle, essentially the speed, position, mass and charge of the particle. It contains the methods to move the particle without drifts, and with drifts due to magnetic and electric effects. Also, it contains methods to set the speed and position of the particle.

Plasm: Object defining a plasma as a group of Particles in a MagneticGrid.

Main Methods:

- Methods to initialise particles from different lines and magnetic surfaces. Particles can be initialised from the surface of any magnetic surface, from a volume inside a magnetic surface, as different flat and triangular distributions, from lines and curves for e-beam experiments.
- Methods to assign particles to the plasma.

GraphicRepresentation: Convert trajectories of particles, coil configurations, surfaces, scalar and vector values on surfaces, etc., in files that can be displayed or used.

SurfaceFourier: Object defining and working with a surface defined both as Fourier coefficients [84] and as a geometrical set of 3D points generated from such Fourier coefficients.

Main Methods and function:

- Linear combination of the Fourier coefficients of two magnetic surfaces.
- Methods for the definition of the Fourier coefficients from data in a file (as a simple series of values or from a VMEC output).
- Save the Fourier coefficients in VMEC and Visual Basic format.
- Method to generate the points of the surface from the Fourier coefficients and accuracy parameters.
- Save a file for the .raw format representation for VisIt visualization code.
- Calculate the mean and maximum error on the LCFS of the normal of a magnetic field created by a CoilSystem on the SurfaceFourier.
- Methods to generate geometrical surfaces (that is, a series of 3D points) by equidistance, or special deformation of the SurfaceFourier.

Shape: Object used mainly for the generation of the straight sections of the UST_2 stellarator. The object contains, and is able to work with, poloidal cuts of magnetic surfaces. There are methods available to expand a poloidal cut in the normal direction, move poloidal cuts, compress poloidal cuts on the magnetic axis, etc.

Descur: Object managing DESCUR and Java-DESCUR related functions. DESCUR [85] is an IPP Max-Plank code able to calculate the Fourier coefficients of a (magnetic) surface from a series of 3D points located on such surface. Java-DESCUR is a Java method similar to DESCUR but implemented in CASTELL code by a Levenberg–Marquardt algorithm from the Apache Commons free libraries. Java-DESCUR is less accurate than DESCUR but allows a simpler integration with the rest of the CASTELL code.

Main Methods:

- Methods to deform in different ways a predefined magnetic surface.
- Save file format to be used by IPP-DESCUR code. The file contains the points of the magnetic axis in cylindrical coordinates and the points of the surface in the correct format.
- The Java-DESCUR method.

xxxDevice (e.g. HSXDevice): Object able to manage the generation of a particular fusion device.

Main Methods:

- Two methods are available for the generation of the MagneticGrid: **i)** generation from the coils and currents of the CoilSystem, the size of the grid and the envelope of the device, and **ii)** direct filling of the MagneticGrid from a file of magnetic grid format.
- Method able to generate a 'vacuum vessel' by initialising particles at the position of the LCFS and saving the occupied cells in a MaterialGrid.
- Generation of equidistant coils to simulate the effect of different layers of conductor.

TreatTrajectories: Object dedicated to the post-processing of the previously saved trajectories of particles.

Main Methods:

- Methods to produce intersection of the trajectories of particles with planes. They are useful to generate Poincaré plots and other representations.
- Method to calculate and save the magnetic well profile.
- Method to calculate and save the magnetic ripple profile.
- To save the modulus of the magnetic field on a trajectory.
- To calculate and save the iota profile.

PotentialFourierCoefs and CurrentSurface: Objects to obtain the modular coils from the Fourier coefficients of the potential generated from NESCOIL code.

5.3 Calculation of UST_2 stellarator

The origin of the UST_2 configuration is the QIPCC3 LCFS [93] defined as Fourier coefficients [84]. QIPCC3 is scaled down to obtain a device about 10 litres of plasma volume. In the next, QIPCC3 means the original QIPCC3 [93] received from the authors and scaled down 21 times (exactly 21.012) to have a reasonable size for UST_2.

The modification performed on the original QIPCC3 configuration is the generation of a straight section at the low field mirror segment of the QIPCC3 LCFS. For that, first the QIPCC3 LCFS is modified by a CAD-like process performed by CASTELL code, e.g. translation of poloidal plasma cuts and scaling poloidal cuts. The obtained magnetic configuration loses part of the original optimization, basically the QIPCC3 excellent neoclassical confinement, stability and iota in a gap without low order rationals. The improvement of such properties is attempted by a CASTELL optimization process.

Summarising, the optimization process follows the next procedure. A loop varies a 6-dimensional space of parameters. Such parameters define the size and current of the large planar coils, three Fourier coefficients, and a slight geometrical gradual expansion of the LCFS at the straight section. Not all the parameters are varied simultaneously to save computation time. An initial value, an end value and an increment is defined for each dimension. Such values are the parameter intervals. All the possible combinations of values in the discrete n-dimensional space are automatically generated. In contrast, the generation of the new intervals for each dimension is performed **manually,** see Fig. 5.1. Experience and heuristics saved much computation time.

For each loop the next computational steps (Fig. 5.1) are produced:

1. New modified Fourier coefficients are generated by adding the respective parameter (Table 9) to each of the three selected original QIPCC3 Fourier coefficients (Table 10) of the $LCFS_1$. The three selected coefficients define the plasma indentation and the vertical excursion of the LCFS. A modified $LCFS_2$ is obtained.
2. A straight section is generated (Fig. 5.2) as 3D points from the $LCFS_2$ defined as Fourier coefficients. Two processes are executed for that: 1) the poloidal cuts of the $LCFS_2$ are properly compressed on the magnetic axis and, 2) new poloidal cuts, identical to the cut at $\varphi = 0$, are generated and translated on the magnetic axis forming a non-circular cylinder at the straight section, Fig. 5.2. A new $LCFS_3$ is obtained as 3D points.
3. The Java-DESCUR optimizer calculates the Fourier coefficients of the $LCFS_3$ from the 3D points.
4. Two consecutive NESCOIL runs calculate the planar coils and the modular coils from the $LCFS_3$ and a winding surface equidistant to $LCFS_3$. In the first run modular coils are generated on an equidistant winding surface located near the $LCFS_3$. Thus, the obtained coil at the straight section is relatively planar. Such initial quasi-planar coil is expanded normally to the $LCFS_3$ to obtain a large coil, Fig. 5.3. The coil is then projected on a plane adjusted to the points of the quasi-planar coil. A planar oval shape is obtained, Fig. 5.4. The filamentary planar oval coil is introduced as background field in NESCOIL. In this second NESCOIL run, modular coils (Fig. 5.5) are obtained to generate the $LCFS_3$. Modular coils tend to not appear at the position where the large planar coil is defined, Fig. 5.6. A planar coil per halfperiod and 14 modular coils per halfperiod are obtained.

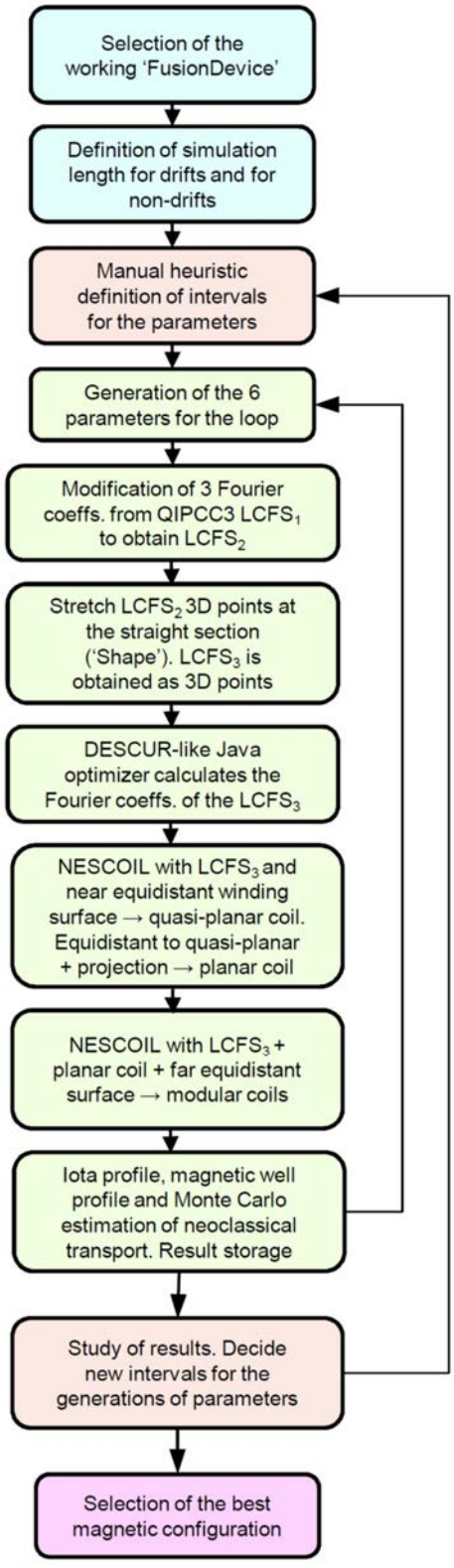

Fig. 5.1. Flow diagram of the computation process.

5. A MagneticGrid is calculated from the coils. The iota profile, magnetic well profile and Monte Carlo estimation of the neoclassical confinement are calculated.
6. The results are saved in a database for subsequent analysis of best configurations.
7. Another loop with modified parameters starts.

After the end of the loop, the database is studied and the initial value, the end value and the increment for each dimension is **manually** and **heuristically** changed. A new loop starts to refine the optimization.

Only ~1200 configurations were compared due to the long lasting neoclassical confinement calculations. A single desktop computer powered by an 'Intel Core i7' quad-core 3.4 GHz processor was used for the calculations.

The parameters added to the original QIPCC3 Fourier coefficients were of the order of magnitude of the ones shown in Table 9. The parameters shown correspond to the ones for the definitive UST_2 magnetic configuration.

m	n	ΔR_{mn}	ΔZ_{mn}
0	**1**	0.0	**0.005**
0	**2**	0.0	**0.0015**
2	**0**	**0.0025**	0.0

Table 9. Parameters added to the original QIPCC3 Fourier coefficients for the final UST_2.

The three QIPCC3 Fourier coefficients of $LCFS_1$, which were subsequently modified in the computation, are listed in Table 10 in bold.

m	n	QIPCC3 R_{mn}	QIPCC3 Z_{mn}
0	**1**	-0.033089	**0.038764**
0	**2**	0.0011502	**-0.0085047**
2	**0**	**0.0029911**	0.0017134

Table 10. Three original QIPCC3 Fourier coefficients ($LCFS_1$).

Some details about the computational step 4.

Some initial tries were performed in the computational step 4 before the parameters and inputs to execute the loop were stabilised. For example, the use of 6 poloidal modes and 6 toroidal modes (named as *6-6 Nescoil modes* in the next) in the second NESCOIL run frequently gave modular coils under the large planar coil, see Fig. 5.5. Later, 6-7 Nescoil modes were used. After such initial tests, most of the optimization loops were executed with the next NESCOIL parameters:

The parameters for the first NESCOIL run were: 3 periods, 6-6 Nescoil modes, no toroidal current and no background magnetic field. CASTELL code generated 12 coils per halfperiod. The coil located at the straight plasma section, which for the chosen coordinate system is the first coil, is the germ of the large planar coil.

The NESCOIL parameters for the second NESCOIL run were: 3 periods, 6-7 Nescoil modes, no toroidal current and background magnetic field from a single large planar coil per halfperiod. CASTELL code generated 14 modular coils.

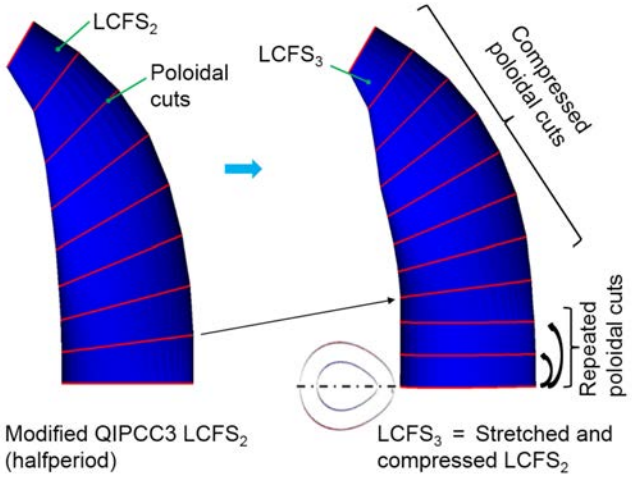

Fig. 5.2. Sketch showing the computation processes to generate the straight plasma sections.

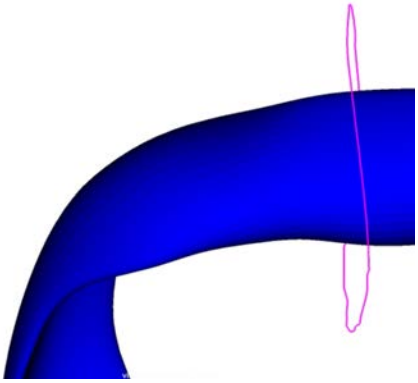

Fig. 5.3. Large quasi-planar coil (magenta). Result at an intermediate process, in computational step 4.

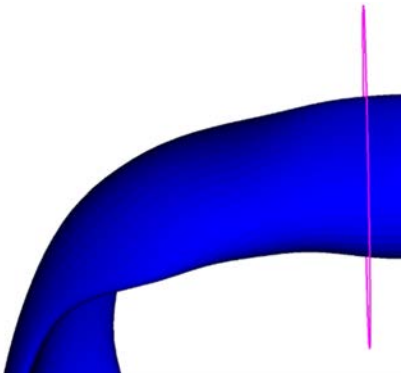

Fig. 5.4. Large planar coil (magenta) obtained after projection on a plane.

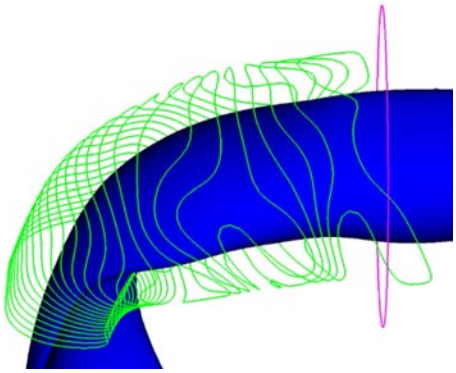

Fig. 5.5. Modular coils (green). Unsatisfactory modular coils under the large planar coil. Case with 24 modular coils per coil frame and 6-6 Nescoil modes in the second run.

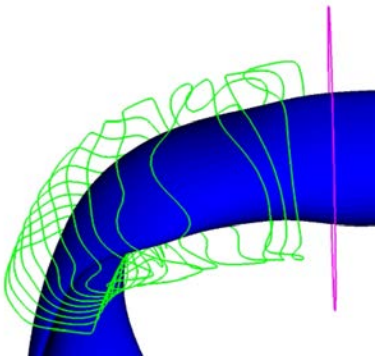

Fig. 5.6. Modular coils (green). Satisfactory modular coils. Case with 14 modular coils per coil frame and 6-7 Nescoil modes in the second run. This case is similar to the definitive UST_2 coils.

5.4 Results and discussion

Among the ~1200 configurations, the selected configuration exhibited: **i)** iota profile in the gap [0.67, 0.74], that is, lacking of low order rationals, **ii)** magnetic well in most of the magnetic surfaces and, **iii)** the lower particle loss rate among all the preselected configurations. Table 11 shows the resulting major LCFS Fourier coefficients utilised for the construction of UST_2.

m	n	R_{mn}	Z_{mn}
0	0	0.30167	0
0	**1**	-0.03555	**0.04962**
0	**2**	0.002746	**-0.00703**
0	3	0.001605	-8.84E-04
1	3	0.001786	-4.36E-04
1	2	-0.00864	0.007629
1	1	0.018215	-0.01469
1	0	0.04475	0.04492
1	-1	0.001393	0.002128
1	-2	5.46E-04	-0.00155
1	-3	0.001737	-3.87E-04
2	3	-0.00248	0.001668
2	2	0.007151	-0.00246
2	1	-0.00468	-0.00316
2	**0**	**0.001103**	-0.00122
2	-1	-6.09E-04	-0.00154
2	-2	-0.00182	-3.38E-04
2	-3	-4.29E-04	-0.00136
3	3	0.001477	-8.66E-04
3	2	-0.00122	-1.13E-04
3	1	0.001189	-7.38E-04
3	0	7.05E-04	-0.00126

Table 11. Major Fourier coefficients of UST_2 LCFS.

The resulting LCFS from the modification of the original QIPCC3 magnetic configuration is shown in Fig. 5.7. This configuration is named ***UST_2 magnetic configuration*** in the next.

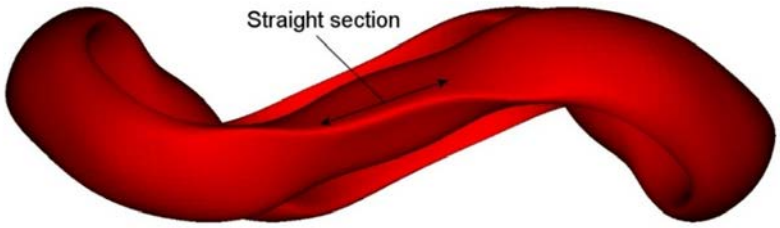

Fig. 5.7. UST_2 LCFS showing the achieved straight section.

Neoclassical confinement in the UST_2 configuration is poorer than in the original QIPCC3 due to the limited optimization loops performed and likely due to the extra conditions imposed to the LCFS. It was observed that the best configuration obtained for a particular length of the straight section showed lower confinement for longer straight sections. A balance between reduction of confinement and length of straight section was attempted.

CASTELL code estimates the neoclassical transport by calculating the particle loss rate through the LCFS. However, CASTELL code is poorly validated for neoclassical calculations. Therefore, a final assessment of the neoclassical confinement was performed by MOCA code [103] after UST_2 configuration was already selected (Table 11). Dr. Joachim Geiger (Max Planck Institute for Plasma Physics) calculated the Fourier coefficients of the magnetic field in Boozer coordinates for QIPCC3 and UST_2 on several magnetic surfaces. From such Fourier coefficients Dr. Víctor Tribaldos calculated the monoenergetic diffusion coefficients of QIPCC3 and UST_2 by MOCA code. The monoenergetic diffusion coefficients are calculated at $\varrho = 0.5$ ($\varrho \equiv \sqrt{s} = r/a$, s is the normalized toroidal flux and a defines the last closed flux surface). From the MOCA calculations and for zero radial electric field, the QIPCC3 magnetic configuration shows approximately 3.5 times lower monoenergetic diffusion coefficients in the low collisionality regime than UST_2.

Considering that QIPCC3 exhibits an excellent neoclassical confinement, similar to QIPCC6 [58], it is predicted an acceptable neoclassical confinement for UST_2. UST_2 neoclassical confinement would be similar or superior to other notable stellarators [58].

From CASTELL and VMEC codes, UST_2 also exhibits lower magnetic well than QIPCC3. The study of the magnetic well and stability of UST_2 remains for a future work.

5.5 Summary and conclusions

The CASTELL code has been developed during a period of 8 years. It is currently capable to perform several calculations required for stellarator development.

The Fourier coefficients of a LCFS presenting a straight non-torsion plasma section at the low magnetic field plasma regions have been calculated from the QIPCC3 magnetic configuration. Neoclassical transport is poorer in the modified UST_2 configuration. In

contrast, the straight section allows modularity of the stellarator, fast assemble and replacement of modules, wide ports for faster maintenance of in-vessel elements and space for potential future large powerful external divertors. A future work might try to further balance the physics and engineering features of the design.

Coils have been obtained for the UST_2 LCFS. It was decided to take advantage of the straight plasma section to generate 6 non-circular large planar coils at the low field plasma region. Two successive NESCOIL executions are performed for the calculation of the planar coils and subsequently of the modular coils.

The generation of a magnetic configuration and coils intended essentially to obtain a design of stellarator so as to test the explored new construction methods. Both aspects, study of magnetic configurations and research of manufacture methods, are produced in parallel though one chapter is written after another.

Section 3.2 reviewed some earlier construction methods. However, the generation of new manufacturing concepts and the acceptance or rejection of such concepts is required previous to the construction of UST_2 stellarator. Consequently, the next chapter studies and compares different alternative manufacturing methods mainly focussed on the coil frame. Finally, the best manufacturing technique for UST_2 is selected.

Chapter 6

Research and selection of construction methods

The three main aspects of stellarator construction according to Section 3.2, mechanical components, fabrication of coils and assembly, are studied next.

The research of construction methods is focused on UST_2 fabrication. Thus, the considered methods might be useless or poor for other larger or different devices. However, it is expected that the developed manufacturing methods will be applicable to some other larger stellarators.

Fast construction methods are sought in order to try to speed up the process from conception of a magnetic configuration to plasma experiments. Lower cost for the same quality and performance is also sought.

6.1 Methods to fabricate mechanical components

The manufacturing methods assessed next are methods capable, in principle, for the fabrication of the considered fusion component. Some of the manufacturing methods have never been utilised for the construction of whole fusion devices while others are common methods in industry.

The two major mechanical components for UST_2 are the coil frames and the vacuum vessel. The base of the device, the legs and other minor components have flat or simple shapes and can advantageously be fabricated by cutting, milling, laser cut or water jet cut.

6.1.1 Alternatives for coil frame fabrication

Metal casting, milling, plastic moulding, non-metal casting, plastic 3D printing and direct metal 3D printing are assessed next.

Metal casting: A molten metal is poured into a mould. Two options are considered, lost wax casting and permanent mould casting.

- Lost wax casting [136]: A replica of the piece, named pattern, is created in wax by different methods. A 3D printed wax pattern is becoming a common technique for complex parts. Refractory plaster is poured around the piece in a bucket to create an expendable mould. The plaster settles. The mould is heated, the wax is extracted from the mould and finally molten metal is poured in the mould under vacuum or at atmospheric pressure. The mould is broken (expendable) to extract the piece. This casting method is accurate and final mechanising might be avoided. For example, the company 'Gorris Comercial de Maquinaria S.L.' produces twisted coils to harden metallic automobile components. The coils are made by lost wax casting with silver or copper. The price of one small 10 cm diameter twisted copper coil is 600-700 €, Fig. 6.5. It would result an estimation of 20000 - 30000 € for one of the six coil frames for UST_2, see Fig. 6.7. The price for the same lost wax casting process is ~18 €/cm^3 in the online 3D printing company Shapeways. One coil frame would consume an order of magnitude of one litre of metal. It results around 20000 € per coil frame. The cost is prohibitive in the framework of the present work.
- Permanent mould casting: Flexible cores in the grooves would be needed to allow opening the mould after casting [136,137] due to the twisted shape of the grooves for the modular coils. The only flexible material withstanding maximum 400 ºC is the high temperature RTV silicone. 400 ºC just allows metal casting of pewter, tin, and low melting point alloys of tin (e.g. Bi-Sn alloys). The design, start-up and use of such mould would be expensive to produce only 6 identical pieces. This casting method is also accurate and final mechanising might be avoided.

Milling: A rotary cutter removes material from a piece. The starting piece for milling may be either a billet or a rough piece. The use of a rough piece reduce milling time and material cost. The two halves (to allow introduction of the vacuum vessel, Fig. 6.7) of the rough coil frame may be produced by metal sand casting, resin casting, plastic injection or other. Finally the coil grooves, legs and other elements of the coil frame would be milled on the rough piece. A company consulted for the fabrication of UST_1 grooves indicated that a 5-6 axis milling machine would be needed. Programming such milling machines is expensive. Locating the piece in position and repositioning the piece to mill the different sectors of the groove require care and operator time. The use of a toroidal milling machine similar to the one utilised for UST_1 is unfeasible for UST_2 due to very convoluted winding surfaces and coils.

Plastic moulding: Plastic moulding requires a strong (metallic) mould to withstand the pressure during thermoplastic injection. Also, the mould would be as complex as in permanent mould casting.

Non-metal casting: Resin, hard plaster and perhaps concrete are some possible materials for non-metal casting. These materials are able to settle or cure. 3D-printed plastic moulds may be used since high strength is not required. The mould only withstands the hydrostatic pressure of the casting liquid. Also, the mould is not loaded at high temperature. Therefore, a 3D printed plastic mould might be a satisfactory option since the coil frame is geometrically complex. Tests will be required to develop and validate the feasibility

and accuracy of the procedure. Resin can be reinforced by chopped glass or carbon fibres. Fibre-reinforced resin can be cast and is simple to use.

Plastic 3D printing: A complete description of the different additive manufacturing methods is found in Ref. [138]. Fused Deposition Modelling (FDM) and Selective Laser Sintering (SLS) are the two main methods for plastic 3D-printing. FDM utilizes one or several nozzles to inject a thin filament of molten plastic at the correct location, layer by layer. SLS uses a steerable laser to melt and fuse small plastic particles (powder) at predefined positions. After the proper particles in a layer of powder have been fused, a new layer of powder of about 0.05-0.1 mm is deposited on the previous layer and the process is repeated.

Direct metal laser sintering: Direct metal laser sintering uses a powerful steerable laser to melt and fuse metallic powder at predefined positions. The powder does not contain binders and the metallic piece is directly produced by the printer. The strength and density of the piece is similar to cast parts.

Table 12 compares the advantages and drawbacks of the different methods for the UST_2 coil frame fabrication.

Method	Cost	Strength	Accuracy
Metal casting	Very expensive for few items. In the range of 20000-30000 € per coil frame	High	Fair. ~ ±0.2-0.5% for lost wax plaster-mould casting and permanent mould
Milling	Expensive due to the programming, piece positioning and machine operation	High if metal. Middle for non-metals	Very accurate
Plastic moulding	Very expensive for few items due to metallic mould cost	Middle	Prone to thermal warping
Non-metal casting	Cheap. 5-30 €/kg depending on casting material	Middle (see Section 6.1.4). Possible fibre reinforced	~ ±0.1 %
Plastic 3D printing	Expensive. About 1.5 €/cm^3 for the material polyamide 12	Middle (see Section 6.1.3)	Deviation ~ ±0.3 % (experimental value, see Section 6.3 and 7.1.3)
Direct metal laser sintering	Very expensive. Checked in i.materialise.com for titanium 3D printing	High	---

Table 12. Comparison of different fabrication methods for the UST_2 coil frame.

6.1.2 Alternatives for vacuum vessel fabrication

Section 3.2.3.2 reviews the techniques utilised for the construction of NCSX, W7-X and HSX vacuum vessels.

The very manual process involved in the construction of contorted vacuum vessels and the diverse mandrels for the sheet forming process are relatively independent on the size of the device. It is a drawback for the small UST_2. As a reference, the cost of the NCSX vacuum vessel was 4.5 M$ [139] and of the TJ-II vacuum vessel 3.9 M€ [111,140]. The vacuum vessel requires relatively low precision if fast variations of coil currents during plasma experiments does not occur. It is the case of UST_2. However, fusion vacuum vessels require smooth metallic internal surfaces and tightness to achieve pressures as low as P ~ 10^{-5} to 10^{-6} Pa. Consequently, uncommon or innovative fabrication methods have to be searched to overcome the difficulties. Some tentative methods are proposed next. They require tests and validation of feasibility.

Metal casting: A small cast vacuum vessel was fabricated for NCSX project for testing purposes. The external diameter of the vacuum vessel is around 0.5 m (scaled-down 10 fold from NCSX). I learned details about this vacuum vessel [141] during my visit to PPPL in October 2013. Such vacuum vessel cost about 40000 $ ($ year 2002). Some pores required closing. Another test for a sand cast vacuum vessel was produced by the Instituto Tecnólogico de Costa Rica (ITCR) for the SCR-1 stellarator. I visited the SCR-1 facilities in January 2014. The interior of the vacuum vessel resulted too rough for good vacuum.

Milling: Two halves should be produced in order to allow milling of the internal of the contorted vacuum vessel. Smoothen and polishing the internal surface of the vacuum vessel would be required. Finally both halves would be tightly welded. The uncomplicated toroidal vacuum vessel for the SCR-1 stellarator has been satisfactorily produced by milling, Fig. 2.18.

Liner: A liner is a thin metallic layer attached to a substrate. The use of a concrete-reinforced steel liner was proposed for the vacuum Test Cell of IFMIF [142]. A patent has been found describing a vacuum vessel formed by a liner and a concrete external reinforcement [143]. Other reinforcement materials can be conceived. The use of a thin-wall vacuum vessel externally reinforced by welded curved beams is a variant of the liner approach. In all the cases a light forming process is required to shape the wall segments that configure the contorted vacuum vessel.

Electrodeposition: A test vacuum vessel made of fibre-reinforced epoxy resin covered internally by electrodeposited cooper thin film was produced [144]. The thin film detached after harsh performance tests. This concept is promising but further research and tests are needed to assure the adherence of the thin film to the epoxy surface. Temperature variations are a concern [144].

Electroforming: The cone for the IFMIF LIPAC beam dump [145] has been produced as a ~6 mm thickness electroformed cone. The cost of the cone was near 18000 €. Electroforming is a relatively common process to generate vacuum vessels.

Forging/forming: It is the method used in the three stellarators studied in Section 3.2.3.2. Explosive forming was utilised for HSX. In the three cases the metal sheet of the

vacuum vessel withstands the atmospheric pressure without the need of external reinforcements.

Table 13 compares the advantages and drawbacks of the different methods for vacuum vessel fabrication.

Method	Cost	Internal surface quality	Other issues
Metal casting	High/middle	Fair	Tendency to have pores
Milling	High for large vessels	Good	Fabrication in two halves
Liner	Middle for small vacuum vessels. Satisfactory for large vacuum vessels.	Excellent	Intensive in low technology work.
Electrodeposition	Would be low if issues solved	Excellent	Detachment of thin film. Many tests required.
Electroforming	Middle	Good	Scarce electroforming companies.
Forging/forming	High for small vacuum vessels	Excellent	Specialised machines, operators and forms needed.

Table 13. Comparison of different fabrication methods for the UST_2 vacuum vessel.

General structure of the vacuum vessel for UST_2

One option is to produce the vacuum vessel as several independent sectors taking advantage of the feasible division of the UST_2 stellarator in 6 sectors. The presence of the plasma straight section and the large planar coils allow this alternative.

Different tests will be carried out to select the best construction methods for UST_2 vacuum vessel. One alternative is to test different techniques in different curved vacuum vessel sectors so as to generate further knowledge and select the best option.

6.1.3 3D printing services and materials

A review of the different additive manufacturing methods is presented in Ref. [138]. The intention of this section is only to: **i)** select between FDM and SLS printing for UST_2, **ii)** identify different companies offering 3D printing services, **iii)** grasp an order of magnitude of the fabrication costs.

FDM is less appropriate than SLS for very hollow pieces since the abundant support material has to be printed and extracted from the interior of the piece. The FDM cost in

such cases is higher than SLS cost. Thus, **Selective Laser Sintering is selected as additive manufacturing method for the UST_2 coil frame.**

Polyamide 12, a type of nylon, is the most common and low cost material for SLS printing. The raw material is nylon powder composed of a precise mixture of particles from ~ 30 to 80 μm in diameter. The cost of 3D printing by SLS in nylon depends on the size and the shape of the piece and of the volume of nylon consumed. The online companies, like www.shapeways.com, www.i.materialise.com or www.ponoko.com, give an instantaneous price for a particular uploaded piece. Shapeways, with headquarters in The Netherlands, have a standard price of 1.4 €/cm^3 (2014) for SLS printed white nylon. This price may vary depending on the hollowness of the piece. The price helps to guide the conceptual design of the pieces if low cost is sought. New nylon powder in small quantities for SLS printers was found from a Chinese company at 70 €/kg. The price is usually higher than that. A 1 kg free sample of polyamide 12 was received in order to assess the fabrication feasibility of the coil frames in the personal laboratory.

Specified **tensile strength** of 3D printed polyamide 12 is 46 MPa and deflection temperature 177 ºC. SLS polyamide has been characterised, e.g. see Ref. [146]. The orientation of the 3D printed elements, e.g. beams and surfaces, with respect the 3D printed layers change the strength and Young's modulus around 30% [146].

In Shapeways company the **delivery time** depends on the size of the piece. Actual average delivery time is from 10 to 20 days. Other companies offer few days delivery at a higher cost.

Also, three Spanish institutions/companies were contacted for estimates: The 'Fundació CIM' in Barcelona, the 'Instituto Tecnológico de Aragón' and, the company 'Ineo prototipos S.L.' in Barcelona.

The maximum **printed size** depends on the available printers. For example, Shapeways allows a maximum piece envelop of 650 × 350 × 550 mm for polyamide 12, enough to print UST_2 in sectors.

6.1.4 Study and test of casting materials

The study of possible non-metal casting materials is carried out because the alternative of casting in hollow pieces is cheap and promising, Table 12.

Possible casting materials are abundant, e.g. several types of resins, plasters and cements. Epoxy, polyurethane and acrylic resins have been assayed. Polyester casting resin was not considered because shrinkage is excessive, ~ 1% to 3 %.

Moulding of thermoplastics is not studied since the mould has to be strong in order to withstand the injection pressure.

Gravity casting, in which the liquid flows by the gravity force, is favourable to produce short series of

Fig. 6.1. Different specimens after fracture.

items. Only 6 identical pieces have to be produced for UST_2. Gravity casting involves simple and safe operations that can be carried out in many companies.

Table 14 lists the results from a series of experiments performed to choose appropriate casting materials for UST_2. Fig. 6.1 shows a photograph of the specimens after the fracture tests. The experiments do not intend to characterise the materials. Only some key properties are assessed for each material, like viscosity and flow, cleanness and simplicity of operations, safety, relation strength and cost, qualitative level of fragility, and impact of fibres and fillers on viscosity and strength. Error in the measured value of force at fracture may reach ±30%. Measurement errors for Shore D hardness (see concept in Section 2.3.4) are lower than 10%.

Sample ref.	Date of pouring	Materials. Conditions	□ [1] (mm)	F [2] (N)	Shore D	Result / Comment
P1	15-11-2013	**Plaster** Hebodent[3] from Hebör. 20 w / 100 p †. No fibres.	5.9 x 14.5	167	85 90 92	No flow. Deposited with a palette knife. Brochure compression strength 130 MPa.
P1'	15-11-2013	Same as P1.	5.7 x 14.45	127	92 85	Same as P1.
P2	15-11-2013	**Cement**-glue brand Axton. 9 w/15 cement.	---	---	---	No flow. Weak. Piece broke when extracting from mould.
P2'	15-11-2013	**Cement**-glue Axton. 9 w/15 cement.	---	---	---	Same as P2.
P3	15-11-2013	**Cement**-glue brand Axton. 9 w/9 cement.	---	---	---	Poor flow. Weak. Piece broke when extracting from mould. Bad settle.
P4	25-11-2013	**Plaster** Exaduro[4] from Hebör. 40 w / 100 p.	5.6 x 14.3	72	82 85	Poor flow. Can be poured.
P5	27-11-2013	**Polyurethane resin**[5] type 327 brand Smooth-Cast (low shrinkage). No fibre. 50% A 50% B components.	6.0 x 14.5	607 *	77	* No fracture, ~ 3 mm deformation. Shore D: 60 61 (24 h cure) / 80 75 76 (4 days cure).
P6	27-11-2013	Same as P5 plus 10% weight of chopped glass fibre ~ 8 mm length cut from Sumbeart company fibres	6.1 x 14.4	392 *	---	* No fracture, ~ 2 mm deformation.
P7	04-12-2013	**Plaster** Exaduro[4] from Hebör. 36 w / 100 p. No fibres.	6.3 x 14.3	122	78 78 83	Poor flow. Can be poured. Loading performed 24h after pouring (≡24h) ‡
P7'	04-12-2013	**Plaster** Exaduro[4] from Hebör. 35 w / 100 p. No fibres.	5.8 x 14.3	101	78 85 81	Poor flow. Can be poured. 50h.
P8	05-12-2013	**Plaster** Exaduro[4] from Hebör. 35 w / 100 p. Glass fibre reinforced, 11 fibres / 100 p.	6.0 x 14.4	64	70 70 75	Impossible to pour the mix. Fibres concentrated at centre of sample. 36h.
P9	05-12-2013	**Plaster** Exaduro[4] from Hebör. 38 w / 100 p. Glass fibre reinforced, 5 fibre / 100 p.	5.6 x 14.4	64	65 70 70	Poor flow. Can be poured. 24h.

P10	11-12-2013	**Acrylic resin** brand RESACRIL[6] C-300 from Sumbeart company. 41 w / 100 powder. No Fibres.	5.9 x 14.3	34	76 80 74	Poor flow. Can be poured. 17h.
P11	12-12-2013	**Acrylic resin** brand RESACRIL[6] C-300 from Sumbeart company. 100 w / 100 powder. No Fibres.	---	---	---	Good flow. The mix lasted long to settle. It is not the brochure proportion of components.
P11'	12-12-2013	**Acrylic resin** brand RESACRIL[6] C-300 from Sumbeart company. 100 w / 100 powder. No Fibres.	6.5 x 14.2	38	62	Good flow. The mix lasted ~1h to settle. Shore D = 60 65 after 3 days.
P12	12-12-2013	Casting **epoxy resin** Epofer[7] EX401+E432 from Feroca supplier. No Fibre.	6.15 x 14.2	392 *	75 78	* No fracture, ~ 2 mm deformation. Also, flow tests with 3 proportions of glass microballoons.
P13	12-12-2013	**Plaster** Exaduro[4] from Hebör. 40 w / 100 p. Chopped pita fibre reinforced, 12 fibre / 100 p.	6.4 x 14.2	85	75 82 79	Impossible to pour the mix. Fibres not well distributed. 22h.
P14	12-12-2013	**Polyurethane resin**[5] type 327. No fibre. 50% A 50% B components. 20% in weight of (A+B) of glass microballoons.	---	---	---	Very thick. Hardly can be poured. Sample volume increased ~50%. Weak and light, like foam.
P15	13-12-2013	**Acrylic resin** RESACRIL[6] C-300 **plus plaster** Exaduro[4]. 3.33 gr of Resacril powder, 6.66 gr Exaduro plaster, 1.33 gr of acrylic resin, 2.66 gr water. No Fibres.	5.1 x 14.3	120	78 82 80	Good flow. The mix was very thick after 5-7 minutes of mixing. 66h
P15'	13-12-2013	Same as P15.	6.0 x 14.3	139	82 80 80	Good flow. 72h.
P16	13-12-2013	**Acrylic resin** brand RESACRIL[6] C-300 from Sumbeart company. 40 w / 100 powder. Chopped glass fibre 5.5 fibre /100 powder.	6.1 x 14.3	160	85 78 80	Very thick. Hardly can be poured. Short chopped glass fibre of ~ 6 mm length. 63h.
P16'	13-12-2013	Same as P16.	5.6 x 14.4	174	80 82 79	Very thick. Hardly can be poured. Short chopped glass fibre of ~ 6 mm length. 72h.
P17	19-12-2013	**Acrylic resin** RESACRIL[6] C-300 **plus plaster** Exaduro[4]. 5.0 gr of Resacril powder, 5.0 gr Exaduro plaster, 2.0 gr of acrylic resin, 2.0 gr water. No Fibres.	6.0 x 14.3	129	85 85 86	Good flow. 84h.
P17'	19-12-2013	Same as P17.	5.4 x 14.3	127	83 82 79	Good flow. 84h.

Table 14. Results from experiments to compare and choose appropriate casting materials for UST_2.

Notes:

† Materials. Conditions: In all cases the proportion of materials is in weight. w = water, p = plaster.

‡ 24h (xxh) ≡ The fracture experiment has been performed 24 hours (xx hours) after pouring the liquid in the mould for specimen production.

Shore D: When available, several measurements are indicated.

[1] □ Section of the specimen at a plane located at the force loading point, see Fig. 6.3.

[2] F : Load on the specimen at fracture.

[3] 'Hebodent' plaster is a type IV plaster. Brochure specified compression strength is 130 MPa and linear expansion 0.1%. Reported tensile strength of type IV dry plasters is ~4 MPa [147]. Service temperature of plasters is lower than 100ºC [148]. Experimental dry flexural strength, measured from specimens in table, is ~11 MPa.

[4] 'Exaduro' plaster is a type IV plaster. Brochure specified linear expansion is 0.1%. Compressive strength is 60 MPa.

[5] Polyurethane resin type 327 has low shrinkage of 0.3 % (0.7% indicated in a brochure), brochure tensile strength of 21.9 MPa, cure time 2-4 hours, mixed viscosity 100 cps.

[6] Supplier specification of tensile strength for Jesmonite AC300 acrylic resin is 20-25 MPa. Linear expansion 0.15%.

[7] Supplier specification of tensile strength for Epofer EX-401-E-432 uncharged epoxy resin is 45 MPa. Shore D 80. Specified shrinkage 0.1%.

A picture of the silicone mould to cast specimens and the hardness gauge is shown in Fig. 6.2. Fig. 6.3 shows a scheme of the experimental setup for fracture assessment of specimens.

Fig. 6.2. Shore D hardness gauge, mould for specimen production and specimen.

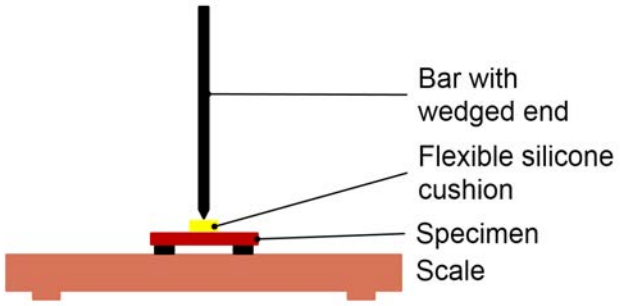

Fig. 6.3. Scheme of the experimental setup for fracture assessment of specimens.

6.2 Methods for coil construction

The winding and the positioning methods capable for UST_2 stellarator construction are studied and selected. A summary of the investigation is described in this section.

6.2.1 Winding methods for UST_2

Several characteristics of each winding method is studied, for example, the need of fasteners to keep the conductor in position during winding, the possibility of winding in grooves or on forms, or the need of a casing to keep the integrity of the coil. In general, it

is favourable to minimise the number of fasteners, casings and winding forms so as to reduce the complexity and the manufacturing time and cost.

A review of earlier winding procedures (from i to iv) is carried out in Section 3.2.1. Other procedures have been devised and are denoted as v) and vi). The different winding procedures are listed next and studied and compared in Table 15.

i) **Use of winding moulds and epoxy impregnation.** See Section 3.2.1.

ii) **Use of winding moulds and casing**. See Section 3.2.1.

iii) **Winding in/on several winding forms or coil frames**. See Section 3.2.1.

iv) **Compressive winding in grooves.** Used in UST_1 stellarator. Section 3.2.1 and Fig. 6.4.

v) **Direct metal laser sintering (DMLS).** Metal 3D printing of copper or aluminium coils would be required. The twisted coils would be produced directly by additive manufacturing. Fabrication of independent coils, or groups of coils, can be imagined. One issue is the uncommon and difficult direct 3D printing of copper and aluminium due to the high thermal conductivity that hampers the laser melting. Nevertheless, the company '3T RPD Ltd' produced a pure copper DMLS piece in October 2014. Another issue is the increase of resistivity of the DMLS material. Recently, Electron Beam Melting additive manufacturing has produced pure copper pieces of resistivity comparable to wrought copper [149,150].

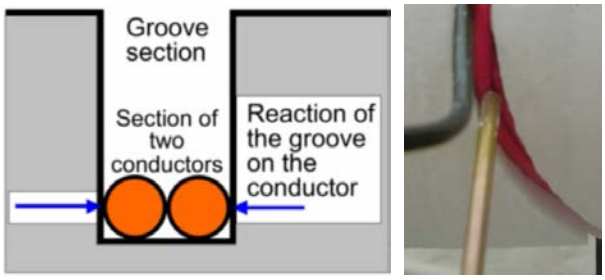

Fig. 6.4. Concept of two conductors per layer compressed on the walls of the winding groove (left). Picture of the winding operation (right).

vi) **Lost wax casting.** This casting method was described in Section 6.1.1. As in direct metal laser sintering, fabrication of independent coils or groups of coils could be considered. Electrical conductivity of the material is kept. Fig. 6.5 shows a contorted coil produced by this method. The diameter of the coil is about 100 mm.

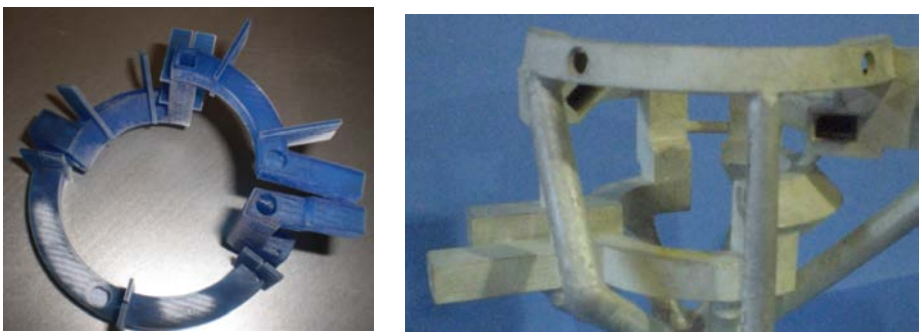

Fig. 6.5. 3D printed wax model for lost wax casting (left). Silver cast coil manufactured from the wax model (right). Pictures courtesy of 'Gorris Comercial de Maquinaria S.L.'.

Table 15 compares the advantages and drawbacks of different techniques used or conceived to wind stellarator coils.

Alternative	Advantages	Drawbacks
i) Use of winding moulds and epoxy	- Casing is not required if magnetic forces are low enough. - Series production can be defined for the equal coils.	- Positioning, adjustment and metrology of each coil are required, increasing complexity and cost. - Numerous fasteners and operator time are necessary for the manufacture.
ii) Use of winding moulds and casing	- Higher magnetic forces can be withstood due to the casing. - Series production can be defined for the equal coils.	- Same as alternative i). - A final casing of the winding pack is required.
iii) Winding in/on several winding forms or coil frames	- Positioning, adjustment and metrology of each individual coil is not required. - Casing is not needed or is impossible.	- Same as alternative i). - Impregnation is needed if magnetic forces are high.
iv) Compressive winding in grooves	**One turn per layer**: - The auxiliary coil (Fig. 6.4-black) is avoided. - Slight higher accuracy than 'Two turns per layer' since the single conductor is better located in the groove. - The same advantages as for 'Two turns per layer'.	- Coils cannot be fabricated and tested off-site. - Series production is difficult or unfeasible. - In-situ epoxy impregnation or external fixation is needed if magnetic forces are high. - A special crossover has to be devised to decrease magnetic errors.
	Two turns per layer: - Fasteners are not needed. Operator worktime decreases. - Coil cases are avoided. - The method is simple.	- Same as for 'One turn per layer' - An auxiliary coil (Fig. 6.4-black) is necessary to avoid unwinding of the first turn wound. - Higher magnetic errors if two symmetric contiguous double pancakes are not defined.
v) Direct metal laser sintering	- Any coil design is feasible: variable or constant coil section, one turn per coil, few turns per coil, coaxial feeds, etc. - Direct production from design. Low operator worktime.	- Size of common direct metal printing machines is small, around 100-200 mm maximum side of piece envelop. - Expensive, ~20 k€ per halfperiod coils (price from i.materialize.com for an estimation of the coils for a halfperiod of UST_2. Obtained 22.8 k€, circa 45 €/cm^3). - Copper and aluminium are the most uncommon and difficult materials for direct metal 3D printing. - Increase of material resistivity. - Many turns per coil may be difficult to produce and isolate (e.g. impregnated isolator).

		- Expensive, about 20000 € per halfperiod in Shapeways.com.
vi) Lost wax casting	- Variable or constant section coils are feasible.	- Several turns per coil hardly would be produced in a single casting operation. Then, magnetic errors increase due to the crossovers. - Isolation must be installed or impregnated.

Table 15. Advantages and drawbacks of different coil winding procedures.

6.2.2 Selection of the winding method for UST_2

The functional requirements for the UST_2 winding method are:
- The winding method shall be fast and simple.
- Be inexpensive.
- Be compatible with the design of the stellarator.

The input information and know-how for the selection is:
- Positioning, adjustment and metrology of each coil should be avoided in order to speed up the process and reduce cost.
- The use of numerous fasteners should be avoided to accelerate the manufacture.
- Method iv) was satisfactorily utilised in UST_1 stellarator. Know-how was acquired.
- A coil frame is the selected coil positioning method (see next Section 6.2.3). The winding method has to be integrated with the positioning method.

The selected winding method for UST_2 is 'Compressive winding in grooves'.

Justification: The previous experience in UST_1, the compatibility with the utilization of a coil frame, and the fast and easy winding process proved in UST_1.

The selected number of turns per layer for UST_2 is one, Fig. 6.6.

Justification: One turn per layer compared to two turns per layer (see also Table 15-iv) is a simpler winding process, slightly more accurate, avoids the auxiliary conductor, and many very twisted coils can be defined (a pair of double pancakes hampers this option). The use of numerous twisted coils decrease magnetic modular ripple and obtain the aimed magnetic configuration more accurately. A disadvantage of the use of only one single pancake per groove is the need of a special type of crossover to decrease the magnetic perturbation from the crossover. Crossovers are studied in Section 7.3.1.

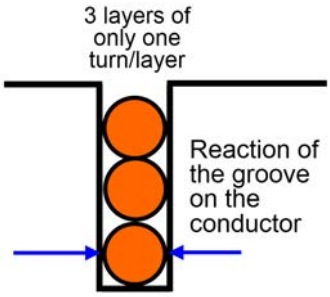

Fig. 6.6. One turn per layer compressed on the walls of the groove.

6.2.3 Positioning methods for UST_2 coils

The study of previous coil positioning methods is performed in Section 3.2.2.

The best positioning method strongly depends on the planned construction and assembling techniques. In general, it is favourable to minimise the adjustments and metrology systems required. Table 16 compares the three positioning methods studied in Section 3.2.2. The meaning of the concepts: 'Independent coils', 'Several frames containing winding grooves' and 'Single monolithic frame with grooves' is given in Section 3.2.2.

Alternative	Advantages	Drawbacks
a) Independent coils	- It is a well-known method used in various stellarators like HSX, TJ-II, and W7-X. - Development risk is low. - Regulation of coil position is possible, if needed.	- Complex and expensive metrology and adjustment of the many elements (coils, supports). - A large number of coils have to be manufactured independently. - A self-supporting coil, a coil casing or a winding form is needed for each coil.
b) Several frames containing winding grooves	- The independent frames can be fabricated in many different ways: metal casting, resin casting, 3D printing, milling, and innovative ways. - Only the metrology and positioning of few frames is required. - Numerous thin and twisted coils can be installed in only one frame. - Resembles to the c) method used in UST_1.	- Assembly, metrology and adjustment of the frames with bolts and shims is required. - The winding process has to be produced in-site, in general. Winding starts after the frames are located on the vacuum vessel. The coils may be wound off-site in a company only if the vacuum vessel could be split in toroidal segments. - Frames cannot be poloidally closed. Frames have to be split at least in two halves to allow installation on the vacuum vessel. Sliding of the frame on the contorted vacuum vessel is impossible in general.
c) Monolithic frame with grooves	- Coil positioning, metrology and adjustment of coils is not necessary. - Many independent coils are not fabricated. - Well-known method since UST_1 was built as a monolithic frame.	- The milling machine to generate the grooves in the monolithic frame has to be developed and built. A commercial robot may be unable to mill the inboard part of the frame due to lack of space. - The milling machine results expensive if only one stellarator is to be produced. - The monolithic frame has to be produced by casting on the vacuum vessel. This operation can only be produced in-site. - The vacuum vessel cannot be separated from the monolithic frame.

Table 16. Advantages and drawbacks of different coil positioning procedures.

6.2.4 Selection of the coil positioning method for UST_2

The functional requirements for the coil positioning method for UST_2 are:
- The method shall be accurate, fast and simple.
- Be compatible with the design of the stellarator and with the selected winding method.

The input information and know-how for the selection is:
- Complex positioning, adjustment and metrology of each coil should be avoided in order to speed up the process and reduce cost.
- Method b) (Table 16) resembles the one utilised in UST_1. Know-how about this method was acquired during UST_1 construction.

The selected coil positioning method for UST_2 is b) 'Several frames containing winding grooves'.

Justification: The know-how obtained from UST_1 construction, the compatibility with the utilization of 'Compressive winding in grooves' procedure, the avoidance of complex metrology for the positioning of each coil and, the possibility of using numerous very twisted coils in grooves on a single frame, justifies this alternative. The use of many twisted coils decreases magnetic modular ripple and reproduces the designed magnetic configuration more accurately.

6.3 Concept, validation and selection of the 3Dformwork method

From the comparison in Table 12, it results that 'Non-metal casting' and 'Plastic 3D printing' fabrication techniques are the two more economical for the manufacturing of the coil frame. However, commercial plastic 3D printing is still relatively expensive. Thus, it was speculated if non-metal casting and plastic 3D printing might be combined in some way to obtain high performance at lower cost.

A concept named 3Dformwork, initially somewhat imprecise, was concocted. The ***3Dformwork*** fabrication method is based on the combination of three known approaches: sparse design (external envelope and internal honeycomb-like patterns commonly used in 3D printing to lighten pieces), truss structures and casting. The concept is named 3Dformwork since it resembles to traditional concrete formwork and to some recent architectural developments to 3D-print buildings. The 3Dformwork pieces are devised as 3D printed hollow light structures composed of narrow beams and optionally thin external walls, whose internal volume is filled with a filler material able to solidify.

The hollow volume is designed to allow the flow of a filler material as in conventional casting or reinforced concrete buildings. After filling the volume, the truss structure and the hardened solidified filler remain attached together as a single monolithic piece. Therefore, the expensive 3D printing material is minimised and the strength is supplied by the low cost strong bulky filler, which may be fibre reinforced.

Filler materials capable for casting in nylon structures are resins, hard plasters, low melting point alloys, cement and concrete. They exhibit different properties and may be useful for particular applications. Fibre reinforcement is possible for most of the materials.

The construction of UST_2 would severely fail at late stages if only one of the innovative concepts were unfeasible or too expensive. Consequently, the higher risk concepts are tested with scaled mock-ups or prototypes. An estimation of the fabrication time and cost of the new concepts was also obtained from the tests.

The design of the pieces for the tests follows the alternative b) 'Several frames containing winding grooves' in Table 16. A preliminary design of the coil frame for a quasi-isodynamic stellarator of two periods [100] was chosen for the tests. Coils were obtained by means of NESCOIL and CASTELL codes. Fig. 6.7 shows the conceptual design of the coil frame, the parting line to split the frame in two parts and an initial representation of the legs.

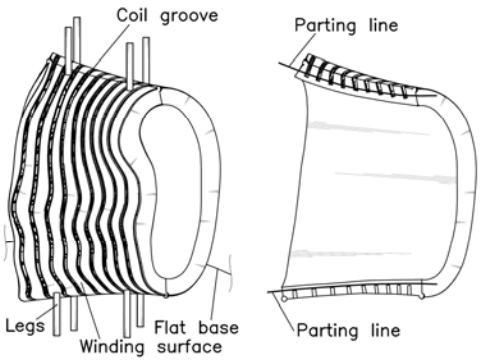

Fig. 6.7. Coil frame (left). Half frame (right).

Two variants of the 3Dformwork concept were assayed. The first variant was named 'Hull Concept'. From the experience gained with the 'Hull Concept' a second concept named 'Truss Concept' was developed.

6.3.1 Experimental validation of the Hull Concept

The concept is based on the combination of (Fig. 6.8 and Fig. 6.9) a sector of the winding surface, a sector of the vacuum vessel surface, internal beams between both surfaces, the walls and bottom of each groove, beams connecting the groove walls, and filling holes to load the double hull volume with a filler. Thus, the coil frame in the Hull Concept is generated as a double hull structure. Each groove has different width in order to test different coils and compression degrees. The structure is automatically generated by a VisualBasic Automation code for CATIA from the filamentary definition of the coils and the Fourier coefficients of the winding and vacuum vessel surfaces. CATIA is a CAD package utilised for ITER design.

The structure was produced by Selective Laser Sintering (SLS) in polyamide 12 by the company Shapeways. Polyamide is the lowest cost 3D printing material found among the strong plastics. Properties of 3D printed polyamide 12 are mentioned in Section 6.1.3. The hardness measured on the polyamide structure was 55 Shore D Hardness. The size of the mock-up is about 1/3 of the planned size for UST_2 stellarator. The envelope of the piece is 12 x 8 x 6 cm. The 3D printed polyamide structure only withstands the hydrostatic pressure during casting. After 3D printing, the interior of the double hull was filled with dental plaster brand 'Hebodent' from the company 'Hëbor Española' (see properties and assays in Table 14).

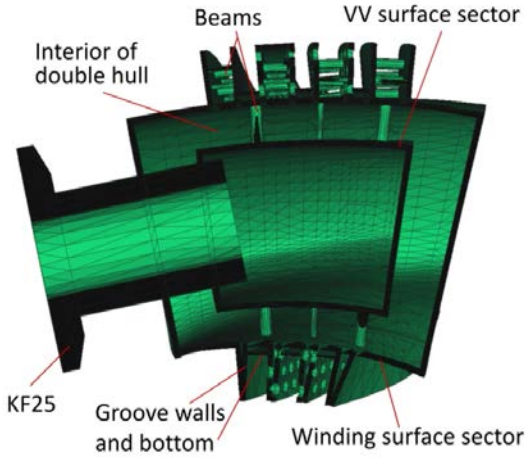

Fig. 6.8. Cross-section of the mock-up coil frame shown as the usual 3D printing STL file format.

Fig. 6.9. Three views of the 3D printed mock-up coil frame. A vacuum flange type KF25, located at an abnormal position, was designed.

The installation of a vacuum vessel inside a coil frame designed as the Hull Concept would be difficult or impossible. Two hardly feasible options might be conceived: **i)** the coil frame would slide on the vacuum vessel similarly to the introduction of the coils on the W7-X vacuum vessel or, **ii)** if possible, the vacuum vessel would be created inside the frame by thick wall electrodeposition, welded metallic sheets, or other means. Finally the vacuum vessel sectors would be welded.

The assessment of compatibility of the 3D printed grooves with one mock-up cable was carried out. The objective of the test is to refine the tolerances to obtain enough compression of the conductor in the groove but still allow an easy winding. The cable is a standard flexible conductor of 3.37 mm average external diameter. Fig. 6.9 shows two turns wound in a groove. Winding and compression of the coil in the groove lasted two minutes. Therefore, the winding worktime will likely have low impact on the total cost of the device.

6.3.1.1 Results and experiences learned

The results are classified next in satisfactory results and experiences learned.

Satisfactory results:

- The measured fabrication dimensional errors are lower than 0.3%. The drawing dimensions and the measured dimensions on the 3D printed mock-up coil frame are compiled in Table 17.

Element	Drawing dimension (mm)	Measured dimensions (mm)			
Width of wide groove	3.50	3.50	3.50	3.45	
Width of middle groove	3.25	3.25	3.25	3.25	
Width of narrow groove	3.00	3.00	2.95	3.05	
Flange external diameter	40.00	39.80	39.70	39.90	
Maximum dimension of the bean shape at the flange side	101.46	101.05	101.05	101.1	101.2

Table 17. Comparison of drawing dimensions and measured dimensions.

- The observed deviations of the groove width are appropriate for the planned 'Compressive winding in grooves'.
- Thermal warping was not observed.
- Filling the inside of the double hull with plaster was simple and effective.
- The conductor was wound quickly and satisfactorily without the use of fasteners.
- Suitable compression of the conductor on the walls of the groove was achieved. The force of the conductor on the groove walls was enough to keep the turn in position.

Experiences learned from poor results:

- The cost of the 3D printed mock-up frame was 80 €. It was considered slightly excessive for the UST_2 definitive coil frame, considering the scaling factor.
- The alternatives for the construction and installation of the vacuum vessel in a Hull Concept coil frame are uncertain and should be carefully validated before construction of UST_2.
- The beams are poorly interconnected among them. Other designs can give higher strength using the same quantity of 3D printed material.
- The high porosity of 3D printed polyamide hampers high vacuum applications. A 3D printed vacuum vessel might be effective if metallic or low outgassing plastics were used.

6.3.2 Experimental validation of the Truss Concept

A lighter and lower cost design was developed from the previous results. A frame structure is created as a truss structure, Fig. 6.10. The frame structure should be preferentially 3D printed, as performed in the piece shown in Fig. 6.10. Finally the frame structure is fully covered by a plastic sheet and internally cast with a filler.

The ***frame structure*** is based on the arrangement of curved beams and reinforcement beams. Four curved beams (Fig. 6.11, external and internal groove edge) define the edges of each winding pack and are parallel to the respective filamentary coil definition.

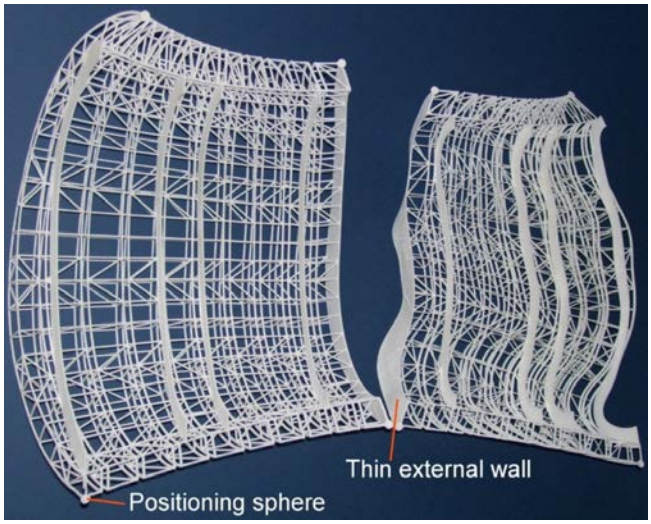

Fig. 6.10. Coil frame halves as received from 3D printing.

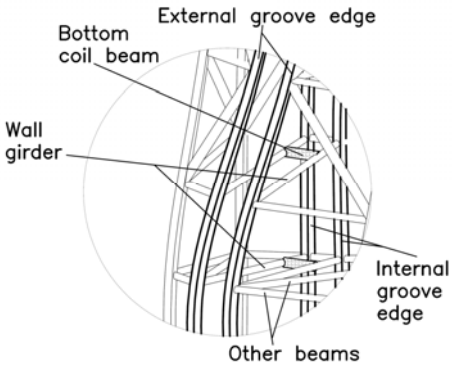

Fig. 6.11. Detail of the design of the truss structure.

The reinforcement beams are or three types (Fig. 6.11):

- **i)** Wall girders: Series of straight beams from the external to the internal curved beam of the same coil. They define the surface of the groove walls.
- **ii)** Bottom coil beams: Series of straight beams, which join each pair of wall girders. The first turn of the winding pack lies on the bottom coil beams and thus, they define the depth of the winding pack.
- **iii)** Other beams: They are perpendicular and tilted bars located at the interspace between the curved beams of consecutive modular coils.

The frame was also automatically generated as in the Hull Concept mock-up and 3D printed with the same polyamide and method. The frame is divided in two halves through a proper parting line (Fig. 6.7) to allow assembling the halves on the vacuum vessel by a horizontal movement (Fig. 6.12, blue arrows). Four positioning spheres, cut in halves, are located at the external vertices of the piece (Fig. 6.10) to help matching the halves. Only one thin external wall (Fig. 6.10) is 3D printed in order to lower the cost of the piece but still assess the ratio performance/cost of such thin walls.

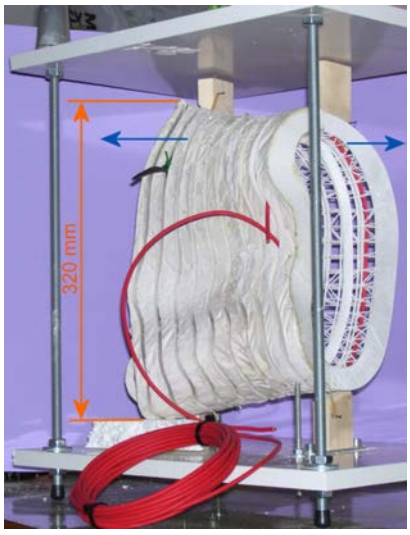

Fig. 6.12. Coil frame assembled on a mock-up flat base.

The maximum dimension of the produced frame is 320 mm (Fig. 6.12), the size required for the UST_2 stellarator. The cross section of the wall girders is 2 x 1.4 mm. The diameter of the beams is 1.4 mm. The width of the grooves is 4 mm, proper width for a commercial flexible copper cable type TXL 10 AWG gauge, red in Fig. 6.12. Such thin insulation cable is preliminarily selected for UST_2.

After the frame structure is 3D printed, a series of processes are required previous to casting since the truss structure is uncovered: **i)** A plastic sheet is glued on the external surface of the piece. **ii)** A silicone core shaped as each winding pack is cut and introduced in-between the four curved beams for each coil. **iii)** Holes are placed at top of the piece for plaster filling. Later, hard plaster was poured into one of the frame structure halves. After settling, the plastic sheet and the moulding cores were removed. The result is shown in Fig. 6.12. Only the half coil frame at the front in Fig. 6.12 was cast. The rear half coil frame remains as the original 3D printed truss frame structure.

6.3.2.1 Results, experiences learned and potential enhancements

The results are classified next in satisfactory results and experiences learned.

Satisfactory results:

- The sparse factor (volume of material / volume of the piece) is 1/16.
- The measured fabrication linear dimensional errors are lower than 0.3%. The measurements are taken between centres of positioning spheres.
- The conductor adjusted correctly in the groove. Fasteners will not be needed to fix the conductor in place during winding.
- The cost scales more favourably than for the Hull Concept since only linear elements compose the truss structure.
- Cost of the 3D printed frame (both halves) was 200 €. Later the Shapeways company changed the price policy and the cost would have been 500 € for another piece. It is considered cost-feasible for UST_2.

Experiences learned from poor results:

- Thermal warping has been far excessive. The positioning spheres of both frame halves mismatched about 2 mm, an unacceptable value. Manual slight rotation of the halves so as to counter warp allowed matching the two halves. An option to try to reduce the thermal warping is to produce both halves joined in position by slender junction bars. The filler would be poured in the structure, the junction bars would be cut after settling, and the two halves would be separated.
- The glued plastic sheet failed at one point and plaster leaked until closing the gap. Fortunately, the volume was satisfactorily filled by pouring extra plaster. 3D printing a thin external envelop surface would avoid such problem.
- About 4 hours were used to prepare, mould and clean the half frame. The working time should be decreased for the UST_2 construction.

6.3.3 Selection of the fabrication concept for the coil frame

The factors for the selection between the Truss Concept and the Hull Concept for UST_2 are: worktime, materials cost, simplicity and integration.

The Hull Concept requires short worktime, materials cost is moderate, the manufacturing process is simple and the generated piece is compatible with the selected winding and positioning method.

The Truss Concept requires long worktime, materials cost is low, the manufacturing process is complex and the generated piece is compatible with the selected winding and positioning method.

Both concepts are somewhat unsatisfactory. A combination of the two methods was considered an adequate solution.

From the previous research, the ***3Dformwork*** method is conceived as a 3D printed truss structure covered by a 3D printed thin envelope surface, and the internal volume is cast with a filler. The grooves and reinforcement bars are defined as in the Truss Concept but they are covered by a thin surface similarly to the Hull Concept.

Fig. 6.13 shows the design of a prototype comprising tree coils of the UST_2 frame structure. The design follows the 3Dformwork technique. The frame structure already corresponds to the coil definition for the definitive UST_2 magnetic configuration. The internal surface of the piece is removed to better observe the internal bars. The piece was also automatically generated as in the Trust Concept and 3D printed with the same polyamide, method and company.

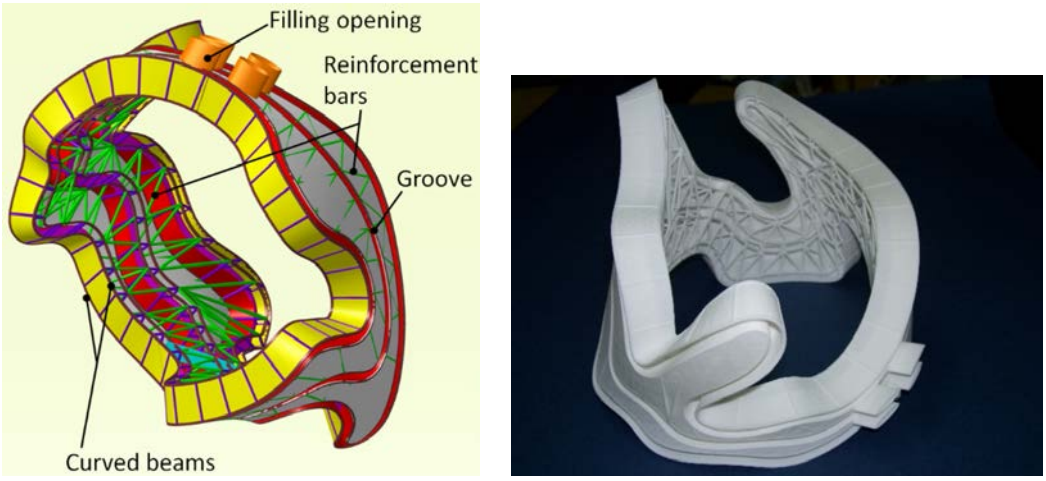

Fig. 6.13. Test of three coils for UST_2 stellarator generated as a 3Dformwork piece. Design (left). Real 3D printed frame structure (right).

The 3-coil prototype includes all the improvements inferred from the results from the Hull Concept and Truss Concept exploration. Summarising, the **principles** for the design of the frame structure are (see Fig. 6.13):

- The frame structure is split in two halves (two independent closed volumes) joined by small joins located at some points at the parting line (see parting line in Fig. 6.7). The internal volume is filled with a filler and, after settling, the joins are cut to split the coil frame in two parts. Splitting in two parts is needed for the introduction of the vacuum vessel in the coil frame. The result is an accurate piece.
- The skeleton of the piece is a truss structure identical to the one defined for the Truss Concept. It gives strength at the minimum cost.
- Reinforcement bars are defined among the curved beams of the same coil and of consecutive coils.

- Four curved beams define the edges of each winding pack and are parallel to the respective filamentary coil definition.
- A thin external surface follows the curved beams to generate twisted grooves where the copper conductor is wound.
- The piece is equipped with upper filling openings for fast and easy casting process.
- Legs are defined as part of the 3D printed frame structure in order to simplify the assembling process. Legs were not designed yet when the prototype shown in Fig. 6.13 was produced.

The initial conjecture about the feasibility of non-metal casting combined with plastic 3D printing has been validated.

Therefore, the **selected alternative for the manufacture of the UST_2 coil frame is a combination of plastic 3D printing and non-metal casting.**

6.4 Tests and selection of manufacturing method for the vacuum vessel

Section 3.2.3.2 reviews earlier methods used for vacuum vessel fabrication. Section 6.1.2 studies unspecific possible methods. Table 13 compares the preselected methods. The information suggests multiple solutions even for a small device. The most restrictive factor is the cost since the available funds are accounted in few thousands Euros for the full UST_2 stellarator. Next, selected data from the above cited sections is summarised:

- Forging/forming and milling are rejected due to unaffordable cost.

- Metal casting gave deficient results in the few attempts for stellarators. Also, cost is unaffordable.

- Electroforming is a well proved method of moderate cost. The cost would be about 1000-3000 € per vacuum vessel sector. The second or third manufactured vacuum vessel sector might be tentatively fabricated by this technique.

- Electrodeposition could have the better ratio performance/cost if some innovations were concocted and tested. Only one real small prototype vacuum chamber has been found in the bibliography [144]. A company able to reliably adhere a copper thin film on epoxy resin is difficult to find. In any case, the cost may be high due to the R&D cost in the company. To avoid the need of specialised electrodeposition companies, a research process could try to find a simple binding method on epoxy resin able for electrodeposition. This alternative has been relegated for a future work. The second or third manufactured vacuum vessel sector might be tentatively fabricated by this technique.

- The only remaining method is the liner externally reinforced technique (Section 6.1.2). The method is proven and gives satisfactory internal surface quality. It requires much working time of delicate soldering/brazing work. Therefore, it was decided to perform some tests to estimate the fabrication time and the feasibility of the concept.

6.4.1 Concept and test of a reinforced liner vacuum vessel

Copper was selected as first wall material since it solders easily, is notably appropriate for high vacuum if well cleaned, and is easily available. Different thickness of copper sheet, 0.1, 0.2, 0.3 and 0.5 mm were tested. Manual forming is the only reasonable solution to avoid the fabrication and use of many mandrels for heavy forming. Thickness of 0.3 mm resulted in feasible manual forming and strength enough for manipulation. Thickness of 0.1 and 0.2 mm gave a weak structure and the subsequent soldering processes would be too delicate.

The concept of a resin reinforced liner vacuum vessel includes (see Section 7.2 for details):

- The vacuum vessel will be formed by 6 identical curved vacuum vessel sectors and 3 straight central vacuum vessel sections, Fig. 6.14. The central vacuum vessel section joins the curved vacuum vessel sectors and allows deviations among them.
- The liner of each curved vacuum vessel sector will comprise two halves in order to comfortably shape the copper surface on a form. The curved VV sector should be split in two halves through points of maximum curvature of each poloidal cut of the vacuum vessel surface in order to easy the forming process. This particular splitting generates parting lines similar, but not equal, to the ones shown in Fig. 6.7 for the coil frame. The two halves will be mutually soldered after fabrication. Finally, flanges will be soldered at both ends of the contorted shape.

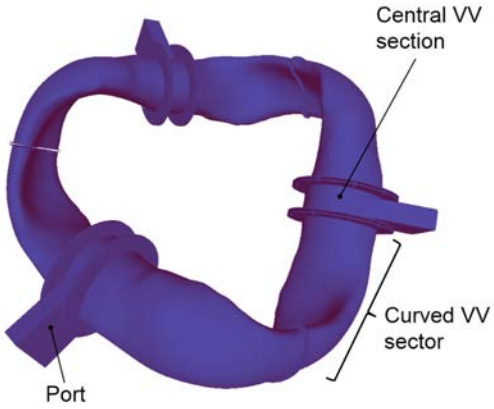

Fig. 6.14. Design of the modular vacuum vessel.

- Each half of curved VV sector is conceived as a series of soldered copper strips shaped on the form.
- Epoxy resin is planned as external reinforcement of the liner for the curved VV sector. Grasping elements, which are firmly attached to the external surface of the liner and to the resin, are devised so as to avoid the separation of the liner from the resin due to the pressure caused by the vacuum in the vessel.


Fig. 6.15. Test of the liner vaccum vessel.

A test of the concept was carried out by means of only 6 strips of the definitive vacuum vessel sector. A flange and a closure cap equipped with a NW 25 vacuum flange were added. Fig. 6.15 shows the result. The test vacuum vessel was satisfactorily loaded under vacuum.

6.4.2 Selection of the fabrication method for the UST_2 vacuum vessel

The concept described in the previous section is not simple at all. However, the vacuum vessel can be produced by simple and inexpensive tools and forms.

Therefore, **the concept of a liner which is externally reinforced by epoxy resin is selected for the fabrication of the first curved vacuum vessel sector for the UST_2 stellarator.**

6.5 Conclusions

Alternatives for the fabrication of the coil frame and the vacuum vessel have been explored and tested. Winding and positioning methods have been studied. Two alternatives of an initially blurred concept named 3Dframework, which is devised for the fabrication of the coil frame, were investigated. From such results, a definitive 3Dframework concept was specified and experienced in a portion of coil frame. It appeared a fast and relatively low cost method for the production of the coil frame for UST_2.

The intention to build a small stellarator is justified in Chapter 1 and in Section 4.1.1. The main reason for the fabrication of a small stellarator is the aim to carry out a stronger and integrated validation of the investigated manufacturing methods.

All the ingredients to prepare a small stellarator in a new manner have been explored. Nonetheless, the application of the concepts in a real object remains. Hence, the next chapter summarises the UST_2 detailed engineering design, the UST_2 construction and the results.

It is appropriate to remember that the scope of the work (Section 1.5.2) does not include mechanical and thermal calculations. The described engineering design is mainly geometrical and integrative.

Chapter 7

UST_2 engineering design and construction

The engineering design and construction of UST_2 is summarised in this chapter. The magnetic configuration and the coils defined in Chapter 4 and 5 are the foundation for the engineering design. Fig. 7.1 shows the design of UST_2 stellarator to be built by the developed construction methods. The external diameter of the device is ~850 mm. The circular base of the stellarator is not shown in the figure for clearness. Also, only four support tables are shown for clarity.

Only one coil frame, one section of the vacuum vessel and the base have been built for the validation of the construction methods in the present work. The remaining stellarator will be built in the future.

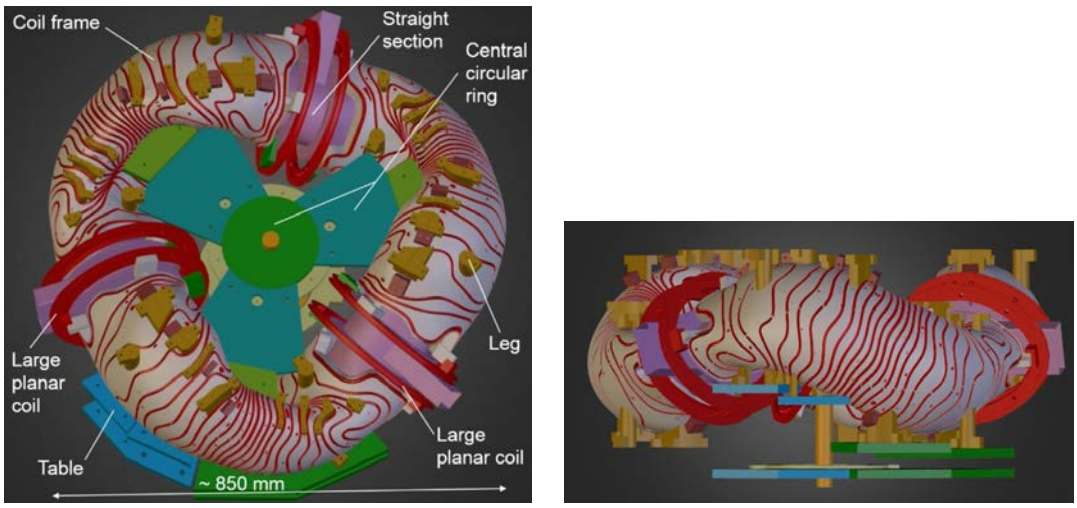

Fig. 7.1. Plan and elevation view of UST_2. It will be manufactured by the researched construction methods.

7.1 Coil frame

The selected alternative for the coil frame fabrication is a combination of plastic 3D printing and non-metal casting, Section 6.3.3. The 3D printed plastic piece is named ***Frame Structure***. The frame structure filled with resin is named ***Coil Frame***.

7.1.1 Frame structure

The frame structure is designed following the method described in Section 6.3. Fig. 7.2 shows the design of the frame structure. It has been particularly devised for additive manufacturing and specifically for Selective Laser Sintering printers.

As in the Hull and Truss Concepts, the frame structure is automatically generated by a VisualBasic Automation code for CATIA from the filamentary definition of the coils and the Fourier coefficients of the winding and vacuum vessel surfaces. Groove surfaces, reinforcement bars, and curved beams (Fig. 6.13) are created by instructions given to CATIA by the Visual Basic code. Several loops successively generate the different modular coils and groove surfaces. The reinforcement bars are generated among contiguous coils. Due to the very contorted shape of the coils, an algorithm decides the origin and end of the reinforcement bars on the contiguous grooves and the thickness of each bar.

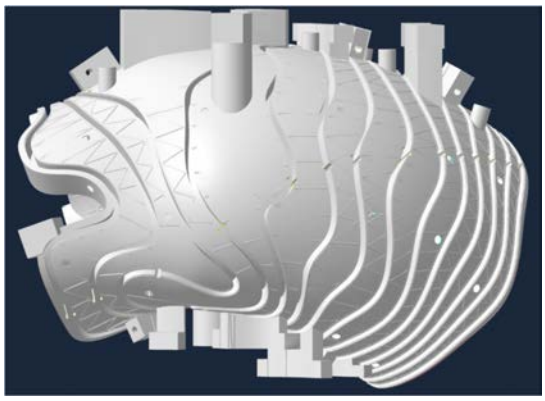

Fig. 7.2. Design of the frame structure.

The legs are CAD designed manually. The legs are located at the top and at the bottom of the frame structure in order to generate stellarator symmetry by rotation of the piece. The base of the legs is defined at two different elevations so as to cope with the large vertical excursion of the magnetic axis of this particular quasi-isodynamic stellarator. The legs of each coil frame rest on two tables of different height.

The attachments used to connect the large planar coils onto the coil frame are shown in Fig. 7.5.

The frame structure was 3D printed by SLS in polyamide 12 by the Shapeways company. Properties of polyamide 12 are indicated in Section 6.1.3. The cost of the piece was 700 €. The envelope of the piece is 216 x 358 x 252 mm. The volume of polyamide is 563 cm^3. Photographs of the obtained 3D printed part are shown from Fig. 7.3 to Fig. 7.8.

Fig. 7.3. Plan view of the frame structure.

Fig. 7.4. Perspective view of the frame structure.

Fig. 7.5. Profile view of the frame structure. Three attachments for the large planar coil are visible.

Fig. 7.6. Profile view of the frame structure viewed from the side of the plasma bean shape.

Fig. 7.7. Detail of the 3D printed reinforcement bars.

Fig. 7.8. Detail of a section of very contorted modular coils. Holes for the extraction of internal nylon powder are also visible.

7.1.2 Resin casting of coil frame

The coil frame is manufactured by filling the frame structure by the material of specimen P15 in Table 14. The material is a mix of acrylic resin brand Jesmonite, type AC-300 and Exaduro plaster. Acrylic resin was selected to cast the first coil frame since it is easier to work with. There are no critical consequences of resin leaks and the tools are cleaned with water. Working with epoxy or polyurethane resins is more complicated. Properties of P15 material and Jesmonite AC-300 are indicated in Section 6.1.4.

Fig. 7.9. 3D printed coil frame prepared for casting with resin.

A picture of the casting set-up is shown in Fig. 7.9. The holes for extraction of polyamide powder (Fig. 7.8) were closed by rubber and silicone tapered plugs. Gross leak testing was carried out to avoid significant leaks of resin. A filler feeding basin was built and the five filling openings were connected to the feeding basin by transparent plastic tubes. Two litres of resin were finally poured for the outboard half of the frame structure. The same process was followed for the inboard half. The set-up operations lasted around 2 hours for each half frame structure and the process of pouring the resin lasted 5 minutes.

The resulting coil frame, combination of the 3D printed frame structure and casting with resin, is displayed in Fig. 7.10. According to the philosophy described in Section 6.3, the coil frame is split in two halves after casting, Fig. 7.11.

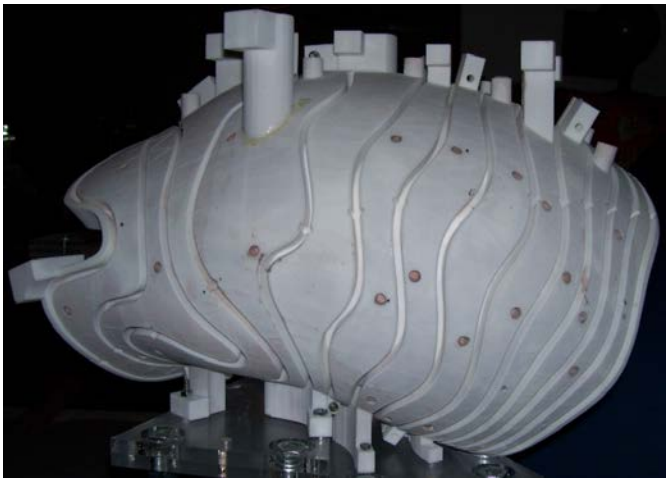

Fig. 7.10. Coil frame, combination of 3D printing and casting.

Fig. 7.11. Coil frame split in two halves.

7.1.3 Results, experiences learned and potential enhancements

The manufacturing of the first coil frame generated know-how and gave insight about the needed improvements for the design and production of the second coil frame. Results from the 3D printing of the frame structure and from the resin casting process are included next. The most relevant results and experiences learned are:

- Dimensional errors: The 3D printed frame structure has been accurately measured before and after filling with resin and compared with the design dimensions. The linear dimensional errors after casting are below ~±0.3 %. The deviations are higher than the recommended 0.1% [110,111]. Nevertheless, it may be acceptable if all the coil frames would have similar deviations, that is, if repeatability were kept among different pieces. **Improvements**: The online Shapeways company is the cheapest found. It was about three fold cheaper than the other companies consulted for the frame structure. A middle point of ratio quality/price might be better. Moreover, other companies may allow the fabrication of the frame structures in the

same 3D printer and with the piece located at the same position and orientation. Thus, the deviations among frame structures, the really important matter, might decrease to 0.2% or even 0.1%.

The design dimensions, the real measured values and the deviation of real and design values for the frame structure (Table 18) and for the coil frame (Table 19) are listed. Several measurements are performed for the same dimension to detect possible measurement errors.

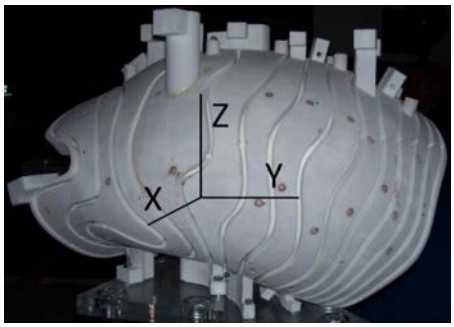

Fig. 7.12. Indication of measurement direction for Table 18 and Table 19.

Measure mnemonic	Design value (mm)	Measured values (mm)	Average measure (mm)	Deviation (%)
1_Z_Outboard	230	230.25 , 230.2 , 230.5	230.3	0.13
2_Z_Inboard	230	230.5 , 230.25	230.38	0.17
3_Z_Outboard	240	240.3 , 240.25 , 240.25	240.27	0.11
4_Y_Outboard	203.525	203.0 , 203.1 , 203.0	203.03	-0.24
5_Y_Top	195.85	195.2 , 195.2	195.2	-0.33
6_Y_Top	220.4	219.45 , 219.4 , 219.5	219.45	-0.43
7_Y_Inboard	244.22	243.2 , 243.25	243.23	-0.41
8_X	216.41	216.75 , 216.8	216.78	0.17
9_X	120.79	120.65 , 120.7	120.68	-0.09

Table 18. Comparison of design dimensions and actual dimensions of the frame structure (before casting).

Measure mnemonic	Design value (mm)	Measured values (mm)	Average measure (mm)	Deviation (%)
1_Z_Outboard	230.3	230.5 , 230.5 , 230.4	230.47	-0.07
2_Z_Inboard	230.38	230.5 , 230.5 , 230.8	230.6	-0.09
3_Z_Outboard	240.27	240.25 , 240.2	240.22	0.02
4_Y_Outboard	203.03	203.25 , 203.3	203.27	-0.12
5_Y_Top	195.2	195.8 , 195.8	195.8	-0.31
6_Y_Top	219.45	220.2 , 220.25	219.22	0.10
7_Y_Inboard	243.23	244.15 , 244.1	243.12	0.05
8_X	216.78	216.9 , 216.8	216.7	0.04
9_X	120.68	120.6 , 120.45 , 120.55	120.53	0.12

Table 19. Comparison of design dimensions and actual dimensions of the coil frame (after casting).

- 3D-printing nylon powder remained in the interior of the frame structure, mainly in the legs and in the narrow inter-groove spaces. Extraction of most of the remaining powder from the interior of the frame structure was performed by means of a kind of glovebox equipped with an air compressor. Some powder still remained in some inter-groove spaces. Full extraction of the internal powder is necessary to completely fill the interior of the piece with resin. Otherwise, parts of the piece are weak due to the discontinuity of the resin structure. **Improvement**: Define more holes at the legs, near inter-groove spaces and at the internal part of the lateral of the frame structure (laterals shown in Fig. 7.5 and Fig. 7.6).
- Major thermal warping was not observed.
- Filling the inside of the frame structure with resin was simple and effective. Leaks did not occur.
- An anticipated issue occurred when filling the top legs. The powder extraction holes were closed by silicone tapered plugs and air in the top inverted legs could not escape. Theory of casting [136,151] indicates the need of venting holes and conduits. **Solutions**: The solution was to manually slightly open the plugs and allow air to scape until a little resin leaked through the hole. However, care will be required when casting with epoxy resin, since such leaks are difficult to clean. The attachment (or 3D printing) of thin vertical vents attached to the powder extraction holes of the top legs is another planned improvement.
- The cost of the 3D printed frame structure was 700 €. It is considered satisfactory for UST_2 and for larger devices due to the particular hollow structure utilised.
- The sparse factor (volume of material / volume of the piece) is ~ 1/7. The value is considered satisfactory since the high cost of 3D printing is much reduced. The reduction will be even higher for larger stellarators since the 3D printed surfaces have to be thicker than 0.7 mm due to requirements of this particular additive manufacturing process, printers and company. The surfaces consume most of the nylon in the frame structure. The truss structure without external surfaces is much lighter.
- The planned TXL 10 copper conductor adjusted correctly in the groove. Fasteners will not be needed to fix the conductor in place during winding.
- About 4 hours were used to prepare and cast the two halves of the coil frame. The production of 2 – 4 coil frames in a batch, taking advance of the know-how from the first coil frame, may last less than two hours per coil frame. It is a reasonable worktime at say 80 €/hour labour cost.

The publication Ref. [152] reports the concept of 3Dformwork, the manufacture procedure and the results corresponding to the work on the UST_2 coil frame.

7.2 Vacuum vessel

The selected alternative for the fabrication of the curved vacuum vessel sectors (Fig. 6.14) is the resin reinforced liner. The concept of resin reinforced liner is described in Sec-

tion 6.4. The detailed procedure for the construction of a curved vacuum vessel sector is described next.

- A plaster form having the shape of half curved VV sector (Fig. 7.13) is generated from a 3D printed plastic mould.
- Each curved vacuum vessel sector is formed by to halves in order to easily shape the surface on the plaster form (Fig. 7.13 and Fig. 7.14).
- Strips of copper (Fig. 7.13) are designed to cover the surface of the vacuum vessel. The strips are cut manually as a matter of test but should be cut by a water jet.
- The strips are shaped manually. Fasteners and bolts help to locate and bend the strip previous to soldering.
- The consecutive strips are overlapped and soldered by Sn-Ag(3%).
- A half sector is finished, Fig. 7.14. Later the second half sector is fabricated.
- The lateral borders of the halves are pre-tinned with Bi-Sn solder paste, Fig. 7.14.
- Two flanges are soldered at both sides of the curved VV sector. Therefore, the different sectors of the vacuum vessel can be joined by o-rings. The flanges are water jet cut.
- The two halves are joined by fasteners and the two end flanges are soldered, Fig. 7.15.
- Both halves are soldered by low temperature Bi-Sn solder in order to avoid unsolder the strips and flanges, Fig. 7.16.
- The liner for the curved VV sector is finished.
- An iterative process of leak testing and leak repair is produced. Different consecutively leak testing methods are used: light for large leaks, water in the vacuum vessel for middle leaks and, pressurised air with the vessel inside a water container for smaller leaks. Helium leak testing was unavailable.
- After leak testing, a grasping element is soldered by Bi-Sn solder on the exterior of the surface. Brass ball chain was selected as a simple element acting as claws, Fig. 7.17. Claws are needed for the attachment of the liner to the reinforcement resin. Gluing alone is unreliable due to differential thermal expansion coefficients.
- The liner of the vacuum vessel is leak tested again.
- The solder junctions among strips are externally covered by a series of thin strips of glued foam, Fig. 7.18. The objective is to allow some leak testing of the vacuum vessel sector after covering the liner with epoxy resin. If a leak appears below the resin it would be extremely difficult to find if not impossible. In such case the vacuum vessel sector would be inoperative.
- The liner equipped with claws is covered by a 3D printed mould (Fig. 7.19), which defines the external surface of the resin reinforcement.
- Epoxy resin is poured in the mould. The vacuum vessel sector is finished, Fig. 7.20.
- Fig. 7.21 shows attachments to allow joining the consecutive curved vacuum vessel sectors at the bean shape side.

The central vacuum vessel section is fabricated by conventional cutting and soldering copper sheets. Fig. 7.22 shows the central vacuum vessel section. The flanges are water jet cut.

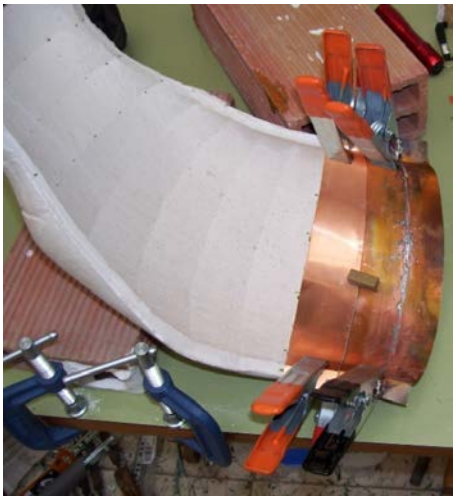

Fig. 7.13. Shaping, fixing and soldering strips on the plaster form.

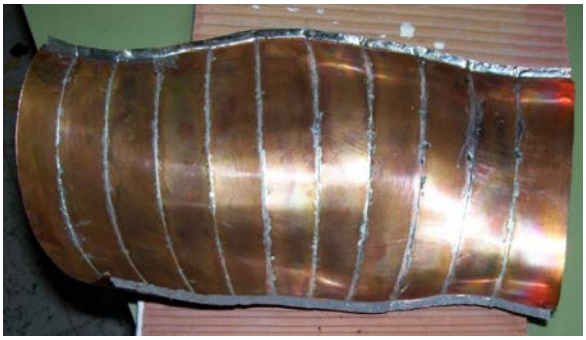

Fig. 7.14. Finished half vacuum vessel sector. It is pre-tinned at the lateral ribs with Bi-Sn solder.

Fig. 7.15. Fixations to solder the large flange on the joined halves.

Fig. 7.16. Soldering the two halves from the interior of the vacuum vessel sector with Bi-Sn.

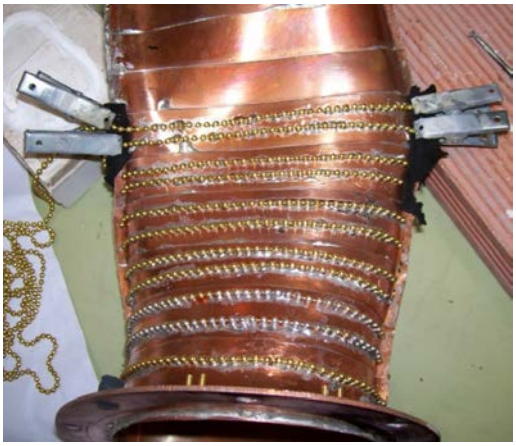

Fig. 7.17. Soldering brass ball chains acting as claws, with Bi-Sn solder.

Fig. 7.18. Finished liner prepared for external resin casting. Shelf-gluing foam strips are located on solder lines.

Fig. 7.19. Casting epoxy resin in the 3D printed nylon mould.

Fig. 7.20. Finished curved vacuum vessel sector.

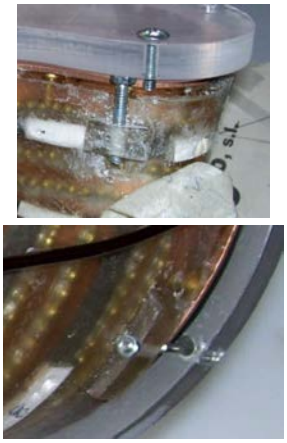

Fig. 7.21. Flange and attachments to join vacuum vessel sectors.

Fig. 7.22. Central vacuum vessel section.

7.2.1 Results, experiences learned and potential enhancements

The production of the curved VV sector was totally prototypical. Thus, the results have been modest and many details require improvement. In contrast, several tests were performed before attempting the fabrication of the first full coil frame.

In spite of the difficulties during production, insight has been obtained for the possible manufacturing of convoluted vacuum vessels by other innovative methods. For example, the production of the external resin reinforcement would be similar to the production of a resin structure for internal electrodeposition. Also, the flanges would likely be similar. The

potential methodology enhancements have been clarified. The most relevant experiences learned and results from the liner vacuum vessel construction are:

- The maximum dimensional errors observed for the liner and the external surface of the vessel are ~±2 mm, about 1 % of the vacuum vessel dimensions. It is acceptable if the global design is performed to cope with such deviations.
- Leaks have not been observed at the curved vacuum vessel sector.
- One small leak at the central VV section was not totally closed. The junction between the port and the oval shape of the central VV section is difficult to solder since the flanges hinder the access for soldering from the outside. The design of the central VV sections should be improved.
- The attachments (Fig. 7.21) planned to join the pairs of curved sectors in order to form a full period were correctly cast. However, as expected, the access to the bolts located inside two contiguous coil frames is very difficult and only a special mechanism would allow releasing the bolts from the exterior of the coil frames.
- Different release agents for the 3D printed mould (Fig. 7.19) were tested: polyvinyl alcohol (PVA), furniture waxes, silicone release agent, butter, and candle wax. Candle wax and butter resulted the best for the very porous 3D printed nylon mould, Fig. 7.19. Finally the interior of the mould was covered by candle wax. The mould released properly.
- The lateral ribs of the 3D printed nylon mould should be improved. Initially the mould was thought for introduction inside the coil frame during casting. So, the ribs were narrow. At the end, the mould was not introduced in the coil frame during casting due to the risk of catastrophic resin leaks inside the coil frame. It forced the use of epoxy glue at the lateral closure ribs for mould tightness. Opening the mould was feasible but some flaws were produced to the mould during opening.
- The manufacturing of the curved VV sector was time consuming, as expected. It compels to attempt other alternatives, like electrodeposition inside epoxy resin or electroforming, see Table 13.
- The cost of materials for the curved VV sector was low, only about 100 €. Most of the cost is labour cost. The technique may be more appropriate for large vacuum vessels since the worktime would be only moderately higher.

7.3 Coil winding

The winding procedures are similar in UST_1 stellarator and UST_2. The conductor is compressed on the laterals of the grooves to avoid unwinding during the winding process. In UST_2 three layers and only one turn per layer are wound, see Section 6.2.2.
Special care was taken in UST_2 for the design of crossovers. Electric coil crossovers are connections or paths of electrical wire communicating different winding turns, or feeder busbars with turns. Differences among the magnetic field produced by different coil frames should be lower than 0.01% [112,113]. Different types of crossovers are possible to avoid as much as possible magnetic errors due to the crossovers. However, the use of only one

turn per layer in stellarator coils is novel and thus, appropriate crossovers are unidentified. Therefore, a brief study of the current crossovers and the test of a new concept is described next.

7.3.1 Alternatives for crossovers and selection

7.3.1.1 Crossovers for a double pancake

A. Fig. 7.23 shows a crossover disposition for a double pancake, that is, two contiguous pancakes wound in opposite direction starting from the bottom of the groove and ending in two parallel busbars. It is the disposition used in UST_1 stellarator. For UST_2 a double pancake is unfeasible since single pancake coils are defined.

B. Fig. 7.24 shows a disposition of two crossovers for to contiguous single pancakes. This configuration is impossible for UST_2 since independent single pancake coils are defined.

C. Fig. 7.25 shows a zig-zag crossover. The coil is wound from the bottom to the top of the groove layer by layer, crossing the centreline of the winding pack each two turns of the conductor. Again this configuration is unviable for UST_2.

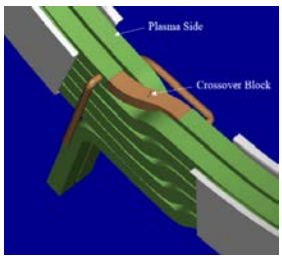

Fig. 7.23. Crossover disposition for a double pancake. Source of figure [153].

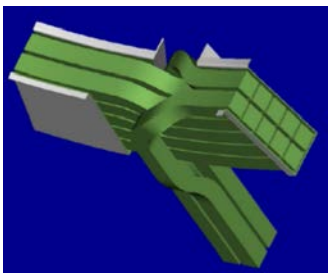

Fig. 7.24. Two single pancakes crossover disposition. Source of figure [153].

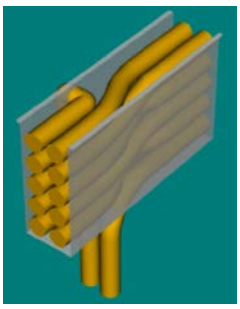

Fig. 7.25. Crossover disposition in zig-zag. Source [153].

7.3.1.2 Crossovers for a single pancake

After thinking and testing some concepts, a named split conductor crossover was devised. The ***split conductor crossover*** consists on cutting certain length of the insulator of the conductor longitudinally by the centreline, splitting the filaments in two identical parts, separating the two bunches of filaments, passing the conductor turns inside the opening between bunches, and finally restore the circular shape of the conductor by a heat-shrink sleeve. The process and result is displayed in Fig. 7.26.


Fig. 7.26. Winding process through the opening between copper filament bunches (left). Finalised winding of three turns. The heat shrink sleeve was not heated yet in this picture, (right).

A named *cylindrical indentation,* which aims at the accurate positioning of the crossover, is designed at each groove. The objective is to locate the magnetic perturbation from each crossover at the same position and orientation in all the coil frames. Thus, the stellarator symmetry will be kept as perfect as possible. The cylindrical indentations are located at different poloidal positions, following a path different to the magnetic field lines, to try to decrease localised perturbations. Fig. 7.27 shows four cylindrical indentations. Fig. 7.26 displays the installation of the conductor in the cylindrical indentation.

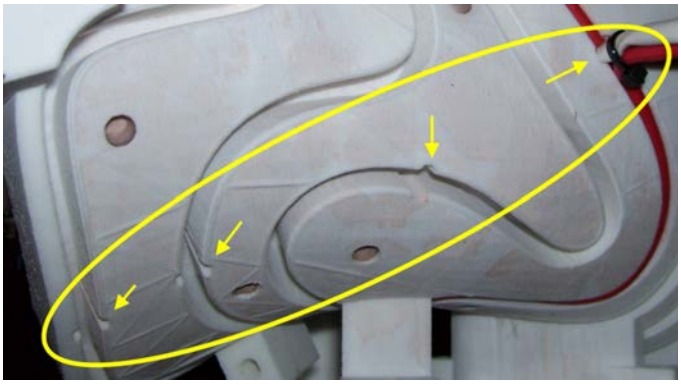

Fig. 7.27. Cylindrical indentations defined at strategic positions in the groove.

7.3.2 Magnetic field errors due to crossovers

Numerical calculations to assess the order of magnitude of the magnetic perturbation produced by the UST_2 crossovers are carried out. Only an estimation is obtained since the model does not replicate exactly the real crossovers. Only calculations for the crossover for the coil number 3 (Fig. 7.27 third coil from left) are performed. The crossover is modelled in CASTELL as a Perturbed CoilSystem that can be composed of arbitrary coils and straight segments.

Model for the estimation of magnetic errors: The filamentary coils (Fig. 7.28 to Fig. 7.35, in black) carry a filamentary current $I_f = 18900$ A-turn that would generate $\langle B_0 \rangle = 1$ T. Therefore, $\Delta B/B$ for such conditions is approximately the value shown in the legend in Fig. 7.30, Fig. 7.33 and Fig. 7.36. The current in each copper bunch (Fig. 7.26) is six times lower than I_f (3 turns per coil and conductor split in two copper bunches). Therefore, the real perturbation will be around six times lower. The real perturbation is located 4 mm nearer the LCFS than the modelled perturbation since the real perturbation

is located at the deeper coil turn and the model locates the perturbation at the central filamentary coil. Three models have been created to better understand the influence of different crossovers on the magnetic field errors. Perturbation currents modelled at the crossover position (Fig. 7.27) as perpendicular currents to the filamentary coil, with currents in opposite directions (Fig. 7.28), is the most similar model to the real perturbation from the coil number 3. The model with a dipole having currents parallel to the filamentary current is shown in Fig. 7.31 and Fig. 7.32. Finally, the model with perturbation currents located perpendicular to the filamentary coil, with currents in the same direction is shown in Fig. 7.34 and Fig. 7.35. The model of current for the three cases is a straight segment of 3.5 mm length. The distance between currents in the parallel dipole (Fig. 7.31) is 7mm.

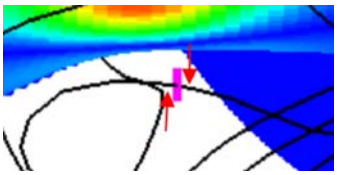

Fig. 7.28. Perturbation currents perpendicular to the filamentary coil.

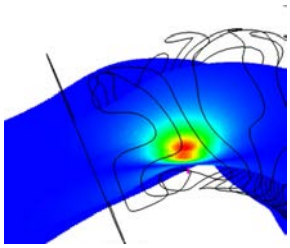

Fig. 7.29. Position of perturbation shown in Fig. 7.28.

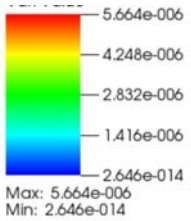

Fig. 7.30. Results obtained for the case in Fig. 7.28.

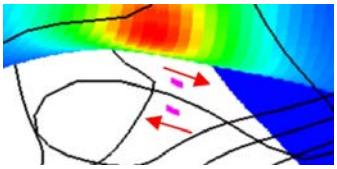

Fig. 7.31. Dipole parallel to the filamentary conductor.

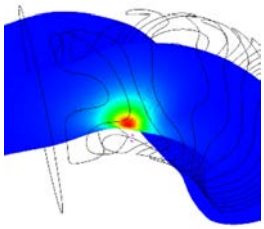

Fig. 7.32. Position of perturbation shown in Fig. 7.31.

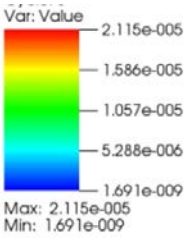

Fig. 7.33. Results obtained for the case in Fig. 7.31.

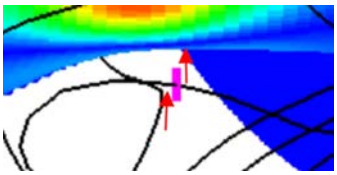

Fig. 7.34. Perpendicular currents in the same direction.

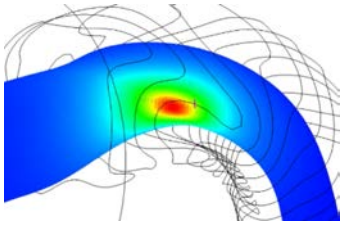

Fig. 7.35. Position of perturbation shown in Fig. 7.34.

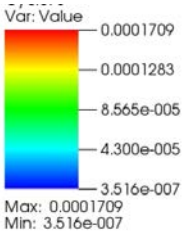

Fig. 7.36. Results obtained for the case in Fig. 7.34.

7.3.2.1 Magnetic field errors due to UST_2 crossovers

Fig. 7.30 shows the result for the estimation of magnetic errors due to the UST_2 crossovers. The maximum error $\Delta B/B$ is lower than 10^{-4}, an acceptable value, [68,113]. Moreover, in UST_2, due to the cylindrical indentation, the geometrical differences among the same crossover for different halfperiods will be low. It reduces the differential magnetic errors among halfperiods.

7.3.3 Winding process and modular coils

Thin wall isolation wire type TXL 10 was ordered and received to assemble two coil frames. However, standard copper flexible wire of 4 mm^2 section was wound for the first coil frame for the e-beam experiments. So, should the conductor be unwound to access to the curved VV sector, the expensive thin wall TXL 10 wire would not be damaged due to the process of winding and unwinding.

The winding process for the 14 modular coils lasted 3 hours. The result of the winding process is displayed in Fig. 7.37.

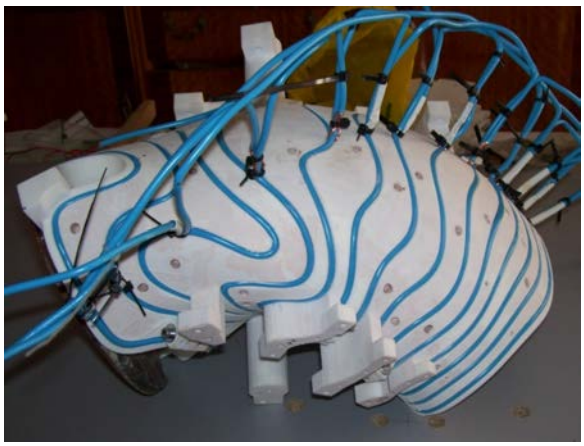

Fig. 7.37. Result of winding 14 modular coils with provisional standard copper conductor.

7.3.4 Results and experiences learned from coil winding

The winding of the modular coils resulted simple and fast, as planned and tested. The results and experiences learned are:

- The winding of the 14 coils lasted only 3 hours. It is an outstanding result. The experience gained during UST_1 development and the use of only one turn per layer allowed the fast process.
- The last turn slightly unwind at some few points due to the lack of pressure from the groove wall. A shim was added and the issue was solved. In any case, it indicates the need of an external pressure cover, or epoxy impregnation of the winding packs, in order to withstand future large magnetic Lorentz forces.
- The split conductor crossover resulted a satisfactory concept. Handling the cable through the opening required only few extra minutes of work. Splitting the copper filaments in two identical bunches was not performed with the maximum possible accuracy, i.e. counting the number of filaments.
- Residues of nylon powder were observed after winding in one groove. Thus, the winding pack was not totally well referenced to the bottom of the groove. Then all the grooves were better inspected and brushed. The coil was unwound, the groove cleaned and the coil wound again.

7.4 Assembly and positioning

The coil frames are assembled contiguous (Fig. 7.1 and Fig. 7.38.) and located on a mechanised circular base to form a full toroidal frame. Consecutive coil frames of a stellarator period are rotated 180º with respect a horizontal axis and located on the respective legs to achieve stellarator symmetry, Fig. 7.38.

Two tables (Fig. 7.38 and Fig. 7.39) are conceived and designed to support each halfperiod. The large excursion of the magnetic axis suggested the use of two tables of different height. Otherwise, the 3D printed legs would have been too long and the strength would have been compromised. The legs are located at the interspaces among contiguous modular coils. Some interspaces are narrow, resulting in slender legs.

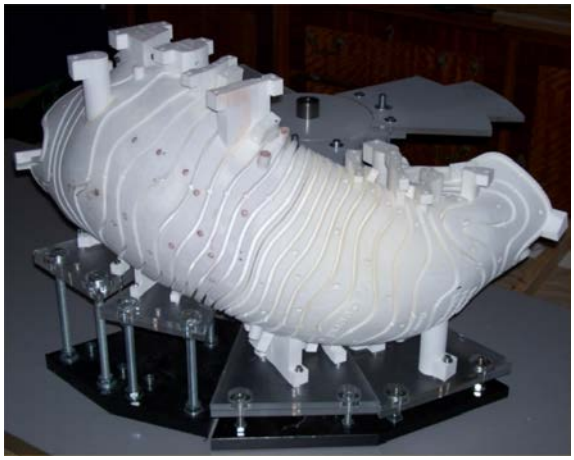

Fig. 7.38. Assembly of two coils frames on the tables.

The positioning strategy for UST_2 coil frames uses some of the remote handling techniques utilised in JET and ITER, like for example edge guides [154]-p.32. Though the assembly of UST_2 is performed hands-on (not remote handling), the UST_2 assembly is fast due to the particular disposition of the elements. The inboard of the coil frame is equipped with two 3D printed positioning stops, Fig. 7.39 and Fig. 7.40. The stops contact on a central circular ring located in the central torus hole at the equatorial plane of the stellarator.

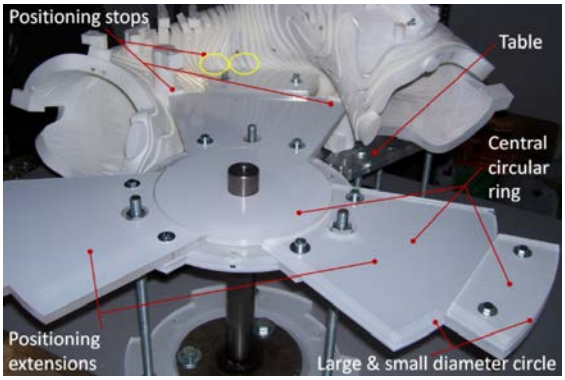

Fig. 7.39. Central circular ring and positioning elements.

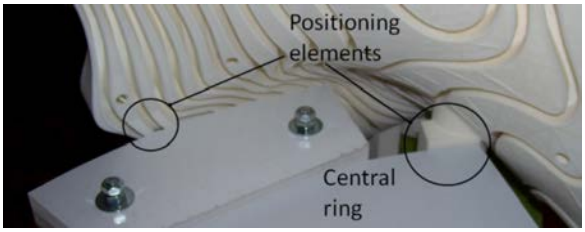

Fig. 7.40. Detail of the 3D printed positioning elements.

Each table lays on a flat smooth circular base of slightly larger diameter than the external diameter of the torus, Fig. 7.46. The circular base is free of obstacles to allow unrestricted horizontal sliding of the tables on the base, Fig. 7.41. The coil frame, located on two contiguous tables, moves freely on the circular base until the positioning stops contact with the central circular ring, Fig. 7.42. At this position, the coil frame has only one turning degree of freedom defined by the stops on the central circular ring. The position of each coil frame is finally completely defined when all the coil frames are located around the central circular ring by successive horizontal movement of the coil frames. This assembling procedure is facilitated if straight mirror sections and large planar coils between periods are designed, as in UST_2 stellarator.

Several particular features are implemented in UST_2 for positioning. The central circular ring (Fig. 7.39) is formed by several bolted pieces to allow the vertical extraction of the central ring. It facilitates the access to the inboard of the coil frames. The central ring contains three positioning extensions since UST_2 is a 3 period stellarator. The positioning extension has two different diameters because the UST_2 magnetic axis viewed from the top is triangular, very different from a circle. One positioning stop contacts with the larger diameter circle of the circular ring and the other positioning stop contacts with the smaller circle, Fig. 7.40.

Fig. 7.41. Flat smooth base and sliding tables on the base.

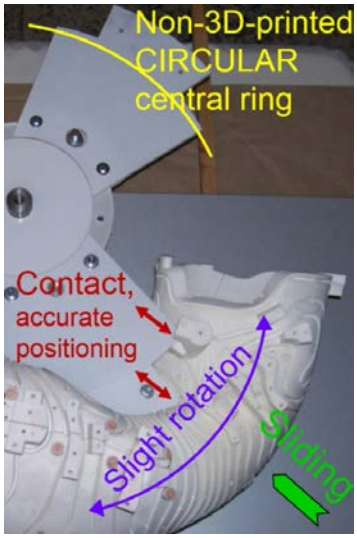

Fig. 7.42. Positioning elements and positioning procedure.

The coil frame is generated as two independent volumes through a parting line, Fig. 6.7. Fig. 7.43 shows the two halves of the coil frame required for assembly. Later, the vacuum vessel is introduced in one of the coil frame halves, Fig. 7.44. Finally, the coil frame is closed with the second half of the coil frame, Fig. 7.45.

Fig. 7.43. Coil frame halves.

Fig. 7.44. Introduction of the VV in one half coil frame.

Fig. 7.45. Closure with the second half coil frame.

The assembly concepts for UST_2 stellarator and the results have been reported in the publication Ref. [155].

7.5 Materials cost

The total cost of the materials for the first halfperiod (coil frame and vacuum vessel sector), copper conductor, one frame structure for the second halfperiod, the four tables for the coil frames and the base of the stellarator, has been ~2400 €. A 10% increase is included to consider minor unaccounted elements.

Element	Cost (€)
Two 3D-printed frame structures	1400
Material for straight vacuum vessel sectors	110
Epoxy and acrylic resin	150
TXL 10 wire	100
Set of tables for two half-periods	90
Circular base	150
Other	400
TOTAL (cost of installed materials)	**2400**

Table 20. Cost of installed materials up to the current construction status.

The instruments, tools, permanent moulds, research materials and elements not utilised yet in UST_2 construction accounted for 3300 €.

The cost of the raw materials for the UST_2 stellarator alone is negligible compared with the cost of the R&D time. It is common in most of the one-of-a-kind complex small devices. In the case of UST_2 stellarator, the device is small, a substantial part of the work is devoted to the research of reduced cost construction methods, the batch produced is only one piece, and the productive process is still in the first stages of R&D. Therefore, almost the full cost corresponds to the research, development and tentative production time.

7.6 Status of the UST_2 construction

Two of the 6 frame structures have been 3D printed and one frame structure has been filled with resin. The base and the central circular ring have been respectively milled and laser cut. A curved VV sector and a central VV section have been satisfactorily manufactured. The curved VV sector has been introduced in the coil frame and the coils have been wound. The central circular ring, the tables and the coil frames have been installed on the base. The finished halfperiod and one frame structure are displayed in Fig. 7.46. The feeder cables were not connected yet when the picture was taken.

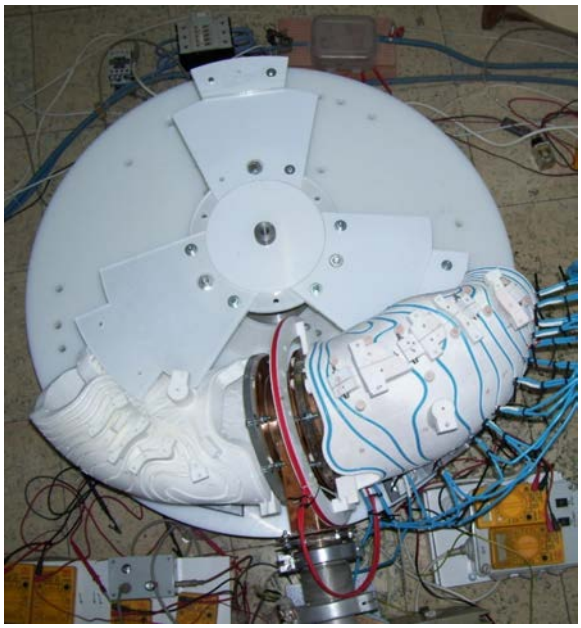

Fig. 7.46. Finished halfperiod and one frame structure.

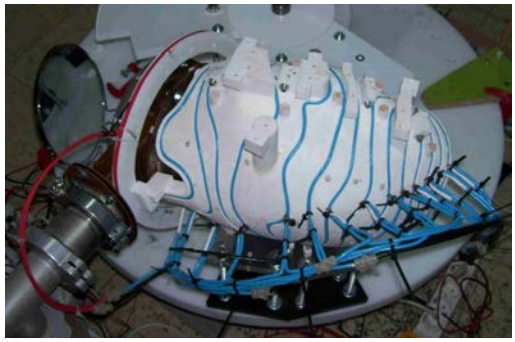

Fig. 7.47. Detail. Cable connections are finished.

The vacuum system is the same as for UST_1 stellarator, Fig. 7.48. The elements of the vacuum system are listed in Section 2.5. Fig. 7.49 shows the construction status during electron beam field line mapping experiments, and the author.

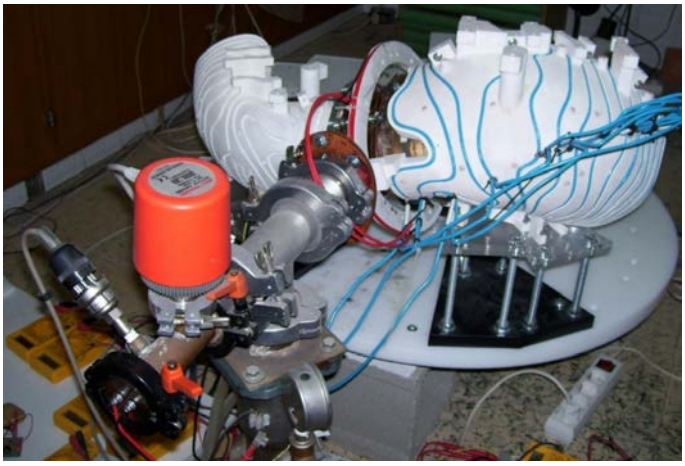

Fig. 7.48. Some elements of the vacuum system and coil frame.

Fig. 7.49. Part of the systems and the author.

7.7 Summary of results from the engineering design and construction

- A hollow 3D printed piece made as a truss structure covered by a thin 3D printed surface has been CAD designed and 3D printed. It was printed in polyamide 12 (a type of nylon) by SLS additive manufacturing.
- The 3D printing cost of the frame structure was 700€.
- The frame structure was satisfactorily internally cast with a mixture of acrylic resin and hard plaster.
- The linear dimensional errors of the coil frame are below ±0.3%, still excessive.
- A curved vacuum vessel sector was fabricated as a resin reinforced liner.
- The liner is composed of two longitudinally soldered halves made by copper strips manually shaped on a form.
- The liner is externally reinforced by epoxy resin. Liner and resin are attached by soldered brass ball chain, which acts as claws.
- The manufacturing of the curved VV sector was time consuming.
- Maximum dimensional fabrication errors of the curved VV were about 1%.
- A crossover is defined as a conductor split in two copper filament bunches. The conductor pass through the opening created by the two bunches. The design is appropriate for single pancake coils.
- The magnetic field errors from the crossover for three turns per coil are acceptable.
- Winding the coils was fast and accurate.
- The positioning of the coil frames to form the torus is based on coil frames sliding on a flat smooth surface until contact on a circular central ring. The property of circularity of the central ring is essential for a simple and accurate positioning.
- Satisfactory assembling and positioning of the halfperiod have been demonstrated.
- The cost of materials for the first halfperiod, the copper conductor, one frame structure for the second half-period, four tables and the base of the stellarator, has been 2400 €.

7.8 Conclusions

The manufacturing of a coil frame and a vacuum vessel sector have been satisfactorily completed. They are the two main components of one UST_2 halfperiod. By means of the gained know-how, the manufacturing of the next coil frames will be fast and of reduced cost. The assembly of the different components has been successfully produced. However, the question whether each phase of the work has been correct arises. An experimental validation of the design and construction would be beneficial so as to increase the certainty about the quality of the concepts, design and construction. The result could be inaccurate or totally wrong if only one mistake during the long process would have been occurred. The next chapter deals with a preliminary validation of the performed work.

Chapter 8

E-beam field mapping experiments for validation

The electron beam field line mapping experiments performed to measure the performance of the construction methods and UST_2 design are described in this chapter. The experimental set-up, the experiments carried out and the comparison of experiments with calculations is summarised next.

Typically, e-beam field line mapping experiments [90] are performed so as to prove the existence of correct magnetic surfaces in a stellarator. Such experiments are unfeasible if only one halfperiod of stellarator is available since the electrons cannot turn toroidally. However, to some extent the validation still may be possible in only one halfperiod of stellarator. For that, an e-gun would be located at one end of the halfperiod and the reception of the e-beam at the other end of the halfperiod. The comparison of the experimental results with calculations may supply evidence that the construction has achieved certain level of accuracy and that there are not major mistakes in the design and construction of UST_2.

The geometrical deviation among periods of a stellarator should be lower than 0.1% (see Section 3.2.3) for good confinement. Such deviations cannot be measured with the means available in UST_2 facility in only one halfperiod of stellarator. In UST_1 the fluorescent points from the 'E-gun 2' (Fig. 8.2) were about 3 mm in diameter and they were not perfectly circular. This phenomenon alone hinders higher accuracy than about ±1 mm.

Therefore, the objective of the current experiments is only to estimate the deviation between the calculated magnetic field lines and the actual experimental magnetic field lines, and to show that major flaws in the design and construction did not occur.

8.1 Experimental set-up

The concept of an e-gun at one halfperiod end and reception of fluorescent points at the other halfperiod end is implemented with an oscillating e-gun (Fig. 8.1) and a fluorescent screen (Fig. 8.3 and Fig. 8.4). The coils of the halfperiod of the stellarator (Fig. 8.3) act as deflexion coils. The coils are energised during a pulse of 2 s. Due to e-gun oscillation, the

e-beam is emitted from a series of points forming an arc (Fig. 8.11) on a plane perpendicular to the magnetic axis of the plasma. The plane of the fluorescent screen is located perpendicular to the magnetic axis at the high field region of the coil frame, Fig. 8.12. The set-up is somewhat similar to the structure of an old CRT television.

A very simple mechanism is utilised for the oscillation of the e-gun. A non-magnetic stainless steel M3 threaded rod supports the e-gun at one end and non-magnetic counterweights are located at the other end. The set is balanced on thin tips at an intermediate point, Fig. 8.1. The distance from the e-beam to the oscillation point is 104 mm. One bit of the counterweight is ferromagnetic. The influence of the ferromagnetic bit on the magnetic field is neglected. The system is equilibrated to hold the threaded rod in horizontal position. A magnetic short impulse on the ferromagnetic part is supplied from the exterior of the vacuum vessel by a permanent magnet. The e-gun starts a free oscillation of about 1 Hz. The oscillation of the e-gun is damped by the thin feeding copper wires but it lasts enough for the duration of the pulse. The e-gun used for the experiment is the model 'E-Gun-2', Fig. 8.2. This e-gun was used in UST_1 stellarator for the first e-beam field line mapping experiments. The e-gun is built from a cut 10 W 12 V commercial halogen light bulb introduced in an internally blackened metallic cover. The extraction hole is 1.25 mm diameter and the distance from the filament to the extraction hole ~0.75 mm. The acceleration voltage is set to have enough bright of the fluorescent points to be recorded by the camera. Acceleration voltage of 59.6 V was used for the present e-beam experiments.

The fluorescent screen is painted with doped ZnO fluorescent powder type P-24-GE, deposited on the surface by a methanol-powder solution. The stock of powder was only around 3 grams. It was decided to paint only some lines on the screen, and not the full screen, in order to save fluorescent powder. The lines are enough to obtain some points on the screen and to compare with the numerically calculated points.

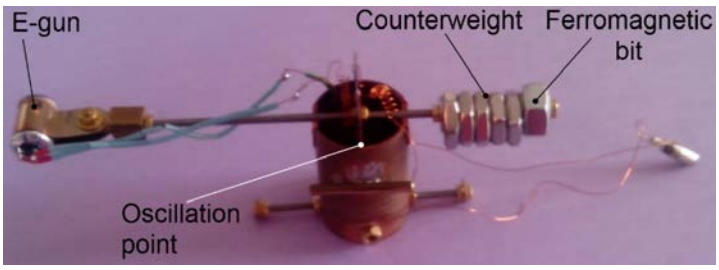

Fig. 8.1. Arrangement of the oscillating e-gun.

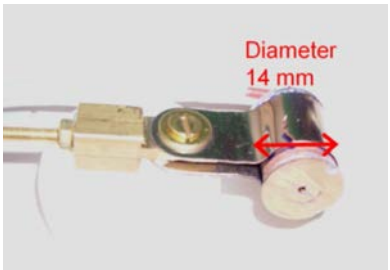

Fig. 8.2. E-gun model 'E-Gun-2' used for the experiments.

The camera is a mobile phone camera of resolution 960x720 pixels. A mirror focussed on the e-gun is utilised in order to synchronically measure the position of the fluorescent points and the e-gun in a sole frame (Fig. 8.4). If two cameras were used, then, either the frame rate would be high to allow good simultaneous resolution in space and time, or the cameras would require an enable sampling signal for frame synchronism. It is intended to avoid any of both alternatives. Simplicity is one of the intended results of the work.

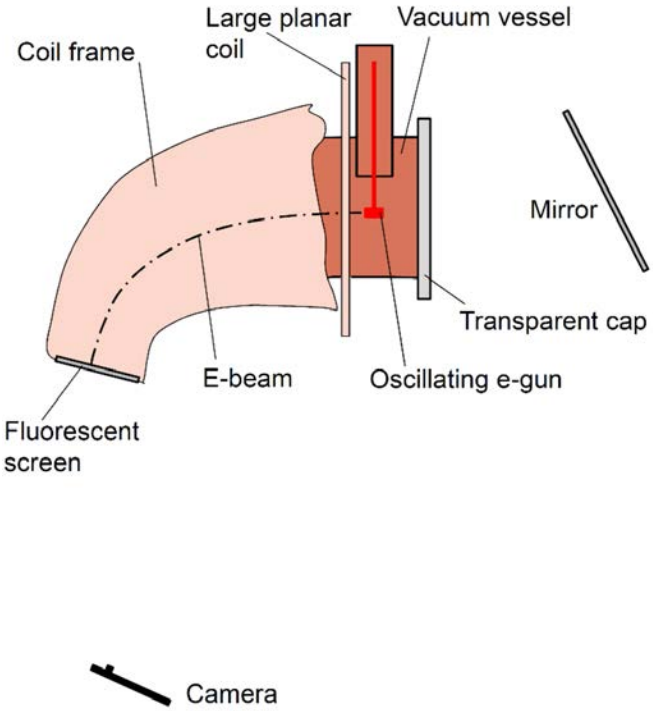

Fig. 8.3. Field line mapping experimental set-up.

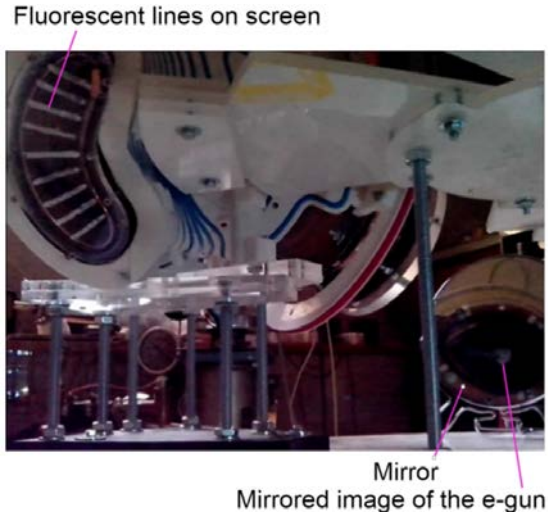

Fig. 8.4. Experimental set-up indicated on a frame of the video recording.

8.2 E-beam field line mapping experiments

A series of experiments were carried out by means of the experimental set-up. All the systems in the UST_2 facility worked together for the experiments. The vacuum system, the e-beam system, the power supplies for one coil frame and the control system. The systems are the same as in UST_1 facility, Section 2.5. One halfperiod of the UST_2 stellarator was operative. The results obtained from the e-beam experiments are listed in Table 21. Videos of the fluorescent points were recorded. E-beam current is approximately 4 mA and tungsten filament heating voltage 9 V.

#	Date of experim.	t	I_{wire}	Pres-sure	U_{ac}	Result / comment
	Units	*s*	*A*	*Pa*	*V*	
11	22-06-2014	2		0.054	59.6	Pulse for batteries set-up
12	22-06-2014	2		0.054	59.6	First fluorescent points *(Video 185750)*
13	22-06-2014	2		0.064	59.6	2nd fluorescent points *(Video 194651)*
14	22-06-2014	2	152	0.064	59.6	3rd fluorescent points *(Video 195332)*
15	22-06-2014	2	152	0.083	59.6	4th fluorescent points *(Video 195659)*

Table 21. Conditions during the e-beam experiments.

Notes and legend:

t : Pulse length.

I_{wire} : Current in the conductor of the modular coils. The current in the conductor is measured from the voltage drop along one busbar cable that feeds the coils.

Pressure: Pressure in the vacuum vessel during the pulses. One small leak was not totally closed at the Central VV. This is one of the reasons of the poor vacuum level during the experiments. Also, wall conditioning was not carried out and pumping down lasted only two hours. The level of vacuum is acceptable for a short beam trajectory since the mean free path of 60 eV electrons is larger than 0.4 m, which is the distance from the e-gun to the screen.

U_{ac} : Acceleration voltage of the e-beam. U_{ac} is the considered electron energy for the CASTELL code calculations.

Pulses #14 and #15 gave acceptable fluorescent points. The frames containing fluorescent points for each pulse are overlapped and an image is generated.

Fig. 8.5 shows a frame of the video recording for pulse #15. The mirrored image of the the e-gun is visible at the right bottom of the image. Fig. 8.6 displays the overlapping of the consecutive frames whose detail is displayed in Fig. 8.7. The curved trajectory of the e-gun is also visible. The top point in Fig. 8.6 almost vanished due to the overlapping process but it is better visible in Fig. 8.7-right frame. Fig. 8.7 shows all the visible fluorescent points in the video recording. One fluorescent point faded due to the background light coming from the e-gun filament.

Fig. 8.5. A frame of the video recording containing one fluorescent point.

Fig. 8.6. Overlapping of the consecutive frames whose detail is displayed in Fig. 8.7.

The fluorescent points define a curve that is the transformation of the position of the e-gun by the rotational transform plus drifts of the guiding centre of the electrons. The drifts are caused by the magnetic field line curvature and magnetic field gradients. The trajectory of the e-gun is an arc of a circle of radius 104 mm (Fig. 8.1) since the distance from the e-beam to the oscillation point is 104 mm. Integration of the guiding centre orbits of electrons is performed by CASTELL code. The model in CASTELL code is summarised in the next section.

Fig. 8.7. Detail of the series of frames containing fluorescent points for pulse #15.

Certain inputs are needed for the CASTELL calculations. The position of the elements cannot be referenced to the vacuum vessel due to the variable gap between the vacuum vessel and the coil frame. It is an extra difficulty since the real positioning of the elements has to be measured by photographic metrology in relation to the coils.

Geometrical inputs needed for the CASTELL code are:

- The position of the e-gun in the neutral initial equilibrated horizontal position with respect the large planar coil. It is obtained by photographic metrology taking as reference the real large planar coil, Fig. 8.8.
- The e-gun traces an arc of 104 mm radius.
- The plane of oscillation of the e-gun. The plane is taken from the engineering design, not measured in the real device. The plane is tilted 0.3629 rad from the vertical at the centre of the straight plasma section and contains the absolute coordinate x-axis of the modelled stellarator in CASTELL. The acceleration hole of the e-gun is not exactly located on such plane due to the length of the e-gun. This deviation is neglected.
- The position of the fluorescent screen. The fluorescent screen is a cap of the vacuum vessel at the bean shape flange. The normal vector of the screen is obtained from the engineering design of the vacuum vessel. The position of the screen is photographed with respect the modular coils, not with respect the vacuum vessel.
- The direction of the current in the real device, Fig. 8.9. It is important since the electron drifts change direction when changing the direction of the magnetic field in the torus.

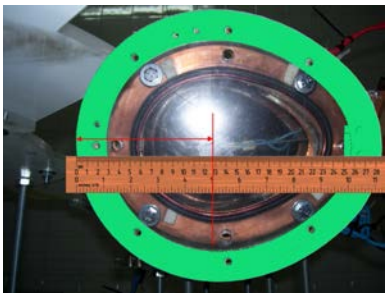

Fig. 8.8. Combination of photograph and designed large coil for metrology of position of the e-gun.

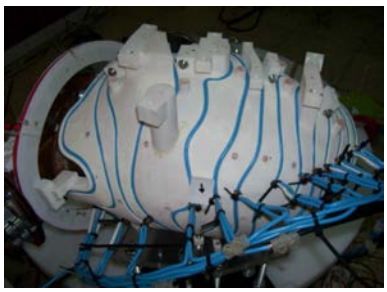

Fig. 8.9. The small arrow in the centre of the photo indicates the direction of the current for the pulses #14 and #15.

8.3 Calculations from CASTELL code

The objective is to compare the experimental fluorescent points with the calculated points under the same conditions. The numerical calculations are carried out by CASTELL code.

The inputs for CASTELL code are: The geometrical inputs listed in the previous section, the definition of the coils of one halfperiod coil frame, current in the conductor ($\mathbf{I}_{wire}$) indicated in Table 21, the acceleration voltage (energy of the electrons), and the number of turns of the coils: the large coil has 4 turns and the modular coils 3 turns. The coils are connected in series.

The model in CASTELL code considers:

- A source of electrons of 59.6 eV and pitch 0 (zero tangential component) is modelled.
- 23 electrons are initialized from equidistant points located on an arc identical to the measured for the real e-gun, Fig. 8.10 and Fig. 8.11.
- Only the 15 coils corresponding to one halfperiod are loaded for the model. One large coil and 14 modular coils are modelled, Fig. 8.10.
- I_{wire} is considered as a reduction of a reference MagneticGrid created by 1000 A in the conductor. Therefore, the scale factor used is 0.152 corresponding to I_{wire} = 152 A, Table 21.
- The sign of the modelled current is properly set. It is concluded that the modelled current is negative for the modelled pulse #14 and #15 due to the order of generation of the points defining the coils and from Fig. 8.9.

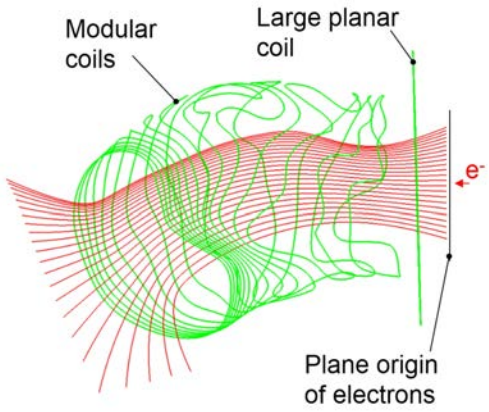

Fig. 8.10. Different elements modelled in CASTELL code.

- The simulation method is set to orbit integration with electron drifts due to magnetic field effects.
- A virtual screen is modelled as a plane located at the same real position of the fluorescent screen, Fig. 8.12. The intersection between the trajectory of each electron and the screen is detected, stored and represented graphically with a similar Java method as the one used for the generation of Poincaré plots. The normal vector to the plane in Cartesian coordinates is (-0.7145 , 0.4125 , -0.5650) m and a point of the plane is (0.16651 , 0.28475 , -0.000903) m in the global coordinates of the modelled stellarator.
- The length of the simulation is set short, only 1000 integration steps, in order to have electron trajectories crossing the virtual screen and some small excess.

It should be noted that the magnetic field in the vacuum vessel under such conditions is not the same as the future magnetic field generated by the full UST_2 stellarator. There are

not magnetic surfaces since the full stellarator is not complete and thus, the magnetic field lines are opened, Fig. 8.10. Nevertheless, the model in CASTELL code is as identical as possible to the real experiment and both results should agree.

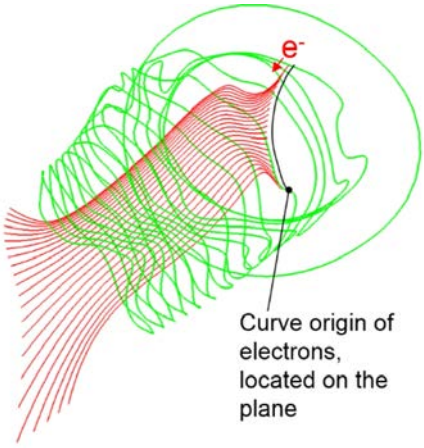

Fig. 8.11. Modelled arc followed by the e-gun.

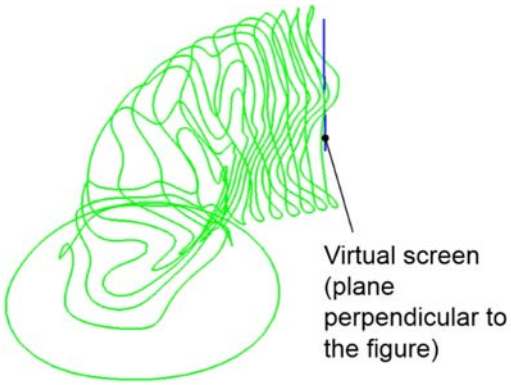

Fig. 8.12. Position of the modelled virtual screen.

8.3.1 Result

The computed intersection of the electron trajectories with the virtual screen for the conditions of experiment #15 is shown in Fig. 8.13.

The graphical representation requires certain conditions and extra information in order to allow a correct overlapping with the experimental fluorescent points. Such information is listed next:

- Fig. 8.13 includes the filamentary representation of the modular coil number 14 (the last coil at the bean shape) in green. The UST_2 winding pack of 3 turns is represented by a central filament in the typical UST_2 model.
- Two lines (Fig. 8.13 in black), which correspond to the engineering design of the parting lines of the coil frame, are included in the model. These two lines allow a slight rotation of Fig. 8.13 for correct overlapping on the photograph (Fig. 8.14) of the fluorescent screen and the coil frame.
- The fluorescent screen is photographed from a line of sight normal to the screen and focussing approximately to the magnetic axis. The angle of view of the recording camera is ~60º. The mobile phone Jiayu G2 is used to record the experiments. Therefore, the graphic representation in Fig. 8.13 is produced by the VisIt code considering a view normal of (-0.7145 , 0.4125 , -0.5650), an angle of view of 60º and the focus located near the intersection of the magnetic axis with the screen at the point (0.1732 , 0.3186 , 0.0137).

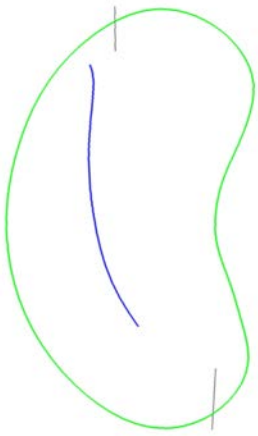

Fig. 8.13. Intersection of the electrons on the virtual screen, in blue. Filamentary coil n. 14 in green.

8.4 Comparison of experiments and calculations

Additional information is required to compare the calculations (Fig. 8.13) and the experimental recorded frames, Fig. 8.7:

- The photograph of the real fluorescent screen, taken with the parameters indicated in Section 8.3.1, is shown in Fig. 8.14.
- The filamentary coil n. 14 is marked as black dashes located on the laterals of the coil frame at the bean shape side (Fig. 8.14) at 7 mm from the edge. This position corresponds to the central turn of coil n. 14. The small difference in position from the filamentary coil to the bean shape lateral is ignored.
- The two parting lines of the coil frame appear in Fig. 8.14. They are the reference for a slight rotation of the calculated e-beam projection, Fig. 8.13.
- The overlapping of the CASTELL result (Fig. 8.13) and the photograph in Fig. 8.14 gives Fig. 8.15. The filamentary coil n. 14 representation (Fig. 8.15-green) notably matches the dashes since the VisIt representation and the photograph are produced with the same conditions. It supports the correction of the overlapping of the calculated intersection represented in blue.
- The video recordings are captured from a shear perspective in order to record simultaneously the fluorescent points and the e-gun position. Thus, the filmed fluorescent points (Fig. 8.6) have to be overlapped to the normal perspective in Fig. 8.15.

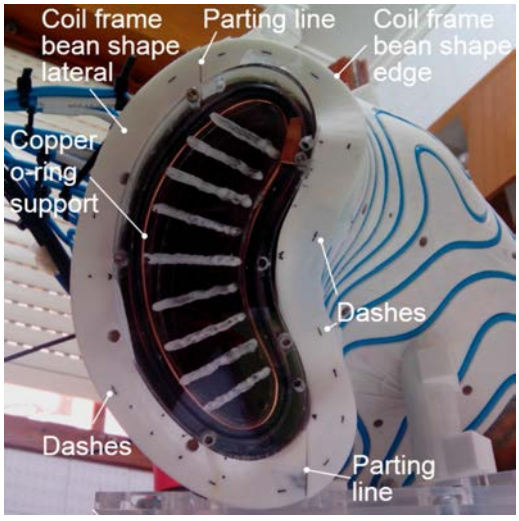

Fig. 8.14. Normal view of the fluorescent screen.

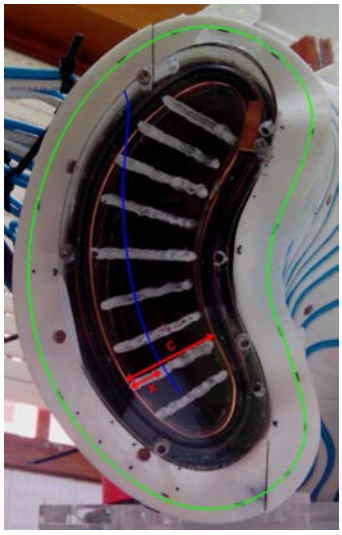

Fig. 8.15. Overlapping of the calculated coil n. 14 and real photograph.

Two approaches are followed for the overlapping:

i) Measurement on fluorescent powder lines. A linear deformation of the image along each fluorescent line painted on the screen (Fig. 8.16) is considered.

ii) Grid method. The position of the fluorescent points on a squared grid (Fig. 8.20) filmed from the same perspective as Fig. 8.16 are translated to the normal view grid, Fig. 8.21.

i) Measurement on fluorescent powder lines.

The position of the centre of the fluorescent points in Fig. 8.16 (or Fig. 8.7 for better definition) is measured in relation to the copper o-ring support (Fig. 8.14) and translated on Fig. 8.15 by linear scaling. The position of the point on Fig. 8.15 is obtained as $x = a \cdot c / b$

The result for pulse #15 is shown in Fig. 8.17 and for the pulse #14 in Fig. 8.19. The diameter of the cyan/turquoise circles in Fig. 8.17/Fig. 8.19 is 3.6 mm. The deviation of the position of the centre of the cyan/turquoise circles with respect the blue line is lower than ±2 mm.

Conclusion: The experimental result and the calculated result agree within a deviation lower than ±2 mm. It cannot be concluded only from the current experiments if the observed deviations between experiments and calculations are caused by measuring errors or by construction flaws.

Fig. 8.16. Fluorescent points. Detail of Fig. 8.6.

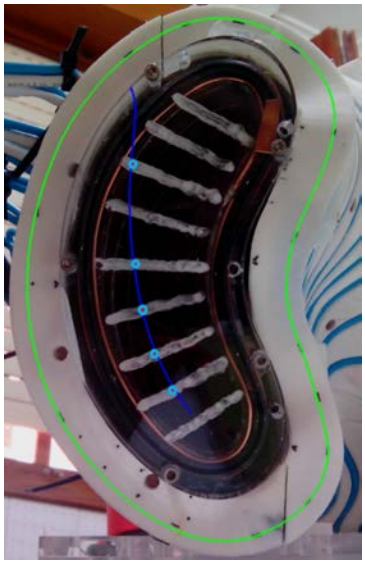

Fig. 8.17. Overlapping of translated experimental points (cyan) for pulse #15 and calculated line (blue).

ii) Grid method.

The squared grid (Fig. 8.20) filmed with the same perspective as Fig. 8.16 is located on a plane parallel to the surface of the fluorescent screen. The distance between planes is 10 mm, the thickness of the plastic plate forming the screen. A normal picture of Fig. 8.20 is shown in Fig. 8.21. A normal view image composed by overlapping of the CASTELL results in Fig. 8.15 and the normal grid in Fig. 8.21 is created in Fig. 8.22.

The background of the grid in Fig. 8.20 is made transparent by a graphics editor. Then, Fig. 8.20 is overlapped to the experimental fluorescent points (Fig. 8.16), resulting Fig. 8.23. A slight translation of the grid shown in Fig. 8.20 is produced in Fig. 8.23 to compensate the slight perspective error due to the 10 mm distance between planes.

Finally, the fluorescent points from Fig. 8.23 are translated to the normal view (Fig. 8.22) resulting Fig. 8.24. The level of agreement of experimental fluorescent points and calculated points is observed in Fig. 8.24. The diameter of the cyan circles is 3.6 mm. The deviation of the position of the centre of the cyan circles with respect the blue line is lower than ±2 mm.

Conclusion: Again, the experimental result and the calculations agree within an error lower than ±2 mm.

Fig. 8.18. Fluorescent points for pulse #14.

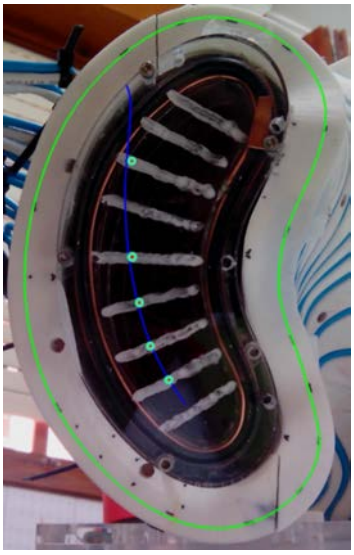

Fig. 8.19. Overlapping of translated experimental points (turquoise) for pulse #14 and calculated line (blue).

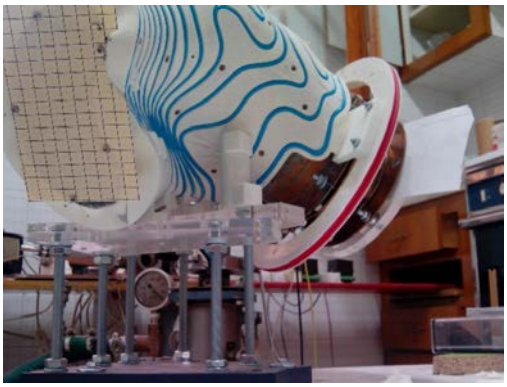

Fig. 8.20. Perspective view of the grid.

Fig. 8.21. Normal view of the grid.

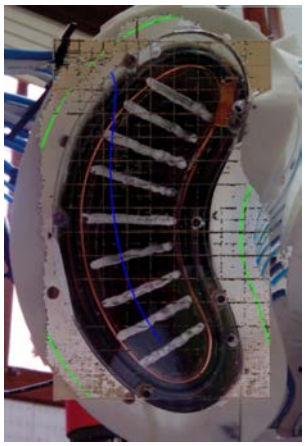

Fig. 8.22. Overlapping of Fig. 8.15 and normal grid (made transparent), Fig. 8.21.

The comparison of the position of the cyan points in Fig. 8.24 and cyan points in Fig. 8.17 with respect the blue line gives an indication about the precision of the utilised methods i) and ii), precision circa ±1 mm.

Fig. 8.23. Overlapping experimental fluorescent points (Fig. 8.16) and grid viewed in perspective, Fig. 8.20.

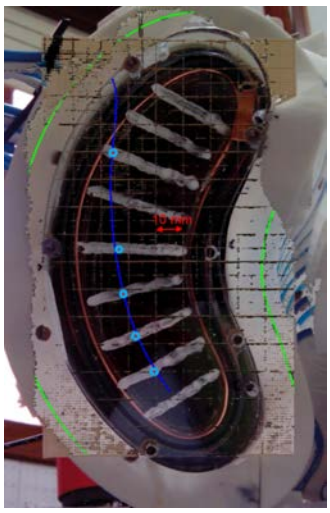

Fig. 8.24. Overlapping of translated experimental points (cyan) from Fig. 8.23 and calculated intersection (blue) for pulse #15.

8.5 Results and conclusions from the e-beam mapping experiments

- The deviation between the experimental results and calculations is smaller than ±2 mm.
- From the previous result, it is concluded that major design or construction mistakes have not been produced. Larger deviations would have been observed or fluorescent points would not have been appeared if design or construction mistakes would exist.
- It cannot be confidently concluded from the current experiments whether the observed deviations between experiments and calculations are caused by measuring errors or by small design or construction flaws.
- Errors smaller than ±1 mm are attributed to measurement errors of the non-circular fluorescent points and the perspective transformation. Other portion of the observed deviations of ±2 mm might be originated by measurement errors of the e-gun position and other measuring errors, if not due to design or construction flaws.
- The CASTELL code is further validated. Though CASTELL code was partially validated by the construction and e-beam field line mapping of the UST_1 magnetic surfaces, further validation is valuable.
- **There is enough evidence in order to confidently continue the construction of the remaining periods of the UST_2 stellarator. Major flaws are not expected.**
- E-beam field line mapping of magnetic surfaces should be carried out after completing UST_2 stellarator.

Chapter 9

Results and discussion

The results from the whole work are summarised next. First, the results coming mainly from poor outcomes are listed as experiences learned. Later, the remaining results are reported. Both results have the same importance but the separation in two groups may be preferable.

9.1 Experiences learned

The results coming particularly from poor or unsatisfactory outcomes are:

- Average dimensional accuracy of the fabricated coil frame was ±0.3%, still excessive. Using high-quality 3D printers and printing all the frame structures, which generate the coil frames, with the same 3D printer and at the same position and orientation may decrease errors.
- Only relatively small pieces can be manufactured by current commercial 3D printers and services. However, recently large prototypical titanium 3D printers of several meters in length have been developed in China. Another strategy, such as the construction of a particular accurate large 3D printer to manufacture one-of-a-kind fusion device, may be expensive, as occurred for the toroidal milling machine used to build just one UST_1 stellarator.
- Only plastic and resin pieces have been studied. Low temperature resistance, relatively low strength and poor radiation hardness of plastics and resins are unsatisfactory for fusion reactors. The potential option of metal additive manufacturing of an external shell and internal metal casting might solve the issue.
- It cannot be confidently concluded from the current e-beam field line mapping experiments if the small deviations observed between experiments and calculations are caused by measuring errors or by small design or construction flaws. E-beam field line mapping of magnetic surfaces, after completion of the UST_2, would achieve higher sensitivity to magnetic errors triggered by geometrical errors.
- Poorer neoclassical confinement has been obtained in the UST_2 magnetic configuration, which has straight plasma sections, than in the original QIPCC3 configuration. Indeed, poor performance can be expected since extra conditions have been imposed

to the magnetic configuration. In any case, plasma properties should be enhanced in a future work for an improved balance between engineering and physics properties.

9.2 Results

- The Fourier coefficients of a LCFS which presents a straight non-torsion plasma section at the low magnetic field plasma segment have been calculated from the QIPCC3 magnetic configuration. QIPCC3 configuration was received as an input from German researchers.
- The straight section facilitates modularity of the stellarator, fast assembly and replacement of modules, the installation of wide ports for faster maintenance of in-vessel elements and space for potential future large powerful external divertors. Nonetheless, neoclassical confinement in the modified UST_2 configuration is poorer than in the original QIPCC3, and modularity may increase magnetic errors.
- A small stellarator named UST_2 has been conceived in order to better validate the explored manufacturing methods. Coils have been calculated and designed for the UST_2 stellarator by NESCOIL code from the obtained LCFS. Six non-circular large planar coils located at the low field plasma section and 84 twisted (modular) coils located at the curved sectors compose UST_2 stellarator. The algorithms implemented in the CASTELL code may be capable to calculate other special coil configurations in the future.
- A construction method for stellarators based on additive manufacturing combined with non-metal casting has been conceived, developed and tested. The method is named 3Dformwork as it resembles to usual concrete formwork and to some recent architectural attempts to 3D-print buildings.
- A hollow 3D-printed piece, named frame structure, defined as a truss structure covered by a thin 3D-printed surface has been conceived, designed and fabricated.
- The frame structure was fast and satisfactorily internally cast with acrylic resin, resulting a coil frame. The concept of casting in a frame structure appears effective for other fusion and non-fusion applications. However, dimensional accuracy of the first coil frame was ±0.3% for the particular price and 3D printing quality utilised for such item.
- The 3D printing cost of the frame structure in a commercial company was 700 € for an exceptionally complex piece whose envelope is 358 x 252 x 216 mm. The piece comprises numerous elements, like a series of twisted grooves, legs, joins, positioning stops, and parting lines. However, the quality of the 3D printing and procedures should be increased to achieve at least ±0.1% relative accuracy. The relative accuracy has to be understood as dimensional errors among the different halfperiods. Higher quality additive manufacturing suppliers, at higher cost, were consulted but they were disregarded.
- The vacuum vessel is conceived as six curved vacuum vessel sectors and three straight vacuum vessel sections. All the vessel segments are joined by demountable

flanges and seals. This feature combined with the independence of the six coil frames and the defined large planar coils generate a stellarator capable to be detached in six modules for easy assembly and maintenance. In the case of a future reactor, the modularity property, together with the potential tilting of the large planar coils, would decrease maintenance downtime and would allow changing full modules in case of failure.

- A curved vacuum vessel sector, which is similar to a curled and convoluted elbow, has been fabricated by a combination of a metallic liner and external resin reinforcement. In this particular application, copper was utilised as liner and epoxy resin as reinforcement but many other combinations are envisaged. This procedure might be more convenient for large vacuum vessels than for small ones due to the long operator labour required for production. The manufacture of one curved vacuum vessel sector for UST_2 took around one week-person.
- Coils composed of a single pancake winding pack are envisaged. The single pancake is created by winding just one turn of conductor per layer of winding pack.
- A crossover, which is worked out as a conductor split in two copper filament bunches, has been implemented. A seemingly new type of crossover was unavoidable because single pancake coils are unknown in stellarator fabrication. In this concept the conductor pass through the opening created by the two bunches of filaments, and therefore, the concept is appropriate for single pancake coils.
- The relative magnetic field errors from such crossover for three cable turns per coil have been calculated lower than 10^{-4}. Consequently, the coils and crossovers are acceptable.
- Winding the coils in grooves was fast, straightforward and accurate. This result arises from the particular design explored and developed in UST_1 and UST_2 stellarators. The particularity of winding a single turn of conductor per layer of winding pack, the compression of the conductor in an appropriate groove, and the positioning of the conductor referenced to the bottom of the groove, allowed the fast and accurate winding. Nonetheless, fabrication of numerous coils, which are actually a single pancake, is not straightforward. It would have been much more expensive or unfeasible by means of traditional manufacturing methods. Accordingly, a noteworthy integration of the design and the manufacturing methods have been achieved. Although the coil pancakes should be impregnated in a strong resin or other material to withstand large Lorentz forces, it does not invalidate the result.
- The positioning of the coil frames to form the torus has been concocted as coil frames sliding on a flat smooth surface until the positioning stops contact on a circular central ring. The property of circularity of the central ring is essential for a simple and accurate positioning. This property is mandatorily complemented by the transfer of complexity of the device to the coil frames, which are additively manufactured. It implies that remarkable integration of the main elements of the stellarator has been achieved since the cost of 3D-printed parts is almost independent of the complexity of the part, and certainly, only the coil frame has been manufactured by 3Dformwork additive manufacturing.

- Satisfactory assembling and positioning of one halfperiod, carried out by those procedures, have been demonstrated.
- A full small or middle size stellarator, built by the researched and developed methods, might hypothetically be fabricated in few weeks. Nevertheless, such speculative possibility does not include the research and design time. Most of the process time becomes R&D labour if additive manufacturing is utilised. Indeed, it is valid for many other industrial applications of rapid manufacturing. Due to the complexity (both physics and engineering complexity) of new stellarators and other fusion devices, and since the knowledge is still not normalised and standardised like in other disciplines (e.g. in aeronautical industry), and since there are not companies developing fusion devices as a routine, hence, the production cycle of new devices will still be considerably long, in spite of the present work. A myriad of factors should be improved in parallel with the construction methods to fully speed up the production cycle of fusion devices.
- E-beam field line mapping experiments have been carried out to validate the performance of the R&D. The experiments are carried out in only one halfperiod of stellarator. A method somewhat similar to an old CRT television has been implemented. The UST_2 coils act as deflexion coils, an oscillating e-gun produces the e-beam and a fluorescent screen reveal the e-beam impact points. Comparison of calculations and experiments is performed.
- The experimental outcome from the e-beam field line mapping experiments and the respective calculations agree within a deviation lower than ± 2 mm.
- The previous result proves that major design or construction mistakes have not occurred.
- The cost of the materials for the portion of UST_2 already built was 2400 €. From the know-how gained in the first halfperiod built, which has been reported in this memory, it is expected that operator cost will decrease for the remaining periods of UST_2 and for other future stellarators. Moreover, the developed particular rapid manufacturing method and the devised assembly technique would accelerate the construction process. In spite of the small UST_2 size, certain cost reduction with respect some traditional construction methods is predicted, at least, for small or medium size stellarators.
- The particular 3Dformwork rapid manufacturing method conceived and, it combined with a proper integration of manufacturing, physics and engineering design, and all properly blended for simple assembling and maintenance, all together in a single object has not been observed in the previous state of the technique for stellarator fabrication. Certainly, most of the combined elements do exist as separated entities, but not together.
- An answer results for the initial question of whether certain manufacturing method might speed up and lower the construction costs of particular stellarators. At least one faster construction method, with reduced costs, has been identified for the construction of a small stellarator.

Chapter 10

Conclusions and future work

A research essentially exploratory is carried out to investigate different construction methods for stellarators. Faster and lower cost manufacturing techniques are sought. As a result, several conceptions of manufacturing methods are identified and validated. Among them, the leading concept is the combination of additive manufacturing of hollow pieces with casting. This concept was named 3Dformwork due to the resemblance to the traditional concrete formwork, which consists of an external wood or metallic shell filled with concrete. But not just a conception is produced, the experimental assay of three concepts is carried out. The Hull concept, the Trust concept and the synthesis of both, the 3Dformwork concept, are tested. Different materials, like resins, hard plasters or cements, capable to solidify or cure may be cast in those 3D-printed hollow structures.

The 3Dformwork concept was selected among the three alternatives. It is implemented as resin casting inside a plastic 3D-printed light truss structure, which is covered by a 3D printed thin surface. Subsequently, this manufacturing method was successfully applied to the fabrication of a coil frame for a small stellarator, UST_2. The construction of such stellarator is intended to better validate the investigated manufacturing methods and assess the integration of all the concepts. Nonetheless, accuracy of the manufactured coil frame is still lower than required for stellarators. Further research is needed to improve such drawback and other concerns. For instance, the study of the dimensional accuracy obtained by using the same printer and the same position and orientation of the piece in the printer. Another foreseen activity is the study of methods combining additive manufacturing and localised milling or trimming. The fast progress of additive manufacturing techniques combined with an endeavour focussed on the production of fusion devices may solve the accuracy concern.

The integration of the engineering and physics design with the developed manufacturing method is implemented in different ways.

For instance, the number of coils for the stellarator was properly integrated with the additive manufacturing capabilities. Since additive manufacturing allows the production of geometrically complex parts at reduced cost, 84 twisted coils are calculated and designed for UST_2 stellarator. The use of numerous coils reduces the modular magnetic ripple generated by the coils and improves neoclassical transport. The utilization of many coils

might appear inconvenient from a traditional point of view. Nevertheless, it is not so in this new paradigm.

In another example of integration, positioning elements for the coil frame, positioning features for the conductor crossovers and legs for the coil frame are additively manufactured as a sole monolithic structure –the coil frame. As a consequence of this choice, the large support structures exhibit simple geometry, such as flat tables or circular supports, resulting in reduced fabrication cost without increasing the manufacturing cost of the 3D-printed coil frame.

From the work it becomes apparent that additive manufacturing provide advantages, in particular to build stellarators, essentially due to the high geometrical complexity of this type of fusion devices and the need of only one or few identical items. Furthermore, since increasing the geometrical complexity of certain components, for example the coils frames, improves the physics properties of the device and simplify the assembly of the system, it results that additive manufacturing is in principle suited to the construction problem of stellarators.

The application of the developed manufacturing method to metallic fusion devices is foreseen from the work. The extension of the investigated technique to additive manufacturing of a metallic shell and internal metal casting emerge from the conducted research. Regarding to this prospect, at least one proposal to build a metallic stellarator by additive manufacturing has been identified –the advanced fabrication of the ARIES-CS stellarator reactor. The aspiration to build, for example, such ARIES-CS reactor would act as a long term goal to stimulate further research on additive manufacturing of accurate, complex and large metallic components. In the same line, the attempt to 3D-print certain geometrically complex components for ITER, such as blankets, the in-vessel coils or elements for the divertors, would boost the research in this field.

From the implementation of proper positioning elements for the conductors and crossovers (grooves and cylindrical indentations respectively) it turns out that faster coil winding is achieved if all the details for the positioning of the winding packs are 3D printed. These elements could be produced without cost increase by additive manufacturing or by 3Dformwork. It could be speculated whether a novel magnetic configuration might only (almost) be built by a still unidentified 3D-printing-like method.

Not only the required high accuracy, but the large size of the necessary components for fusion is a concern. Though at least a titanium 3D-printed flat piece, which is larger than 4 metres length, has been tentatively produced recently in China, and a large 6 m x 6 m and accurate 3D printer (the D-Shape) exists, still, high accuracy and a diversity of materials need to be proven at a reasonable cost. To some extent, the solution may come from the application of additive manufacturing to major industrial sectors requiring large and singular pieces, for example, the aeronautical industry.

Cost of additive manufacturing services from commercial high quality companies is still relatively expensive. High amortization cost of 3D printers, patents, high cost of specialised operators, maintenance cost of the printers, and expensive 3D printing materials lead to the current high prices per unit of volume. Still, a kilogram of any geometrically simple metallic piece produced by conventional casting, forging, cutting, milling and welding is far more economical than the same simple piece produced by additive manufacturing. The strategy

to reach competitiveness resides in fully making use of the integration possibilities of all the components of the geometrically complex stellarators, in order to, already today, try to produce certain stellarators faster and cheaper than with traditional fabrication methods. In the case of the geometrically simpler tokamaks, when and how additive manufacturing will be competitive for certain components, e.g. low thermal stress divertor materials or complex cooling circuits for blankets, will depend on the research carried out on such particular endeavours. Overall, it will be a new and magnificent fusion technology research line that is, sometimes, hardly envisioned today.

A positive answer results for the initial question, whether a manufacturing method, based partially on additive manufacturing, and fully integrated with the physics and engineering design, may speed up and lower the construction costs of certain stellarators. This thesis identified at least one manufacturing method, based on the combination of additive manufacturing and resin casting, which being properly integrated with the engineering and physics design, resulted a fast construction method, at reduced cost, for a small stellarator.

Inspiration and encouragement might be generated from the present work in the future, similarly to the stimulus produced by UST_1 stellarator on other researcher groups, for instance, inspiring the development of the SCR-1 stellarator, currently operational in Costa Rica.

If it were true that the pace of technology is behind plasma physics, as stated by a prominent fusion researcher, this thesis could be deemed as a modest, but significant, thrust for technology to catch plasma physics.

Acknowledgments

First, I would like to thank my PhD adviser Dr. Víctor Tribaldos for his excellent guidance during the development of the research work, for the detailed explanations about different matters about stellarators and the advice during the writing of the present memory. Also, for his help during the previous R&D work for the UST_1 stellarator, almost ten years ago.

Also, I am in great debt to Dr. Jesús A. Romero and Dr. José A. Ferreira for the ideas raised during our breaks in CIEMAT. Sometimes the discussions dealt about the best types of fusion devices to produce competitive fusion energy, other about the best types of divertors or magnetic configurations. The brainstormings gave me ideas about what line of research to follow and about some concepts to research and develop.

Special thanks to my friend and IT expert Cristobal Bellés who taught me with great patience the Object Oriented programming paradigm.

Also, my gratitude to all the researchers of the National Fusion Laboratory in CIEMAT who helped me with different particular aspects of the research. Special thanks to the researches that taught me the use of certain codes: Jesús Romero (NESCOIL), Antonio Lopez-Fraguas (DESCUR), Gerardo Veredas (Visual Basic automation for CATIA) and J.A. Jimenez (VMEC), and to CIEMAT for granting the use of such codes and means.

To my grandfather Pascual, who only attended few years to school due to poverty. But at 95 years old (he lived 104) he was still capable to calculate cubic roots manually. He learned many things from thrown away books. When I was about 14 I used to read his university-level physics book from year 1898. In the book they still speculated that energy from the sun might come from meteors continuously falling on the sun!.

Also, I would like to thank all the contributors to the crowdfunding campaign '3D-printed clean fusion energy for the World' raised in the platform Indiegogo. The contributions funded almost half of the materials cost for UST_2 development and construction.

Finally I would like to thank the researchers who provided the definition of coils or Last Closed Flux Surfaces for different stellarators. Also, I am in debt to the members of the teams developing such configurations. In particular thanks to:

Drs. Long-Poe Ku and Farrokh Najmabadi for the supply of the definition of ARIES-CS coils.

Drs. A. Werner and J. Baldzuhn, HSR-3 and HSR-4 Helias reactor coils.

Drs. Donald Spong and Jeffrey Harris, QPS coils and LCFS definition.

Dr. H. E. Mynick for the supply of a NCSX-like configuration potentially optimised for turbulent transport.

Drs. J. Nührenberg and M.I. Mikhailov for the QIPCC2, QIPCC3 and QIPCC6 LCFS.

Bibliography

[1] Colin McEvedy and Richard Jones, Atlas of World Population History, ISBN 0140510761, Ed. Puffin, 1978.

[2] G.R. McPherson, http://guymcpherson.com/wp-content/uploads/2013/06/human-population-and-energy-use.jpg, 2014.

[3] International Energy Agency, 'Key world energy statistics 2013'.

[4] Thomais Vlachogianni and Athanasios Valavanidis, Energy and Environmental Impact on the Biosphere Energy Flow, Storage and Conversion in Human Civilization, *American Journal of Educational Research* **1** (3) 68–78, 2013.

[5] G.R. Elizarraás and G. Sanchez, Mankind and Energy: Needs, Resources, Hopes: Proceedings of a Study Week at the Pontifical Academy of Sciences, Ed. Andre Blanc-Lapierre, p. 509, 1980.

[6] International Energy Agency, 'World Energy Outlook 2004'.

[7] International Energy Agency, 'World energy outlook 2008', p. 221, 2008.

[8] I. Cook, G. Marbach, L. Di Pace, C. Girard, N. P. Taylor, Safety and environmental impact of fusion, Report EFDA-S-RE-1, April 2001.

[9] D.J. Ward, The contribution of fusion to sustainable development, *Fusion Engineering and Design* **82** 528–533, 2007.

[10] D. McMorrow, 'Tritium', Report JSR-11-345, The MITRE Corporation, 7515 Colshire Drive, McLean, Virginia 22102-7508, USA, November 2011.

[11] K. Yamazaki and T.J. Dolan, Impact of plasma, magnet and wall performances on tokamak and helical reactor economics, *Fusion Engineering and Design* **81** 1145–1149, 2006.

[12] T. J. Dolan, K. Yamazaki, and A. Sagara, Helical fusion power plant economics studies, *Fusion Science and Technology* **47** 60–72, 2005.

[13] S. Sanders, A. Rolfe, S.F. Mills, A. Tesini, Application of remote handling compatibility on ITER plant, *Fusion Engineering and Design* **86** 1989-1992, 2011.

[14] V. Queral, A. García, G. Miccichè, A. Ibarra, N. Casal, F. Mota and D. Rapisarda, Proposal of an improved design of IFMIF Test Cell components for enhanced handling and reliability, *Fusion Engineering and Design* **84** 1548–1552, 2009.

[15] O. Crofts and J. Harman, Maintenance duration estimate for a DEMO fusion power plant, based on the EFDA WP12 pre-conceptual studies, *Fusion Engineering and Design* **89** 2383–2387, 2014.

[16] L. M. Waganer, R. J. Peipert, X. R. Wang, S. Malang and ARIES Team, ARIES-CS maintenance system definition and analysis, *Fusion Science and Technology* **54** 787–817 2008.

[17] L. El-Guebaly, V. Massaut, K Tobita, L. Cadwallager, Evaluation of recent scenarios for managing fusion activated materials: recycling and clearance, avoiding disposal, Published by Fusion Technology Institute, Wisconsin, September 2007.

[18] M. Kikuchi, K. Lackner, M. Quang (editors), 'Fusion Physics', ISBN 978–92–0–130410–0, IAEA, Vienna, September 2012.

[19] D. Maisonnier, I. Cook, S. Pierre, B. Lorenzo, B. Edgar, et al., The European power plant conceptual study, *Fusion Engineering and Design* **75–79** 1173–1179, 2005.

[20] Mitsuru Kikuchi, Frontiers in Fusion Research: Physics and Fusion, Chapter 10 Towards the Realization of Fusion Energy, ISBN 978-1-84996-410-4, Springer-Verlag London Limited, 2011.

[21] C. Llewellyn, The need for fusion, *Fusion Engineering and Design* **74** 3–8, 2005.

[22] P. E. Stott, The feasibility of using D–3He and D–D fusion fuels, *Plasma Phys. Control. Fusion* **47** 1305, 2005.

[23] J. F. Santarius, G. L. Kulcinski, L. A. El-Guebaly and H. Y. Khater, Could Advanced Fusion Fuels Be Used with Today's Technology?, *Journal of Fusion Energy* **17** (1) 33–40, 1998.

[24] L. El-Guebaly, M. Zucchetti, Recent developments in environmental aspects of D–3He fuelled fusion devices, *Fusion Engineering and Design* **82** 351–361, 2007.

[25] L. El-Guebaly, P. Wilson, D.Henderson, M. Sawan, G. Sviatoslavsky, et al., Designing ARIES-CS compact radial build and nuclear system: neutronics, shielding, and activation, *Fusion Science and Technology* **54** 747–770, 2008.

[26] T. Nishitani, M. Yamauchi, S. Nishio, M. Wada, Neutronics design of the low aspect ratio tokamak reactor, VECTOR, *Fusion Engineering and Design* **81** 1245–1249, 2006.

[27] J. Jordanova, U. Fischer, P. Pereslavtsev, Y. Poitevin, A. Li Puma, et al., Evaluation of nuclear heating, tritium breeding and shielding efficiency of the DEMO HCLL breeder blanket, *Fusion Engineering and Design* **75–79** 963–967, 2005.

[28] H. Kottowski, O. Kranert, C. Savatteri, C. Wu and M. Corradini, Studies with respect to the estimation of liquid metal blanket safety, *Fusion Engineering and Design* **14** 445–458, 1991.

[29] B.J. Merrill, M. Sawan, C. P.C. Wong, R.E. Nygren, L.C. Cadwallader, et al., Safety assessment of two advanced ferritic steel molten salt blanket design concepts, *Fusion Engineering and Design* **72** 277–306, 2004.

[30] T. Hayashi, K. Tobita, S. Nishio, S. Sato, T. Nishitani, M. Yamauchi, Possibility of tritium self-sufficiency in low aspect ratio tokamak reactor with the outboard blanket only, *Fusion Engineering and Design* **81** 2779–2784, 2006.

[31] M. Nishikawa, Study on tritium balance in a D-T fusion reactor, *Fusion Science and Technology* **57** 120-128, 2010.

[32] R. C. Kirkpatrick, I. R. Lindemuth, M. S. Ward, Magnetized Target Fusion: An Overview, *Fusion Science and Technology* **27** (3) 201–214, 1995.

[33] S. Woodruff, An Overview of Tokamak Alternatives in the US Fusion Program with the Aim of Fostering Concept Innovation, *Journal of Fusion Energy* **23** (1) 27–40, 2004.

[34] K. Ishida, K. Nagamine, T. Matsuzaki, and N. Kawamura, Muon catalyzed fusion, *J. Physics G: Nuclear Particle Physics* **29** 2043–2045, 2003.

[35] Edmund Storms, The science of low energy nuclear reaction. A Comprehensive Compilation of Evidence and Explanations about Cold Fusion, ISBN-10 981-270-620-8, Ed. World Scientific, 2007.

[36] J. Meyer-ter-Vehn, S. Atzeni, R. Rami, Inertial Confinement Fusion, *Europhysics News*, November/December 1998.

[37] R. K. Kirkwood, J. D. Moody, J. Kline, E. Dewald, S. Glenzer, et al., A review of laser-plasma interaction physics of indirect-drive fusion, *Plasma Physics Controlled Fusion* **55** 103001, 2013.

[38] A. H. Boozer, Physics of magnetically confined plasmas, *Reviews of modern physics* **76**, 2004.

[39] D. Campbell (Max-Planck-Institut für Plasmaphysik, Germany), Magnetic Confinement Fusion, *Europhysics News*, November/December 1998.

[40] T. J. Dolan, Fusion Research, ISBN 0-08-025565-5, Ed. Pergamon Press, 1980.

[41] J.E. Menard, L. Bromberg, T. Brown, T. Burgess, D. Dix, et al., Prospects for pilot plants based on the tokamak, spherical tokamak and Stellarator, *Nuclear Fusion* **51** 103014, 2011.

[42] G.M. Vossa, S. Allfreya, A. Bondb, Q. Huangc, P.J. Knighta, et al., A conceptual design of a spherical tokamak power plant, *Fusion Engineering and Design* **51–52** 309–318, 2000.

[43] R.C. Wolf and the Wendelstein 7-X Team, A stellarator reactor based on the optimization criteria of Wendelstein 7-X, *Fusion Engineering and Design* **83** 990–996, 2008.

[44] F. Najmabadi, A. R. Raffray and the ARIES-CS Team, The ARIES-CS compact stellarator fusion power plant, *Fusion Science and Technology* **54** 655–672, 2008.

[45] M. Li, R. Liu, X. Shi, W. Yi, et al., Preliminary design of hybrid energy reactor and integral neutron experiments, *Fusion Engineering and Design* **87** 1420–1424, 2012.

[46] S.V. Ryzhkov, Alternative Fusion Reactors as Future Commercial Power Plants, *J. Plasma Fusion Research SERIES* **8** 35–38, 2009.

[47] J. Scheffel and J-E. Dahlin, Confinement scaling in the advanced reversed-field pinch, *Plasma Physics Controlled Fusion* **48** L97–L104, 2006.

[48] J. Kesner, D.T. Garnier, A. Hansen, M. Mauel and L. Bromberg, Helium-catalyzed D-D fusion in a levitated dipole, *Nuclear Fusion* **44** 193–203, 2004.

[49] K. I. Thomassen, E. B. Hooper, and D. D. Ryutov, The Spheromak Path to Fusion, *Journal of Fusion Energy* **17** (3) 193–199, 1998.

[50] D.A. Sutherland, T.R. Jarboe, K.D. Morgan, M. Pfaff, E.S. Lavine, Y. Kamikawa, et al., The dynomak: An advanced spheromak reactor concept with imposed-dynamo current drive and next-generation nuclear power technologies, *Fusion Engineering and Design* **89** 412–425, 2014.

[51] S. Knowlton, G. Hartwell, J. Hanson, C. Montgomery, J. Munoz, et al., 'Overview of the Compact Toroidal Hybrid (CTH) experiment', Presentation in 2nd US-Japan Workshop and Kyoto University 21st Century COE Symposium on New Approaches in Plasma Confinement in Helical Systems, 15 November 2006.

[52] Web site http://www-fusion-magnetique.cea.fr/gb/fusion/principes/principes02.htm, 2014.

[53] C.D. Beidler, E. Harmeyer, F. Herrnegger, J. Kisslinger, Y. Igitkhanov, H. Wobig, Stellarator fusion reactors – an overview, *J. Plasma Fusion Res. SERIES* **5** 149–155, 2002.

[54] P. Helander, J.H.E. Proll, G.G. Plunk, Collisionless microinstabilities in stellarators I - analytical theory of trapped-particle modes, (AIP) *Physics of Plasmas* **20**, 122505, 2013.

[55] J.H.E. Proll, P. Xanthopoulos, P. Helander, Resilience of Quasi-Isodynamic Stellarators against Trapped-Particle Instabilities, *Physical Review Letters* **108** 245002, 2012.

[56] J.H.E. Proll, P. Xanthopoulos, P. Helander, Collisionless microinstabilities in stellarators II - numerical simulations, (AIP) *Physics of Plasmas* **20** 122506, 2013.

[57] U. Stroth, Transport in Toroidal Plasmas, *Lecture Notes in Phys*ics **670** 213–267, 2005.

[58] C.D. Beidler, K. Allmaier, M.Yu. Isaev, S.V. Kasilov, W. Kernbichler, G.O. Leitold, H. Maaßberg, D.R. Mikkelsen, S. Murakami, M. Schmidt, D.A. Spong, V. Tribaldos and A.Wakasa, Benchmarking of the mono-energetic transport coefficients - results from the International Collaboration on Neo-classical Transport in Stellarators (ICNTS), *Nuclear Fusion* **51** 076001, 2011.

[59] K. Tobita, S. Nishio, M. Enoeda, M. Sato, T. Isono, Design study of fusion DEMO plant at JAERI, *Fusion Engineering and Design* **81** 1151–1158, 2006.

[60] J.F. Lyon, L.P. Ku, L. El-Guebaly, L. Bromberg, L.M. Waganer, M.C. Zarnstorff, and ARIES-CS Team, Systems studies and optimization of the ARIES-CS power plant, *Fusion Science and Technology* **54** 694-724, 2008.

[61] J. Sheffield, R. A. Dory, S. M. Cohn, J. G. Delene, L. F. Parsly, D. E. T. F. Ashby, W. T. Reiersen, Cost Assessment of a Generic Magnetic Fusion Reactor, Report ORNL n. ORNL/TM-9311, March 1986.

[62] P. Helander, C.D. Beidler, T. M. Bird, M. Drevlak, Y. Feng, R. Hatzky, et al., Stellarator and tokamak plasmas: a comparison, *Plasma Physics Controlled Fusion* **54** 124009, 2012.

[63] Farrokh Najmabadi, 'Towards Attractive Fusion Power Plants', Presentation in the Korean National Fusion Research Center, Daejon (Korea), 20 April 2006.

[64] S. Knowlton, G. Hartwell, J. Armstrong, et al., Auburn University, 'The Compact Toroidal Hybrid Experiment', Unpublished result supplied by the authors, ~2003.

[65] G.J. Hartwell, S.F. Knowlton, J. Armstrong, J. Peterson, C. Montgomery, et al., Construction Progress of the Compact Toroidal Hybrid, Poster presentation in ANS 45th Annual Meeting of the Division of Plasma Physics, Albuquerque, New Mexico (USA), 27-31 October 2003.

[66] E. Ascasibar, L. Almoguera, J. alonso, J. Botija, J. Moreno, et al., Engineering Design and Construction of a Low Aspect Ratio Torsatron: The TJ-I Upgrade, *Fusion Technology*, Proceedings of the 16th Symposium on Fusion Technology, 3–7 September 1990, 577–581, 1990.

[67] PPPL Digests, 'Advanced Technology Essential in NCSX Component Fabrication', February 2007.

[68] M. Wanner and the W7-X Team, Construction and assembly of WENDELSTEIN 7-X, *Fusion Engineering and Design* **81** 2305–2313, 2006.

[69] B. Heinemann, M. Gasparotto, C. Damiani, M. Fröschle, B. Giesen, et al., Design of Narrow Support Elements for Non Planar Coils of Wendelstein 7-X, Conference proceedings of the 21th IEEE/NPS SOFE 2005, Knoxville, Tennessee (USA), 26-29 September 2005.

[70] J. Duhovnik, B. Jerman, T. Kolšek , J. Kramar J., N. Mole et al. (University of Ljubljana), Analysis of Narrow Support Element of The W7-X Magnet System under Design Loads, Annual Report 2005 – Fusion Physics Programme, Slovenian Fusion Association (EURATOM-MHEST), 21–27, 2005.

[71] A. F. Almagri, D. T. Anderson, S. F.B. Anderson, K. M. Likin, P. G. Matthews, et al., Design and Construction of HSX: a Helically Symmetric Stellarator, *Journal of Plasma Fusion Research SERIES* **1** 422-425, 1998.

[72] L.M. Waganer, T.S. Kevin, J.C. Waldrop III, and ARIES Team, ARIES-CS coil structure advanced fabrication approach, *Fusion Science and Technology* **54** 878-889, 2008.

[73] R. Sacristán, G. Veredas, I. Bonjoch, I. Peñalva, E. Calderón, et al., Fuskite® preliminary experimental tests based on permeation against vacuum for hydrogen recovery as a potential application in Pb15.7Li loop systems, Fusion Engineering and Design **89** 1551–1556, 2014.

[74] V.I. Vargas, J. Mora, J. Asenjo, E. Zamora, C. Otárola, et al., Engineering Issues to the Stellarator of Costa Rica 1, Proceedings of the 25th Symposium on Fusion Engineering, San Francisco, CA (USA), 10-14 June 2013.

[75] T. Mizuuchi, F. Sano, K. Nagasaki, H. Okada, S. Kobayashi, et al., Configuration control for the confinement improvement in Heliotron J, *Fusion Science and Technology* **50** 352-360, 2006.

[76] T. Sunn Pedersen, A. H. Boozer, J. P. Kremer, R. G. Lefrancois, W. T. Reiersen, F. Dahlgren and N. Pomphrey, The Columbia Nonneutral Torus: a new experiment to confine nonneutral and positron-electron plasmas in a stellarator, *Fusion Science and Technology* **46** 200-2008, 2004.

[77] A. W. Clark, M. Doumet, K. C. Hammond, Y. Kornbluth, D. A. Spong, R. Sweeney, F. A. Volpe, Proto-CIRCUS tilted-coil tokamak–torsatron hybrid: Design and construction, *Fusion Engineering and Design* **89** 2732–2737, 2014.

[78] Paul E Moroz, Low-aspect-ratio stellarators with planar coils, *Plasma Physics Controlled Fusion* **39** 1841–1859, 1997.

[79] F.A. Volpe, C. Caliri, A.W. Clark, A. Febre, K.C. Hammond, et al., 'Stellarator Research at Columbia University', Presentation in PPPL, 2013.

[80] V. Queral, Coil fabrication of the UST 1 modular stellarator and potential enhancements, *Fusion Engineering and Design* **88** 683-686, 2013.

[81] Presentation 'D-Shape', company 'Monolite UK Ltd', web site: www.d-shape.com, August 2014.

[82] AVIC Laser (AVIC Heavy Machinery subsidiary), '16th China International High-tech Expo', Beijing, 21-26 May 2013, web site www.france-metallurgie.com, August 2014.

[83] V. Queral, Concept, production and validation of a 3D-printed coil frame for the UST_2 modular stellarator, *Fusion Engineering and Design* **89** 2145–2149, 2014.

[84] P. Merkel, Solution of stellarator boundary value problems with external currents, *Nuclear Fusion* **27** 867, 1987.

[85] E. Strumberger and M. Hölzl, User manual: iterative computation of 3D ideal MHD equilibria and magnetic fields, IPP Max-Planck-Institut, Report IPP 5/113, May 2005.

[86] G. J. Hartwell, S. F. Knowlton, C. Watts, J.D. Hanson, T. Brown, Design and construction progress of the Compact Toroidal Hybrid, Paper N. PIIB.7, Proceedings of the 13th International Stellarator Workshop, Canberra (Australia), 25 February - 1 March 2002.

[87] C. Beidler, G. Grieger, F. Herrnegger, E. Harmeyer, J. Kisslinger, et al., Physics and engineering design for W7-X, *Fusion Technology* **17** 148-167, 1990.

[88] K. Risse K, Th. Rummel, L. Wegener, R. Holzthüm, N. Jaksic, et al., Fabrication of the superconducting coils for Wendelstein 7-X, *Fusion Engineering and Design* **66-68** 965-969, 2003.

[89] J. H. Chrzanowski, P. J. Fogarty, P. J. Heitzenroeder, T. Meighan, B. Nelson, et al., Manufacturing development of the NCSX modular coil windings, Conference proceedings of the 21th IEEE/NPS SOFE 2005, Knoxville, Tennessee (USA), 26-29 September 2005.

[90] X. Sarasola X, T.S. Pedersen, J. P. Kremer, R. G. Lefrancois, Q. Marksteiner and N. Ahmad, Field line mapping results in the CNT stellarator, P-1.058, 32nd EPS Conference on Plasma Phys. Tarragona (Spain), 27 June - 1 July 2005, ECA 29C, 2005.

[91] V. Queral, web site www.fusionvic.org , January 2014.

[92] J. Mora, V. I. Vargas, L. F. Villegas, L. Barillas, J. I. Monge and L. Rivas, Major issues in the design and construction of the stellarator of Costa Rica: SCR-1, *Journal of Physics Conf. Ser.* **370** 012066, 2012.

[93] M. J. Mikhailov, W. A. Cooper, M.F. Heyn, M.Yu Isaev, V.N. Kalyuzhnyj, et al., Comparison of the properties of Quasi-isodynamic configurations for Different Number of Periods, Proceedings of the 31st EPS Conference on Plasma Phys. London, 28 June - 2 July 2004, ECA 28G, P-4.166, 2004.

[94] Y. Nakamura, S. Masuzaki, T. Morisaki, H. Ogawa, T. Watanabe, et al., Impact of real-time magnetic axis sweeping on steady state divertor operation in LHD, *Nuclear Fusion* **46** 714–724, 2006.

[95] A.R. Raffray, L. El-Guebaly, S. Malang, X.R. Wang, L. Bromberg, et al., Engineering design and analysis of the ARIES-CS power plant, *Fusion Science and Technology* **54** 725-746, 2008.

[96] N. Pomphrey, A. Boozer, A. Brooks, R. Hatcher, S.P. Hirshman, et al., NCSX magnetic configuration flexibility and robustness, *Fusion Science and Technology* **51** 181-202, 2007.

[97] B.E. Nelson, R.D. Benson, L.A. Berry, A.B. Brooks, M.J. Cole, et al. Design of the quasi-poloidal stellarator experiment (QPS), *Fusion Engineering and Design* **66-68** 205-210, 2003.

[98] A.A. Subbotin, M.I. Mikhailov, V.D. Shafranov, M.Yu. Isaev, C. Nührenberg, J. Nührenberg, et al., Integrated physics optimization of a quasi-isodynamic stellarator with poloidally closed contours of the magnetic field strength, *Nuclear Fusion* **46** 921–927, 2006.

[99] H.E. Mynick, N. Pomphrey and P. Xanthopoulos, Reducing turbulent transport in toroidal configurations via shaping, *Physics of Plasmas* **18** 056101, 2011.

[100] M. Samitov, W. Cooper, M. Isaev, M. Mikhailov, J. Nührenberg, et al., Quasi-isodynamic Configuration with Small Number of Periods, *J. Plasma Fusion Research SERIES* **6**, 2004.

[101] D.J. Strickler, S.P. Hirshman, D.A. Spong, M.J. Cole, J.F. Lyon, et al., Development of a robust quasi-poloidal compact stellarator, *Fusion Science and Technology* **45** 15-26, 2004.

[102] D.A. Spong, J.H. Harris, A.S. Ware, S.P. Hirshman and L.A. Berry, Shear flow generation in stellarators-configurational variations, *Nuclear Fusion* **47** 626-633, 2007.

[103] V. Tribaldos, Monte Carlo estimation of neoclassical transport for the TJ-II stellarator, *Physics of Plasmas* **8** 1229, 2001.

[104] M.A Samitov, W.A. Cooper, M.F. Heyn, M. Yu. Isaev, A.A. Ivanov, et al. 'Numerical Optimization of Three Period Stellarator Configuration with Respect to Quasi-isodynamicity', Presentation in IAEA Technical Meeting on Innovative Concepts and Theory of Stellarators, Greifswald (Germany), 29 September - 1 October 2003.

[105] E. Mazzucato, A midsize tokamak as a fast track to burning plasmas, *AIP Advances* **1**, 012101, 2011.

[106] S.P. Hirshman and J.C. Whitson, Steepest descent moment method for three-dimensional magnetohydrodynamic equilibria, *Physics of Fluids* **26** 3553, 1983.

[107] R.K. Maix, V. Bagnato, M. Fricke, K. Heyn, T. Kluck, et al., Design, Production and QA Test Results of the NbTi CIC Conductors for the W7-X Magnet System, *Journal of Physics: Conference Series* **43** 753–758, 2006.

[108] L.E. Dudek, J. H. Chrzanowski, P. J. Heitzenroeder, S. Raftopoulos, M. E. Viola, et al., Status of the NCSX construction, *Fusion Engineering and Design* **84** 351–354, 2009.

[109] M.E. Viola, T. Brown, P. Heitzenroeder, W. Reiersen, P. Goranson, et al., NCSX vacuum vessel fabrication, Proceedings of 21st IEEE/NPS Symposium on Fusion Engineering (SOFE 05), Knoxville, Tennessee (USA), September 2005.

[110] M. Fujiwara, O. Motojima, Y. Hamada, T. Watari, M. Okamoto, et al., Overview of LHD (Large Helical Device) project, *J. Plasma Fusion Research SERIES* **1** 52-61, 1998.

[111] Javier Alonso, 'Design, construction and assembly of the Spanish stellarator TJ-II. Engineering experience', Presentation in ITER Business Forum 2007 (IBF/07), Nice (France), 10-12 December 2007.

[112] J.H. Feist, M. Wanner and the W7-X construction team, Status of Wendelstein 7-X construction, 28th EPS Conference on Controlled Fusion and Plasma Physics, Funchal (Portugal), 18-22 June 2001, ECA 25A 1937-1940, 2001.

[113] Allen H Boozer, Stellarators and the path from ITER to DEMO, *Plasma Physics Controlled Fusion* **50** 124005, 2008.

[114] G. Hartwell, S. Knowlton, Helical coil frame for the CTH experiment, Unpublised internal report supplied by the CTH team, January 2002.

[115] J. Reich, W. Gardebrecht, B. Hein, B. Missal, J. Tretter, et al., Manufacture of the vacuum vessels and the ports of Wendelstein 7-X, *Fusion Engineering and Design* **75–79** 565–569, 2005.

[116] D. Chauvin, T. Koppe, A. Cardella, B. Missal, D. Pilopp, et al., Completion of designing and manufacturing of the coil support structure of W7-X, *Fusion Engineering and Design* **86** 640–644, 2011.

[117] Web site http://www.hsx.wisc.edu/pictures/construction/Support-structure_on-diagonal_no-coils.jpg, December 2014.

[118] Y. Tanaka, S. Kitajima, H. Yakahashi, H. Utoh, M. Sasao and M. Takayama, Study of Impurity Influx of H-mode Plasma in Hot-Cathode-Biasing Experiment in the Tohoku University Heliac, *Journal of Plasma Fusion Research SERIES* **6** 371–375, 2004.

[119] M.A. Pedrosa, M.A. Ochando, J.A. Jiménez, R. Balbín, J. Qin, and C. Hidalgo, Magnetic configuration effects on the TJ-IU torsatron plasma edge turbulence, *Plasma Physics and Controlled Fusion* **38** 365, 1996.

[120] M.A. Abdou and The APEX Team, Exploring novel high power density concepts for attractive fusion systems, *Fusion Engineering and Design* **45** 145–167, 1999.

[121] P. Norajitra, S. I. Abdel-Khalik, L.M. Giancarli, T. Ihli, G. Janeschitz, et al., Divertor conceptual designs for a fusion power plant, *Fusion Engineering and Design* **83** 893–902, 2008.

[122] A.R. Raffray, High heat flux components - Readiness to proceed from near term fusion systems to power plants, *Fusion Engineering and Design* **85**, 2010.

[123] R.A. Krakowski, R.L. Hagenson, N.M. Schnurr, C. Copenhaver, C.G. Bathke, R.L. Miller and M.J. Embrechts, Compact reversed-field pinch reactors (CRFPR), *Nuclear Engineering and Design/Fusion* **4** 75-120, 1986.

[124] V.M. Kulygin, V.V. Arsenin, V.A. Zhiltsov, A.V. Zvonkov, A.A. Skovoroda, A.V. Timofeev, Project EPSILON – the way to steady state high β fusion reactor, Ref. IC/P7-1, Proceedings of the IAEA XXI Fusion Energy Conference (Chengdu, China), 16 -21 October 2006.

[125] V.M. Kulygin, V.V. Arsenin, V.A. Zhiltsov, A.V. Zvonkov, A.A. Skovoroda, A.V. Timofeev, 'Project EPSILON – a way to steady state high β fusion reactor', Presentation in IAEA XXI Fusion Energy Conference (Chengdu, China), 16 -21 October 2006.

[126] T. Imai, M. Ichimura, Y. Nakashima, I. Katanuma, M. Yoshikawa, et al., Status and plan of GAMMA 10 tandem mirror program, *Transactions of Fusion Science and Technology* **59**, 2011.

[127] Donald A. Spong and Jeffrey H. Harris, New QP/QI Symmetric Stellarator Configurations, *Plasma and Fusion Research: Regular Articles* **5** S2039, 2010.

[128] Vicente M. Queral, J.A. Romero, J.A. Ferreira, High-field pulsed Allure Ignition Stellarator, *Stellarator News* 125, Editor: James A. Rome, April 2010.

[129] F. Wagner, S. Bäumel, J. Baldzuhn, N. Basse, R. Brakel, R. Burhenn, A. Dinklage, W7-AS: One step of the Wendelstein stellarator line, *Physics of Plasmas* **12**, 072509, 2005.

[130] V. Queral, J. Urbón, A. García, I. Cuarental, F. Mota, G. Miccichè, A. Ibarra, D. Rapisarda and N. Casal, Preliminary definition of the remote handling system for the current IFMIF Test Facilities, *Fusion Engineering and Design* **86** 1941–1945, 2011.

[131] X.R. Wang, S. Malang, A.R. Raffray, the ARIES Team, Maintenance Approaches for ARIES-CS Compact Stellarator Power Core, *Fusion Science and Technology* **47**(4) 1074-1078, 2005.

[132] M. Gryaznevich, V. Svoboda, J. Stockel, A. Sykes, N. Sykes, et al., Progress in application of high temperature superconductor in tokamak magnets, *Fusion Engineering and Design* **88** 1593– 1596, 2013.

[133] T. Sunn Pedersen, J. P. Kremer, R. G. Lefrancois, Q. Marksteiner, N. Pomphrey, et al., Construction and initial operation of the Columbia Nonneutral Torus, *Fusion Science and Technology* **50** 372-381, 2006.

[134] P. C. Stangeby, A tutorial on some basic aspects of divertor physics, *Plasma Physics Controlled Fusion* **42** B271–B291, 2000.

[135] H. Renner, J. Boscary, H. Greuner, H. Grote, F.W. Hoffmann, J. Kisslinger, E. Strumberger and B. Mendelevitch, Divertor concept for the W7-X stellarator and mode of operation, *Plasma Physics Controlled Fusion* **44** 1005-1019, 2002.

[136] C.W. Ammen, Metalcasting, ISBN 978-0-07-134246-9, Ed. McGraw-Hill, 2000.

[137] B. Terry Aspin, The backyard foundry, ISBN 978-185486-146-7, Ed. Special Interest Model Books Ldt, 2002.

[138] Ian Gibson, David W. Rosen and Brent Stucker, Additive Manufacturing Technologies, ISBN 978-1-4419-1120-9, Ed. Springer, 2009.

[139] P.J. Heitzenroeder, T.G. Brown, J.H. Chrzanowski, M.J. Cole, P.L. Goranson, et al., Component Manufacturing Development for the National Compact Stellarator Experiment (NCSX), PPPL Report n. PPPL-4019, November 2004.

[140] J. Botija, J. and M. Blaumoser, Vacuum vessel design for the TJ-II device, Proceedings of the 14th IEEE/NPSS Symposium on Fusion Engineering, 30 September - 03 October 1991.

[141] Article 'Team Proves Casting Sound For Vacuum Vessel Use', *NETCASTER newsletter* (http://www.buycastings.com), Issue 5, Winter 2003.

[142] V. Heinzel, P. Bem, E. Esposito, S. Gordeev, U. Fischer, A. Moeslang, et al. Overview on the IFMIF Test Cell development, *Journal of Nuclear Materials* **329-333 A** 223-227, 2004.

[143] Alexander S. Polyak, Tom K. Cho and Joseph Yudovsky, 'Concrete vacuum chamber', Patent application number: 20100021273, Publication date: 28 January 2010.

[144] F. Burri, M. Fertl, P. Feusi, R. Henneck, K. Kirch, et al., Copper coated carbon fiber reinforced plastics for high and ultra high vacuum applications, arXiv:1308.2563 [physics.ins-det], 12 August 2013.

[145] F. Arranz, B. Brañas, D. Iglesias, O. Nomen, D. Rapisarda, et al., Manufacturing prototypes for LIPAC beam dump, *Fusion Engineering and Design* **89** 2199–2203, 2014.

[146] B. Caulfield, P.E. McHugh and S. Lohfel, Dependence of mechanical properties of polyamide components on build parameters in the SLS process, *Journal of Materials Processing Technology* **182** 477–488, 2007.

[147] S.S. Azer, R.E. Kerby, L. A. Knobloch, Effect of mixing methods on the physical properties of dental stones, *Journal of dentistry* **36** 736–744, 2008.

[148] J.J. Fuller, 'Predicting the Thermo-Mechanical Behavior of A Gypsum-To-Wood Nailed Connection', Master's Thesis. 6 April 1990.

[149] P. Frigola, O.A. Harrysson, T.J. Horn, H.A. West, R.L. Aman, et al. Fabricating Copper Components with Electron Beam Melting, *Advanced Materials & Processes* 20-24, July 2014.

[150] Timothy Horn, 'Material Development for Electron Beam Melting', Presentation from the Center for Additive Manufacturing and Logistics, North Carolina State University, 2013.

[151] Tim McCreight, Practical casting, ISBN 0-9615984-0-9, Ed. Brynmorgen Press Inc., Boylston, Massachusetts, 1986.

[152] V. Queral, 3D-printed fusion components concepts and validation for the UST_2 stellarator, *Fusion Engineering and Design*, doi:10.1016/j.fusengdes.2015.03.028, in Press, 2015.

[153] 'Status of Non-Axisymmetric Coils Study', Handouts for Project Workshop, NCSX Project, 23-25 September 1998.

[154] S. Rajendran, ITER Remote Handling Code of Practice (IRHCOP), ITER Report Ref. ITER_D_2E7BC5, 2 July 2009.

[155] V. Queral, Construction concepts and validation of the 3D printed UST_2 modular stellarator, *Journal of Physics: Conference Series* **591** 012015, 2015.

Acronyms

3D : Three-dimensional
BSCOO : Bismuth Strontium Calcium Copper Oxide HTS
CAD : Computer Aided Design
CIEMAT : Centro de Investigaciones Energéticas, Medioambientales y Tecnológicas
CNC : Computer Numerical Control
CNT : Columbia Non-neutral Torus
COE : Cost of Electricity
CRT : Cathode-ray tube
CTH : Compact Toroidal Hybrid
DMLS : Direct Metal Laser Sintering
ECRH : Electron Cyclotron Resonant Heating
FDM : Fused Deposition Modelling
fps : Frames per second
HSR : Helias Stellarator Reactor
HSX : Helically Symmetric Experiment
HTS : High Temperature Superconductor
IAEA : International Atomic Energy Agency
ICF : Inertial Confinement Fusion
IFMIF : International Fusion Materials Irradiation Facility
IPP : Institute of Plasma Physics
ITCR : Instituto Tecnólogico de Costa Rica
ITER : International Thermonuclear Experimental Reactor
JET : Joint European Torus
LCFS : Last Closed Flux Surface
LHD : Large Helical Device
LIPAC : Linear IFMIF Prototype Accelerator
MCF : Magnetic Confinement Fusion
MHD : Magnetohydrodynamics
MTF : Magnetized Target Fusion
NCSX : National Compact Stellarator Experiment
PC : Personal Computer
PPPL : Princeton Plasma Physics Laboratory
PVA : Polyvinyl Alcohol
QIPCC : Quasi-isodynamic with Poloidally Closed Contours
QPS : Quasi-Poloidal Stellarator
R&D : Research and Development
SCR-1 : Stellarator of Costa Rica 1
SLS : Selective Laser Sintering
TBR : Tritium Breeding Ratio
TEC : Instituto Tecnológico de Costa Rica
TF : Toroidal Field
UST_1 : Ultra Small Torus 1
UST_2 : Ultra Small Torus 2
VV : Vacuum Vessel
W7-X : Wendelstein 7-X stellarator
YBCO : Yttrium barium copper oxide

Publications and contributions

Publications in international peer reviewed journals

- **V. Queral**, 3D-printed fusion components concepts and validation for the UST_2 stellarator, *Fusion Engineering and Design*, doi:10.1016/j.fusengdes.2015.03.028, in Press, 2015.
- **V. Queral**, Concept, production and validation of a 3D-printed coil frame for the UST_2 modular stellarator, *Fusion Engineering and Design* **89** 2145–2149, 2014.
- **V. Queral**, Coil fabrication of the UST_1 modular stellarator and potential enhancements, *Fusion Engineering and Design* **88** 683–686, 2013.

Conference Contributions

Conference Proceedings publications

- **V. Queral**, Construction concepts and validation of the 3D printed UST_2 modular stellarator, *Journal of Physics: Conference Series* **591** 012015, 2015.
- L. Barillas, V. I. Vargas, A. Alpizar, J. Asenjo,..., **V. Queral**, et al., SCR-1: Design and Construction of a Small Modular Stellarator for Magnetic Confinement of Plasma, *Journal of Physics: Conference Series* **511** 012037, 2014.

Oral contributions

- **V. Queral**, '3D-printed UST_2 stellarator status and first e-beam mapping experiments'. Oral contribution in the 21st Topical Meeting on the Technology of Fusion Energy (TOFE), Anaheim, CA (USA), 9-13 November 2014.
- **V. Queral**, '3D printed modular stellarator UST_2'. Oral contribution in the 21st IAEA Technical Meeting on 'Research Using Small Fusion Devices' (RUSFD), San José (Costa Rica). 27-29 January 2014.

Poster contributions

- **V. Queral**, 3D-printed fusion components concepts and validation, Poster P1.014 in the 28th Symposium on Fusion Technology (SOFT), San Sebastián (Spain), 29 September - 3 October 2014.

- **V. Queral**, Concept, production and validation of a 3D-printed coil frame for the UST_2 modular stellarator, Poster P1.140 in the 11th International Symposium on Fusion Nuclear Technology (ISFNT), Barcelona (Spain), 16-20 September 2013.
- **V. Queral**, Coil fabrication of the UST_1 modular stellarator and potential enhancements, Poster P1.7 in the 27th Symposium on Fusion Technology (SOFT), Liège (Belgium), 24-28 September 2012.

Other publications in international peer reviewed journals

- **V. Queral**, J. Urbón, A. García, I. Cuarental, F. Mota, G. Miccichè, A. Ibarra, D. Rapisarda, N. Casal, Preliminary definition of the remote handling system for the current IFMIF Test Facilities, *Fusion Engineering and Design* **86** 1941–1945, 2011.
- **V. Queral**, A. García, G. Miccichè, A. Ibarra, N. Casal, F. Mota, D. Rapisarda, Proposal of an improved design of IFMIF Test Cell components for enhanced handling and reliability, *Fusion Engineering and Design* **84** 1548–1552, 2009.
- Elena V. Rosa, Luis Rios, **Vicente Queral**, Progress on the interface between UPP and CPRHS (Cask and Plug Remote Handling System) tractor/gripping tool for ITER, *Fusion Engineering and Design* **88** 2168–2172, October 2013.
- G. Miccichè, L. Lorenzelli, D. Bernardi, **V. Queral**, Enhancement of the remote handling strategy for the refurbishment of the backplate bayonet concept of IFMIF target system, *Fusion Engineering and Design* **86** 2109–2112, 2011.
- A. Ibarra, M. Perlado, R. Aracil, D. Blanco, M. Ferre, … **V. M. Queral**, L. Ríos, R. Román, TechnoFusión, a relevant facility for fusion technologies: The Remote Handling area, *Fusion Engineering and Desing* **85** (7-9) 1659–1663, 2010.
- N. Casal, A. García, A. Ibarra, F. Sordo, D. Rapisarda, **V. Queral**, F. Mota, Tritium permeation experiment at IFMIF Medium Flux Test Module, *Fusion Engineering and Design* **84** 559–564, 2009.
- David Rapisarda, Angela García, Óscar Cabellos, Fernando Mota, Jose M. Gómez-Ros, Ángel Ibarra, Natalia Casal, **Vicente Queral**, Javier Sanz, Feasibility of fission chambers as a neutron diagnostic in the IFMIF Test Cell, *Fusion Engineering and Design* **84** 1570–1574, 2009.
- N. Casal, F. Sordo, ... **V. Queral**, IFMIF suitability for evaluation of fusion functional materials, *Journal of Nuclear Materials* **417** 1316-132, 2011.
- D. Rapisarda, L. Vermeeren, A. García, O Cabellos, J.M. García, A. Ibarra, J.M. Gómez-Ros, F. Mota, N. Casal, **V. Queral**, Study on the response of IFMIF fission chambers to mixed neutron-gamma fields: PH-2 experimental tests, *Fusion Engineering and Design* **86** 1232–1235, 2011.
- F. Mota, C. Ortiz, A. Garcia, N. Casal, R. Vila, A. Ibarra, D. Rapisarda, **V. Queral**, Analysis of displacement damage in materials in nuclear fusion facilities (DEMO, IFMIF and Technofusion*), Fusion Engineering and Design* **86** 2425–2428, 2011.